NUMERICAL SIMULATION OF ELECTROPHORESIS SEPARATION PROCESSES

by

D.K. Ganjoo (1)

and

T.E. Tezduyar (2)

Department of Mechanical Engineering

University of Houston

Houston, TX 77004

Interim Report for the

Work Performed Under NASA-Johnson Space Center

Contract NAS 9-17380

(NASA-CR-180124) NUMERICAL SIMULATION OF ELECTROPHORESIS SEPARATION PROCESSES Interim Report (Houston Univ.) 104 p CSCL 07D G3/25

N87-16087

Unclas 43382

(1) Graduate Research Assistant
(2) Assistant Professor

ABSTRACT

A new Petrov-Galerkin finite element formulation has been proposed for transient convection-diffusion problems. Most Petrov-Galerkin formulations take into account the spatial discretization, and the weighting functions so developed give satisfactory solutions for steady state problems. Though these schemes can be used for transient problems, there is scope for improvement. The schemes proposed here, which take into account temporal as well as spatial discretization, provide improved solutions.

Electrophoresis, which involves the motion of charged entities under the influence of an applied electric field, is governed by equations similiar to those encountered in fluid flow problems, i.e., transient convection-diffusion equations. Test problems are solved in electrophoresis and fluid flow. The results obtained are satisfactory. It is also expected that these schemes, suitably adapted, will improve the numerical solutions of the compressible Euler and the Navier-Stokes equations.

TABLE OF CONTENTS

TABLE OF CONTENTS

LIST OF FIGURES

LIST OF FIGURES

CHAPTER 1

INTRODUCTION

In recent years finite-element methods have been applied to problems of fluid dynamics, and various other transport problems. Some of their advantages over other methods are the following: ease in modelling intricate geometries and consistent treatment of the boundary conditions. However, problems with convection dominated flows have not been solved as successfully as problems in solid mechanics, structures, and heat conduction. The reason being that symmetric positive-definite operators - which are dominant in differential equations governing solid mechanics problems - lead to a "best approximation" of the exact solution by the finite-element method. On the other hand, problems in fluid mechanics(and some other transport problems) are governed by both, symmetric positive-definite operators and nonsymmetric operators(convection terms). Thus, in convection dominated flows, the "best approximation" property of the Galerkin finite element is lost and spurious oscillations are observed.

It is well known that "upwind " differencing in finite-difference schemes may produce a wiggle-free solution, but in most cases the side effect is loss of accuracy due to overly diffuse solutions. Efforts to improve the results by adding artificial diffusion terms to the differential equations may again result in unacceptable levels of amplitude error or smearing of discontinuities. This artificial diffusion concept has been the subject of substantial controversy and criticism [1,2,3]. Various "upwind" finite-element schemes have been proposed, such as those by Christie et al.[4], Heinrich et al. [5], Hughes[6], and Hughes and Atkinson[7]. These methods are based on modified weighting functions, modified quadrature rules, and variational principles, which yield satisfactory results for one-dimensional problems. However in multi-dimensional cases the solutions are overly diffuse especially in the presence of transient or source terms.

It has been demonstrated that the above mentioned problems can be avoided by using proper Petrov-Galerkin (PG) schemes [8,9]. As opposed to regular Galerkin formulations, PG formulations involve trial and weighting functions from different spaces. Such schemes have been applied to various fluid dynamics and convection-diffusion problems by Brooks and Hughes [10], Hughes and Tezduyar[11], Hughes et al. [12], and Hughes, Mallet and Franca[13]. These schemes have been developed to obtain steady state solutions, and though they have been tested for transient cases, it was felt that there was considerable scope for improvement.

Chapter 2 highlights the development and testing of new weighting functions which improve the performance of transient schemes. The underlying philosopy in

conceptualizing such functions is the belief that in addition to depending on spatial discretization, the weighting functions must also depend on the temporal discretization. Johnson et al. [14] have also approached the problem with a similiar objective in mind.

1.1 APPLICATIONS

FLOW FIELD SIMULATION Simulation of flow fields has become exceedingly important today with the advent of the space age and the increasing demand for understanding of other related properties. Although the governing equations (i.e., the full Navier-Stokes equations) would require tremendous computational resources, depending on specific problems, simplifications can be made leading to feasible models. In this thesis a two-dimensional, incompressible flow model has been assumed which has a wide range of applications.

The governing equations are the two momentum equations and the continuity equation[15] which can be solved numerically[16]. However by further simplifications, the number of transient equations can be reduced to one and the number of unknowns to two. This is possible by introducing new variables, the vorticity and the stream function[17]. This approach, known as the vorticity-stream function approach, has been adopted in Chapter 3.

ELECTROPHORESIS SEPARATION SIMULATION Electrophoresis involves motion of dissolved or suspended material under the influence of an applied electric field. The entities may be simple ions, complex macromolecules, colloids, or living cells. The rate of migration depends on factors such as the amount of charge, the size and shape of the entity, and the solvent properties.These properties are conveniently combined into a single factor, termed the "particle mobility". Thus, when particles of different mobilities are subjected to the same electric potential, they tend to move at different speeds and thus separate out . This is the basic principle of electrophoresis[18]. Electrophoresis, particularly in gels, affords a higher resolving power for biopolymers than any other method, and is therefore universally used for the analysis of protein preparations[19]. Figure 1.1.1 shows the electrophoretic pattern of blood serum proteins of normal and diseased people which is useful as a clinical tool.

However, current methods in electrophoresis separation suffer from disadvantages like complicated design, construction, and operation of apparatus, low production

capacity, precipitation of proteins at high concentrations, etc. Evidently more research has to be done to make electrophoresis commercially viable. Hence simulation of this phenomenon can aid in further development .

Specifically, the following goals can be accomplished :

- Simulation can be used to correlate mobility/dissociation data with experimental data. A typical problem in this field is the general lack or inaccuracy of data. Using computational models can help to narrow down inaccuracies .
- Computational models reveal details of boundary structures like concentration, pH, and conductivity not easily amenable to direct experimental observation.
- Simulations can be used to develop new techniques which are not yet available experimentally. This may be used to develop commercial high volume production techniques.
- Numerical models can provide a rational basis for understanding many separation techniques. Existing theories are too restrictive in the sense that one theory can only be used to explain a particular technique. However, a mathematical model based on the governing equations can be simulated and can predict all techniques (as will be illustrated in Chapter 4).

Briefly, the thesis outline is as follows:

Chapter 2 gives details on the development and testing of Petrov-Galerkin schemes.
Chapter 3 outlines the algorithm used for flow field simulation along with test cases.
Chapter 4 gives a detailed description of various electrophoretic techniques and their simulation.
Chapter 5 gives the conclusions for Chapters 2, 3, and 4.

CHAPTER 2

DEVELOPMENT OF PETROV-GALERKIN SCHEMES FOR CONVECTION-DIFFUSION PROBLEMS

In this chapter a new Petrov-Galerkin finite-element formulation has been developed for transient convection-diffusion problems. Most Petrov-Galerkin formulations take into account the spatial discretization and the weighting functions so developed give satisfactory solutions for steady state problems. Though these schemes can be used for transient problems, there is scope for improvement. Basically the weighting functions used for the steady state problems are obtained by perturbing the functions which would otherwise lead to a Galerkin formulation. These perturbations are dependent only on the spatial discretization. However, for transient problems it was felt that this perturbation should also depend on the temporal discretization. The schemes proposed here, which take into account temporal as well as spatial discretization, provide improved solutions. In view of the generality of the differential equation being solved, these schemes can be used to solve any physical problem which is governed by the transient convection-diffusion equation.

2.1 PROBLEM STATEMENT

The transient convection-diffusion equation in n_{sd} space dimensions is given as

$$\phi_{,t} + \mathbf{u} \bullet \nabla\phi = \nabla \bullet (\boldsymbol{\kappa} \bullet \nabla\phi) + f \qquad \text{on } \Omega \tag{2.1.1}$$

where $\phi = \phi (\mathbf{x},t)$ is the dependent variable, a function of the spatial position $\mathbf{x} \in \Omega \subset \Re^{nsd}$ and time $t \in]\, 0,T\, [$ where $T > 0$. The velocity field $\mathbf{u} = \mathbf{u} (\mathbf{x})$ is given, and $\boldsymbol{\kappa}$ is the conductivity matrix. The source term is given as $f = f (\mathbf{x})$. The boundary Γ of the domain Ω is assumed to have the following decomposition:

$$\Gamma = \overline{\Gamma_g \cup \Gamma_h} \tag{2.1.2}$$

$$\varnothing = \Gamma_g \cap \Gamma_h \tag{2.1.3}$$

where Γ_g and Γ_h represent the Dirichlet and Neumann type boundaries, respectively. Hence,

$$\phi(\mathbf{x},t) = g(\mathbf{x},t) \qquad \forall\ \mathbf{x} \in \Gamma_g,\ t \in\ ]0,T[\tag{2.1.4}$$

$$\mathbf{n}(\mathbf{x}) \bullet \boldsymbol{\kappa} \bullet \nabla\phi(\mathbf{x},t) = h(\mathbf{x},t) \ \forall\ \mathbf{x} \in \Gamma_h,\ t \in\ ]0,T[\tag{2.1.5}$$

where $\mathbf{n}$ is the unit normal vector to the boundary, and g and h are prescribed functions.

The initial condition is

$$\phi(\mathbf{x},0) = \phi_0(\mathbf{x}) \qquad \mathbf{x} \in \Omega \tag{2.1.6}$$

where ϕ_0 is a given function.The initial/boundary-value problem is to find $\phi = \phi(\mathbf{x},t)$ which satisfies eqs. (2.1.1) and (2.1.4)-(2.1.6).

2.2 FINITE-ELEMENT FORMULATION

Consider a discretization of Ω into element subdomains Ω^e, e = 1,2,..., n_{el} where n_{el} is is the number of elements. Let Γ^e denote the boundary of $\bar{\Omega}^e$. We assume

$$\bar{\Omega} = \bigcup_{e=1}^{n_{el}} \bar{\Omega}^e \tag{2.2.1}$$

$$\varnothing = \bigcap_{e=1}^{n_{el}} \Omega^e \tag{2.2.2}$$

The interior boundary is defined as

$$\Gamma_{int} = \bigcup_{e=1}^{n_{el}} \Gamma^e - \Gamma \tag{2.2.3}$$

Let V and S denote the finite-dimensional variational and trial-solution spaces such that

$$V = \{ w \mid w \in H^1(\Omega),\ w(x) = 0 \qquad \forall\ x \in \Gamma_g \} \tag{2.2.4}$$

$$S = \{ \Phi \mid \Phi \in H^1(\Omega),\ \Phi(x) = g(x) \quad \forall\ x \in \Gamma_g \} \tag{2.2.5}$$

It is also assumed that both the spaces consist of the typical C^0 finite-element interpolation functions.

The discrete variational form of eq. (2.1.1) and the associated initial condition in eq. (2.1.6) are

$$\int_\Omega \{ w\Phi_{,t} + w\mathbf{u}\bullet\nabla\Phi + \nabla w \bullet (\boldsymbol{\kappa} \bullet \nabla\Phi) \}\, d\Omega$$

$$+ \sum_{e=1}^{n_{el}} \int_{\Omega^e} p\{ \Phi_{,t} + \mathbf{u}\bullet\nabla\Phi - \nabla \bullet (\boldsymbol{\kappa} \bullet \nabla\Phi) - f \}\, d\Omega$$

$$= \int_{\Gamma_h} wh\, d\Gamma + \int_\Omega wf\, d\Omega \tag{2.2.6}$$

$$\int_\Omega w(\Phi - \Phi_0)\, d\Omega = 0 \tag{2.2.7}$$

where p is a C^{-1} perturbation to the weighting function w. The Euler-Lagrange equation corresponding to eq. (2.2.6) is

$$\sum_{e=1}^{n_{el}} \int_{\Omega^e} \tilde{w}\{ \Phi_{,t} + \mathbf{u}\bullet\nabla\Phi - \nabla\bullet(\boldsymbol{\kappa}\bullet\nabla\Phi) - f \}\, d\Omega$$

$$+ \int_{\Gamma_h} w\{ \mathbf{n}\bullet\boldsymbol{\kappa}\bullet\nabla\Phi - h \}\, d\Gamma + \int_{\Gamma_{int}} w\, [\, \mathbf{n}\bullet\boldsymbol{\kappa}\bullet\nabla\Phi]\, d\Omega = 0 \tag{2.2.8}$$

where [ ] is the "jump" operator.

Remarks

(1) $\tilde{w}$ is obtained by perturbing the weighting function w which when unperturbed leads to Galerkin formulation, i.e., the modified weighting function is given by

$$\tilde{w} = w + p \tag{2.2.9}$$

(2) The perturbation component weighs only on the element interiors and hence does not affect the boundary term h.

(3) Brooks and Hughes [10] have shown that for rectangular elements the perturbation term does not affect the weighting of the diffusion term and it is expected that for reasonable element shapes the contribution is negligible.

(4) The unknown ϕ is interpolated with multilinear isoparametric interpolation functions.

A consistent finite-element spatial discretization of equation (2.2.8) leads to the following set of ordinary differential equations:

$$\mathbf{M}\,\dot{\mathbf{d}} + \mathbf{C}\,\mathbf{d} = \mathbf{F} \tag{2.2.10}$$

where $\mathbf{M}$, $\mathbf{C}$, and $\mathbf{F}$ are the mass matrix, stiffness matrix, and the generalized force vector respectively; and $\mathbf{d}$ and $\dot{\mathbf{d}}$ represent the dependent variable and its temporal derivative at the nodes.

This initial value problem is solved by a family of Predictor/Multi-corrector algorithms proposed by Hughes et al. [20].

The proposed weighting functions are the following:

SUPG - a modified version of Streamline Upwind/Petrov-Galerkin formulation proposed by Brooks and Hughes[10].
TW - a scheme based on Transport Weighting proposed by Hughes et al.[12].
SW - a scheme based on Sigma Weighting proposed by Hughes et al.[12].

For all the above schemes the weighting function associated with element node number a is expressed as

$$\tilde{N}_a = N_a + z\,\tilde{P}_a \tag{2.2.11}$$

where N_a is the multilinear weighting function (associated with node a) leading to

Galerkin formulation.

The parameter z depends on the element Peclet number and is given [10] as

$$z = \begin{cases} \alpha/3 & 0 \le \alpha \le 3 \\ 1 & \alpha > 3 \end{cases} \qquad (2.2.5)$$

where $\alpha \in [0,\infty)$ is the element Peclet number(= ||u||h / 2k , where **u** is the flow velocity, h the element length along the advection direction, and k the diffusivity). This expression for z is a doubly asymptotic approximation of the form which leads to nodally exact solutions in one-dimensional steady state problems [10]. For convection-dominated flows z = 1 as $\alpha \to \infty$.

The perturbation function $\tilde{P}_a$ for steady state cases is given as

$$\tilde{P}_a = P_a^* \qquad (2.2.13)$$

where

$$P_a^* = N_a^* - N_a \qquad (2.2.14)$$

Here N_a^* is the weighting function for pure convection (i.e., for z = 1). The Streamline-Upwind/Petrov-Galerkin formulation given in [10] defines P_a^* as

$$P_a^* = (h/2)\, \mathbf{s}\bullet\nabla N_a \qquad (2.2.15)$$

where h is the element length along advection direction **s**.

The Transport Weighting formulation proposed in [12] defines N_a^* as follows:

$$N_a^*(\mathbf{x}) = Na(\tilde{\mathbf{x}}), \quad \mathbf{x} \in \Omega^e \qquad (2.2.16)$$

$$\tilde{\mathbf{x}} = \mathbf{x} + \varepsilon \mathbf{s}, \qquad \varepsilon \ge 0 \qquad (2.2.17)$$

Here $\tilde{\mathbf{x}}$ represents the intersection with the element boundary of the line emanating from **x** in the direction **s**.

The Sigma Weighting formulation proposed in [12] defines N_a^* as follows:

$$N_a^* = \sigma_a / \sigma \ , \ x \in \Omega^e \tag{2.2.18}$$

$$\sigma_a = < s \bullet \nabla N_a > \tag{2.2.19}$$

$$\sigma = \sum_{a=1}^{n_{en}} \sigma_a \tag{2.2.20}$$

where n_{en} is the number of element nodes, Ω^e is the element domain, and $< \bullet >$ is the Macauley bracket (i.e., $<y> = y$ if $y > 0$, else $<y> = 0$).

Note that P_a^* for SW and TW is derived from eq.(2.2.14).

For SUPG, $\tilde{P}_a$ is given as

$$\tilde{P}_a = \tau \, \mathbf{u} \bullet \nabla N_a \tag{2.2.21}$$

where τ is a parameter having the dimension of time [10]. Based on τ, an "algorithmic Courant number" [11] can be defined as

$$C_{2\tau} = \frac{(2\tau) \| \mathbf{u} \|}{h} \tag{2.2.22}$$

For transient problems, we propose

$$\tilde{P}_a = C_{2\tau} P_a^* \tag{2.2.23}$$

where $C_{2\tau}$, in general, is selected to be different from unity. For steady state problems, SUPG formulation has $C_{2\tau} = 1$. Hughes and Tezduyar[11] have used

$$C_{2\tau} = C_{\Delta t} \tag{2.2.24}$$

for various problems governed by hyperbolic equation systems where $C_{\Delta t}$ is the element Courant number based on the time step, i.e.,

$$C_{\Delta t} = \frac{(\Delta t) \| \mathbf{u} \|}{h} \tag{2.2.25}$$

where Δt is the time step of the transient algorithm. In the next section a Neumann stability/accuracy analysis is carried out. This analysis is useful in arriving at estimates for the algorithmic Courant number $C_{2\tau}$.

Remark

Combining eqs. (2.2.11), (2.2.14), and (2.2.23), we obtain the expression,

$$\tilde{N}_a = (1 - z\, C_{2\tau})\, N_a + z\, C_{2\tau}\, N_a^* \quad , \tag{2.2.26}$$

which is convenient for implementation purpose especially for weighting functions SW and TW because, unlike SUPG, for these weighting functions there is no explicit definition for $\tilde{P}_a$.

2.3 STABILITY AND ACCURACY ANALYSIS

Tezduyar and Hughes [21] have performed a detailed phase accuracy and damping ratio analysis for one-dimensional transient pure advection. In this analysis, the exact solutions were assumed to be of the form:

$$\phi(x,t) = e^{-(\xi + i\omega)t} \; e^{-ikx} \tag{2.3.1}$$

and approximate linear finite-element solutions are of the form:

$$\phi(x_A,t_n) = e^{-(\bar{\xi} + i\bar{\omega})\, n \Delta t} \; e^{-ik x_A} \tag{2.3.2}$$

where ξ and $\bar{\xi}$ represent exact and approximate algorithmic damping ratios (ADR) respectively; ω and $\bar{\omega}$ represent the exact and approximate frequency ratios(FR); and k denotes the wave number ($k = 2\pi/\lambda$ where λ is the wavelength). A dimensionless wave number can be defined based on k and the element length h as follows:

$$q = k\, h \tag{2.3.3}$$

The ADR is related to the amplitude decay of a wave while the FR indicates the presence of trailing or leading waves which are seen as oscillations. A good scheme should display minimum damping with a FR close to unity. Using these attributes as the guidelines and using the analysis in [21] ,various plots were obtained for ADR vs q and FR vs q for a set of element Courant numbers, different weighting functions, and various forms of $C_{2\tau}$. The optimal value of $C_{2\tau}$ for a given $C_{\Delta t}$ was retained, and from this optimal data, $C_{2\tau}$ was constructed as a function of $C_{\Delta t}$.

Figure 2.3.1 shows various weighting functions for one-dimensional linear elements using various forms of $C_{2\tau}$ (for z = 1 and $C_{\Delta t} = 0.5$).

Figures 2.3.2 to 2.3.7 show the ADR and FR characteristics of various forms of $C_{2\tau}$ for SUPG and TW(or SW) weighting functions.

Remarks

(1) The various forms of $C_{2\tau}$ are expressed as polynomial functions of $C_{\Delta t}$, i.e.,

$$C_{2\tau} = a + (1 - a) C_{\Delta t}^{n}$$

where a and n are constants to be determined.

(2) The forms $C_{2\tau} = 1$ and $C_{2\tau} = C_{\Delta t}$ have been extensively studied in [21].

(3) TW and SW weighting functions are identical in one-dimensional cases; for $C_{2\tau} = 1$ they correspond to the Padé finite-difference approximation [22].

Implicit Algorithms

(1) Although algorithmic damping is zero for Galerkin formulation (i.e., $C_{2\tau} = 0$), a rapid departure of FR (not shown) from unity predicts oscillations in numerical solutions.

(2) For the SUPG weighting function, the best FR response is for the form,

$$C_{2\tau} = 2/\sqrt{15} + (1 - 2/\sqrt{15})\, C_{\Delta t}, \quad 0 \le C_{\Delta t} \le 1 \qquad (2.3.4)$$

with a reasonable ADR. As $C_{\Delta t}$ approaches zero, this scheme reduces to the one which has fourth-order phase accuracy [23] for the semi-discrete equations.

(3) For the SUPG formulations, the forms $C_{2\tau} = 2/\sqrt{15}$ and $C_{2\tau} = C_{\Delta t}$ lead to satisfactory FR response. However, the corresponding ADR is not as good as for the case mentioned in remark (2).

(4) For the TW(or SW) weighting function of the form

$$C_{2\tau} = 1/4 + (1 - 1/4) C_{\Delta t}^4 , \quad 0 \le C_{\Delta t} \le 1 \qquad (2.3.5)$$

yields superior FR response. This form satisfies the unit CFL condition[24].

Explicit 1-pass Algorithms

(1) Galerkin (not shown) is unconditionally unstable.

(2) SUPG ($C_{2\tau} = C_{\Delta t}$) is second-order accurate.

(3) SUPG ($C_{2\tau} = 1$) and TW ($C_{2\tau} = 1$) are identical.

(4) TW ($C_{2t} = 1/4 + (1 - 1/4) C_{\Delta t}^4$) is conditionally stable; the stability limit is $C_{\Delta t} \cong 0.253$.

Explicit 2-pass Algorithms

(1) Galerkin (not shown) is unconditionally unstable.

(2) All algorithms are second-order accurate.

(3) TW ($C_{2\tau} = 1/4 + (1 - 1/4) C_{\Delta t}^4$) is conditionally stable; the stability limit is $C_{\Delta t} \cong 0.303$.

2.4 NUMERICAL EXAMPLES

In an effort to verify the improvements made in the weighting functions, a number of standard test problems were solved for convection dominated flows in one and two dimensions for various combinations of the weighting functions, algorithmic Courant number (not to be confused with the element Courant number which is based on Δt), and the element Courant number. For one-dimensional problems even though the results

shown in figures are for $C_{\Delta t} = 0.6$, the related discussions and conclusions also account for different value of $C_{\Delta t}$. The problems are classified as follows:

Advection of a Cosine-wave in One Dimension

This consists of a cosine-wave initially on the extreme left and Neumann type boundary condition on the extreme right. The diffusion is set to zero, and the mesh and the convection velocity remain fixed. Tests were conducted for various time steps (i.e., for different element Courant numbers). The exact solution consists of pure advection of the initial condition to the right. Solutions are compared at the end of the same time interval. Figure 2.4.1 depicts the results for various weighting functions, various forms of $C_{2\tau}$, and a fixed value of $C_{\Delta t}$. Since weighting functions TW and SW are identical in one dimension, only TW has been shown. Moreover, when $C_{2\tau} = 0$, all weighting functions lead to Galerkin formulation.

For SUPG for all forms of $C_{2\tau}$, the peak amplitudes are comparable, and only trailing waves are observed. When $C_{\Delta t}$ is decreased, all forms of $C_{2\tau}$ yield comparable solutions, and exhibit both leading and trailing waves. When $C_{\Delta t}$ is increased, the peak amplitudes are comparable; however, for the $C_{2\tau} = 2/\sqrt{15} + (1 - 2/\sqrt{15}) C_{\Delta t}$ form the trailing wave amplitude is halved compared to the other forms. For SUPG formulation, the form $C_{2\tau} = 2/\sqrt{15} + (1 - 2/\sqrt{15}) C_{\Delta t}$ performs better for high or low Courant numbers, while for medium Courant numbers, all forms of $C_{2\tau}$ perform similarly.

For TW (or SW) the form $C_{2\tau} = 1$ produces leading oscillations; for other forms of $C_{2\tau}$ the solutions are reasonable and comparable. A similiar trend is observed when the Courant number is decreased. With increasing Courant number all forms of $C_{2\tau}$ give better results, and when $C_{\Delta t} = 1$, the solutions are identical. For TW(or SW) formulation the forms $C_{2\tau} = C_{\Delta t}$ and $C_{2\tau} = 1/4 + (1 - 1/4) C_{\Delta t}^4$ provide satisfactory results for

a wide range of Courant numbers.

Advection of a Discontinuity in One Dimension

This is similiar to the previous problem of one-dimensional cosine-wave advection except that the initial profile has a discontinuity spread over one element. The exact solution again consists of pure advection of the initial profile to the right. Figure 2.4.2 shows these results for $C_{\Delta t} = 0.6$. For the SUPG formulation, all forms of $C_{2\tau}$ provide comparable solutions (the peak overshoots are 7-9.5% of initial peak value and the undershoots are 0.7-2% of the initial peak value).When the Courant number is decreased the overshoots are higher for the $C_{2\tau} = C_{\Delta t}$ form, and oscillations occur. This is not surprising because as $C_{\Delta t}$ tends to zero the scheme approaches Galerkin formulation. As the Courant number is increased, the solutions converge and become identical for $C_{\Delta t} = 1$ for all forms of $C_{2\tau}$. For the SUPG formulation all forms of $C_{2\tau}$ yield reasonable solutions for medium to high Courant numbers. For low Courant number, the forms $C_{2\tau} = 1$ or $C_{2\tau} = 2/\sqrt{15} + (1 - 2/\sqrt{15}) C_{\Delta t}$ perform better.

For the TW(or SW) formulation, $C_{2\tau} = 1$ produces severe leading oscillations, while for the $C_{2\tau} = C_{\Delta t}$ the undershoot is too high. However, much less overshoot and undershoot occur for the form $C_{2\tau} = 1/4 + (1 - 1/4) C_{\Delta t}^4$. For TW(or SW) the form $C_{2\tau} = 1/4 + (1 - 1/4) C_{\Delta t}^4$ performs optimally for the entire range of Courant numbers.

Translation of a Cosine-hill in Two Dimensions(Translating Puff)

The domain is a square region of size 1x1 in the positive x_1-x_2 plane with 30x30 elements. A cosine-hill initial profile, distributed over 12 elements, is centered at coordinates (0.27, 0.50). The diffusion is set to 10^{-6}. The velocity is unity in the x_1-direction and the time step is adjusted to give $C_{\Delta t}$ of approximately 0.25 at the tip of the hill. All boundaries are of Dirichlet type and homogeneous except at $x_1 = 1.0$ which is of Neumann type and homogeneous. The problem was run for 120 time steps, in which time the hill should be transported out of the region with minimal amplitude loss and minimal oscillations in front or in the wake.

Figures 2.4.3, 2.4.4, and 2.4.5 show the results for different weighting functions and various forms of $C_{2\tau}$.

For SUPG formulation at step 80 it is observed that the peak amplitude is 99.2% (as a percentage of the initial peak amplitude) for $C_{2\tau} = C_{\Delta t}$, 96.8% for $C_{2\tau} = 1$, and 97.9% for the $C_{2\tau} = 2/\sqrt{15} + (1 - 2/\sqrt{15}) C_{\Delta t}$ form. The trailing wave amplitudes are comparable (< 2%).

For the TW (or SW) formulations and all forms of $C_{2\tau}$ the solutions are vastly superior to those obtained by using SUPG formulations(Peak height drop is less than 1% while trailing wave amplitude is less than 0.01%). Notice, however, that for $C_{2\tau} = 1$ the solution is marred by the presence of leading oscillations.

For cosine-hill advection in two dimensions, the TW(or SW) formulations perform quite well when the form $C_{2\tau} = C_{\Delta t}$ or $C_{2\tau} = 1/4 + (1 - 1/4) C^4_{\Delta t}$ is used.

Rigid Rotation of a Cosine-hill in Two Dimensions(Rotating Puff)

The setup conditions are the same as in the previous problem of two-dimensional cosine-hill advection except that the velocity field is rotational with respect to the center of the domain (i.e., $u_1 = -x_2$ and $u_2 = x_1$), and all boundaries are of Dirichlet type and homogeneous. The problem was run for 200 time steps during which period the hill should perform one complete rigid body rotation.

Figures 2.4.3, 2.4.6, 2.4.7, and 2.4.8 show the results for different weighting functions and various forms of $C_{2\tau}$.

For the SUPG formulation the form $C_{2\tau} = C_{\Delta t}$ is apparently superior in terms of peak amplitude which drops less than 2% after 200 steps. For $C_{2\tau} = 2/\sqrt{15} + (1 - 2/\sqrt{15}) C_{\Delta t}$ form, the peak amplitude drop is less than 5% for the same trailing wave amplitude (<2%).

For the SW formulation, the forms $C_{2\tau} = C_{\Delta\tau}$ and $C_{2\tau} = 1/4 + (1 - 1/4) C^4_{\Delta t}$ give comparable results(the peak amplitude drop is only 2% and trailing wave amplitude is less than 2% after 200 steps). However, $C_{2\tau} = 1$ fails totally for this problem, which

is not surprising in view of the one-dimensional problem results.

For the TW formulation, the results are comparable to those of the SW formulation except that the form $C_{2\tau} = 1$ does not fail totally; however, the latter form produces leading waves with an amplitude of 9.5% which is quite unacceptable.

CHAPTER 3

APPLICATION TO FLOW FIELD SIMULATION BY VORTICITY-STREAM FUNCTION APPROACH

Flow field simulations for two-dimensional incompressible flows are generally based on either the primitive variable approach or on the vorticity-stream function approach. By using the vorticity-stream function formulation, the number of unknowns and transient equations are reduced, simplifying the problem for computational purposes. Since the governing equations involve transient convection- diffusion terms, the Petrov-Galerkin schemes developed in Chapter 2 were used for this formulation.

3.1 VORTICITY-STREAM FUNCTION FORMULATION

The fundamental equations for two-dimensional, incompressible flow of a Newtonian fluid with no body forces, and constant properties are the two momentum equations (Navier-Stokes) and the continuity equation [15],

$$\partial u/\partial t + u\,\partial u/\partial x + v\,\partial u/\partial y = -1/\rho\,\partial P/\partial x + \nu\,(\partial^2 u/\partial x^2 + \partial^2 u/\partial y^2) \qquad (3.1.1)$$

$$\partial v/\partial t + u\,\partial v/\partial x + v\,\partial v/\partial y = -1/\rho\,\partial P/\partial y + \nu\,(\partial^2 v/\partial x^2 + \partial^2 v/\partial y^2) \qquad (3.1.2)$$

$$\partial u/\partial x + \partial v/\partial y = 0 \qquad (3.1.3)$$

These equations are in the **primitive variable** form involving velocity components, u, v and pressure P, and the fluid properties of mass density, ρ, and kinematic viscosity, ν. The equations have been written in an Eulerian frame of reference and although it is possible to obtain numerical solutions from these equations[16], they can be further simplified both in terms of the number of dependent variables , and the number of transport equations being solved . This simplification leads to the **vorticity-stream function** formulation which has been used successfully for numerical simulations. By appropriate vector and algebraic operations on eqs.(3.1.1), (3.1.2), and (3.1.3), and introduction of vorticity and stream function as the new variables, the above three equations reduce to the following equations:

Vorticity Transport Equation

$$\omega_{,t} + \mathbf{u}\bullet\nabla\omega = \nu\,\nabla^2\omega \qquad \text{on } \Omega \tag{3.1.4}$$

where ω is the vorticity, and $\mathbf{u}$ is the velocity vector.

The boundary Γ is assumed to have the following decomposition ,

$$\Gamma = \overline{\Gamma_{\tilde{g}} \cup \Gamma_{\tilde{h}} \cup \Gamma_G} \tag{3.1.5}$$

$$\varnothing = \Gamma_{\tilde{g}} \cap \Gamma_{\tilde{h}}\,,\ \varnothing = \Gamma_{\tilde{g}} \cap \Gamma_G\,,\ \varnothing = \Gamma_G \cap \Gamma_{\tilde{h}} \tag{3.1.6}$$

Hence,

$$\omega(\mathbf{x}) = \tilde{g}(\mathbf{x}) \qquad \forall\ \mathbf{x} \in \Gamma_{\tilde{g}} \tag{3.1.7}$$

$$\nu\,\mathbf{n}(\mathbf{x})\bullet\nabla\omega(\mathbf{x}) = \tilde{h}(\mathbf{x}) \qquad \forall\ \mathbf{x} \in \Gamma_{\tilde{h}} \tag{3.1.8}$$

Nothing can be specified about the vorticity on the no-slip boundary, Γ_G . Here $\mathbf{n}$ is the unit normal vector to the boundary, and $\tilde{g}$ and $\tilde{h}$ are prescribed functions.

The initial condition is

$$\omega(\mathbf{x},0) = \omega_0(\mathbf{x}) \qquad \mathbf{x} \in \Omega \tag{3.1.9}$$

Remark

Vorticity is defined as $\nabla \times \mathbf{u}$, a vector quantity. In two dimensions it reduces to a single component and can be treated as a scalar.

Poisson's Equation for the Stream Function

$$\nabla^2\Psi + \omega = 0 \qquad \text{on } \Omega \tag{3.1.10}$$

where Ψ is the stream function.

The boundary Γ is assumed to have the following decomposition,

$$\Gamma = \overline{\Gamma_g \cup \Gamma_h \cup \Gamma_G} \tag{3.1.11}$$

$$\varnothing = \Gamma_g \cap \Gamma_h\,,\ \varnothing = \Gamma_g \cap \Gamma_G\,,\ \varnothing = \Gamma_G \cap \Gamma_h \tag{3.1.12}$$

Hence,

$$\Psi(\mathbf{x}) = g(\mathbf{x}) \qquad \forall\ \mathbf{x} \in \Gamma_g \tag{3.1.13}$$

$$\mathbf{n}\bullet\nabla\Psi(\mathbf{x}) = h(\mathbf{x}) \qquad \forall\ \mathbf{x} \in \Gamma_h \tag{3.1.14}$$

$$\left.\begin{aligned}\Psi(\mathbf{x}) &= G(\mathbf{x})\\ \mathbf{n}\bullet\nabla\Psi(\mathbf{x}) &= H(\mathbf{x})\end{aligned}\right\} \quad \forall\ \mathbf{x} \in \Gamma_G \tag{3.1.15}$$

Remark

The stream function Ψ is defined such that $u = \partial\Psi/\partial y$ and $v = -\partial\Psi/\partial x$. Thus in eq.(3.1.15), H is the wall velocity parallel to the boundary Γ_G.

It is required to find $\omega = \omega(x,t)$ and $\Psi = \Psi(x,t)$ for the two coupled partial differential equations.

The flow is thus governed by the nonlinear vorticity equation, which is parabolic in time, and the elliptic Poisson equation for the stream function. For steady state solutions, which are of interest in many cases, the temporal derivative can be eliminated. However, interestingly, most numerical studies concerning steady state flows are based on the time-dependent equations, the steady state solution being obtained as an asymptotic limit of the unsteady state equation. This procedure allows the treatment of steady flows as parabolic in time, so that the solution marches in time to the steady state result. Frequently, the elliptic stream function equation is also treated as a time-dependent problem, with the steady state solution obtained for large time steps[25].

It is also worth noting that the vorticity transport equation serves as a model for many other transfer processes and the techniques used to solve it can be extended to application for processes including compressible flow.

3.2 BOUNDARY CONDITIONS

On no-slip boundaries both components of the velocity vector are specified. Hence it is necessary to specify boundary conditions for vorticity which are consistent with the stream function boundary conditions. Figure 3.2.1 shows the wall details at a boundary. If Ψ is expanded by a Taylor series out from a wall which is parallel to x-direction and where the values are denoted by Ψ_1, we get

$$\Psi_2 = \Psi_1 + (\partial\Psi/\partial y)_1 \Delta y + 1/2(\partial^2\Psi/\partial y^2)_1 \Delta y^2 + 1/6(\partial^3\Psi/\partial y^3)_1 \Delta y^3 + O[(\Delta y)^4] \quad (3.2.1)$$

From the no-slip condition specified at the wall in eq.(3.1.15), $(\partial\Psi/\partial y)_1 = H$, and $\partial v/\partial x = 0$.

Also $\partial u/\partial y = \partial^2\Psi/\partial y^2$. Thus for a wall moving along x direction with velocity H, the vorticity is

$$-\omega_1 = \partial u/\partial y - \partial v/\partial x = (2/h^2)(\Psi_2 - \Psi_1 - H\ h) + O[h] , \quad (3.2.2)$$

where h is the normal distance from the wall node to the adjacent node. Higher order forms have also been implemented though they tend to cause instability at high Reynolds number[26]. For stationary walls, eq.(3.2.2) reduces to

$$\omega_1 = \partial u/\partial y - \partial v/\partial x = (2/h^2)(\Psi_2 - \Psi_1) + O[h] \quad (3.2.3)$$

Remarks

(1) On no-slip boundaries the boundary value of the vorticity depends on the stream function values and thus are time-dependent.

(2) The above derivation is based on element boundaries normal to the no-slip boundary. This restricts the type of elements which can be used adjacent to the boundaries. The boundary conditions on vorticity can be imposed in a more consistent way within the finite-element context by a proper weak formulation of the problem. We were reminded of this by Glowinski[27].

(3) On outflow boundaries, a homogeneous Neumann boundary condition is usually specified for ω and Ψ. Such a "traction-free" boundary condition, although suitable for Navier-Stokes equations, is not the best one for the vorticity-stream function formulation. A more appropriate "absorbing" boundary condition has been proposed by Glowinski[28].

3.3 FINITE-ELEMENT FORMULATION

Consider a discretization of Ω into element subdomains Ω^e, e = 1,2,..., n_{el} , where n_{el} is the number of elements. Let Γ^e denote the boundary of $\bar{\Omega}^e$. We assume

$$\bar{\Omega} = \bigcup_{e=1}^{n_{el}} \bar{\Omega}^e \tag{3.3.1}$$

$$\varnothing = \bigcap_{e=1}^{n_{el}} \Omega^e \tag{3.3.2}$$

The interior boundary is defined as

$$\Gamma_{int} = \bigcup_{e=1}^{n_{el}} \Gamma^e - \Gamma \tag{3.3.3}$$

Weak form of the Vorticity Transport Equation

Let $\tilde{V}$ and $\tilde{S}$ denote the finite-dimensional variational and trial solution spaces such that

$$\tilde{V} = \{ w \mid w \in H^1(\Omega), w(x) = 0 \ \forall \ x \in \Gamma_{\tilde{g}}, \Gamma_G \} \tag{3.3.4}$$

$$\tilde{S} = \{ \omega \mid \omega \in H^1(\Omega), \omega(x) = \tilde{g}(x) \ \forall \ x \in \Gamma_{\tilde{g}}, \quad \omega(x) = \omega_G(x) \forall \ x \in \Gamma_G \} \tag{3.3.5}$$

where ω_G represents the value attained by vorticity on boundary Γ_G.

The variational form of eq. (3.1.4) and the associated initial condition in eq.(3.1.9) are

$$\int_\Omega \{ w\omega_{,t} + wu\bullet\nabla w + \nu \nabla w \bullet \nabla\omega \} d\Omega + \sum_{e=1}^{n_{el}} \int_{\Omega^e} p \{ \omega_{,t} + u\bullet\nabla\omega - \nu \nabla^2 \omega \} d\Omega = \int_{\Gamma_{\tilde{h}}} w\tilde{h} \, d\Gamma \, d\Gamma \quad \forall w \in \tilde{V} \tag{3.3.6}$$

$$\int_\Omega w(\omega - \omega_0) d\Omega = 0 \quad \forall w \in \tilde{V} \tag{3.3.7}$$

where p is a C^{-1} perturbation to the weighing function w, i.e., the modified weighting function is given by

$$\tilde{w} = w + p \qquad (3.3.8)$$

The Euler-Lagrange form of the above equation can be derived and is similiar to the one derived in Chapter 2, i.e.,

$$\sum_{e=1}^{n_{el}} \int_{\Omega^e} \tilde{w}\{\omega_{,t} + \mathbf{u}\bullet\nabla\omega - \nu\nabla^2\omega\}\, d\Omega + \int_{\Gamma_{\tilde{h}}} w\{\nu\, \mathbf{n}\bullet\nabla\omega - \tilde{h}\}\, d\Gamma + \int_{\Gamma_{int}} w\,[\nu\, \mathbf{n}\bullet\nabla\omega]\, d\Omega = 0 \qquad (3.3.9)$$

where [ ] is the "jump" operator.

Weak Form of the Poisson's Equation

Let V and S denote the finite dimensional variational and trial solution spaces such that

$$V = \{w \mid w \in H^1(\Omega),\ w(x) = 0\ \forall\ x \in \Gamma_g,\ \Gamma_G\} \qquad (3.3.10)$$

$$S = \{\Psi \mid \Psi \in H^1(\Omega),\ \Psi(x) = g(x)\ \forall\ x \in \Gamma_g,\ \Psi(x) = G(x)\ \forall\ x \in \Gamma_G\} \qquad (3.3.11)$$

The variational form of eq. (3.1.10) is

$$\int_{\Omega} \nabla w\bullet\nabla\Psi\, d\Omega = \int_{\Omega} w\omega\, d\Omega + \int_{\Gamma_h} wh\, d\Gamma \qquad \forall\ w \in V \qquad (3.3.12)$$

where w is the weighting function leading to Galerkin formulation.

3.4 MATRIX FORM OF THE DISCRETIZED EQUATIONS AND THE ALGORITHM

A consistent finite-element spatial discretization of eqs. (3.3.8) and (3.3.12) leads to the following set of ordinary differential equations:

$$\tilde{\mathbf{M}}\,\dot{\mathbf{d}} + \tilde{\mathbf{K}}\,\mathbf{d} = \tilde{\mathbf{F}} \tag{3.4.1}$$

$$\mathbf{K}\Psi = \mathbf{F} - \mathbf{M}\,\mathbf{d} \tag{3.4.2}$$

where $\tilde{\mathbf{M}}$ and $\mathbf{M}$ are the mass matrices, $\tilde{\mathbf{K}}$ and $\mathbf{K}$ stiffness matrices, $\tilde{\mathbf{F}}$ and $\mathbf{F}$ the generalized force vectors, $\mathbf{d}$ and $\dot{\mathbf{d}}$ the vorticity and its temporal derivative at the nodes, and Ψ the stream function at the nodes. Note that the mass matrices in eqs.(3.4.1) and (3.4.2) are not identical since the weighting functions used for the equations come from different spaces.

Predictor/Multi-Corrector Algorithm

The algorithm used to solve eqs. (3.4.1) and (3.4.2) is a modified version of the Predictor/Multi-corrector algorithm used by Hughes and Brooks[20] and is shown below:

(1) Predictors

$$\mathbf{d}_{n+1}^{(0)} = \mathbf{d}_n + \Delta t(1-\gamma)\,\dot{\mathbf{d}}_n$$

$$\dot{\mathbf{d}}_{n+1}^{(0)} = 0$$

Set i = 0 and go to step (2a) or (2b)

Predict the vorticity at next time step based on the current step.

(2a) Solution alternative I

$$\mathbf{C}\Psi_{n+1}^{(i)} = \mathop{\mathbf{A}}_{e}\{\,\mathbf{f}^{e} - \mathbf{m}^{e}\,(\mathbf{d}_{n+1}^{(i)})^{e}\,\}$$ Stream function calculation

$$(\mathbf{d}_G)_{n+1}^{(i)} = \mathbf{L}\,\Psi_{n+1}^{(i)}$$ Update vorticity boundary condition

(5) Convergence check

If the vorticity equation residue norm is within the tolerable limit, then increment n by 1 and go to step (1). Else increment i by 1 and go to step (2a) or (2b).

If the vorticity has converged, then go to next time step else keep correcting it.

Remarks

(1) Δt is the time step chosen and γ is the Euler parameter chosen between 0 and 1, while subscript n represents time levels and superscript i represents the iteration level. Symbol **A** represents assembly over the elements $e = 1,2,..n_{el}$.

(2) $\mathbf{M}^*$ is defined as follows:

$$\mathbf{M}^* = \tilde{\mathbf{M}} + \Delta t\, \gamma\, \tilde{\mathbf{K}} \quad \textbf{for implicit solutions}$$

$$\mathbf{M}^* = \mathbf{M}^L \quad \textbf{for explicit solutions}$$

where $\mathbf{M}^L$ is the lumped mass matrix.

(3) For step (2a), if N is not large enough the solution diverges. From practical experience it is seen that convergence is slow with step (2a) and hence step (2b) is used .

(4) Weighting functions developed in Chapter 2 are used for the vorticity transport equation since they have good stability/accuracy characteristics.

(5) Matrix **L** is obtained from eq. (3.2.3) which relates the wall vorticity($\mathbf{d}_G$) with the stream function.

(6) Since matrices $\tilde{\mathbf{M}}$ and $\tilde{\mathbf{K}}$ for the vorticity equations depend on the spatial and temporal discretization besides the flow field they are reformed every iteration within each time step. However matrices **M** and **K** for the stream function are formed only once in the first iteration of the first time step since the weighting function depends only on the spatial discretization.

3.5 NUMERICAL TEST CASES

Flow Past Step

This is a relatively stringent problem for testing the algorithm because of sharp boundaries which result in steep gradients of variables. Convergence in this problem is thus not expected to be as good as for problems involving smooth geometries like flow past a cylinder.(The latter case and associated phenomenon of vortex shedding is currently being studied by Glaisner[29], and, results obtained are in strong agreement with those obtained by Fornberg[30], Smith and Brebbia[31], and Brooks and Hughes[32]). Figure 3.5.1 gives a problem description and the appropriate boundary conditions used. This problem was solved using a crude(210 elements) mesh and a fine mesh (804 elements) for Re = 200 . The mesh was not refined near the walls in order to study the effects of a uniform mesh.

The solutions obtained for Re = 200 cases are shown in Figures 3.5.2 and 3.5.3 . Results obtained compare quite well with those obtained by Hughes et al.[32] using a penalty formulation. However, in our computations the Dirichlet boundary values are allowed to reach the full values after 10 time steps. Thus solutions obtained should be compared with caution.

The following observations can be made:

(a) As the mesh is refined, the time step has to be reduced even for the implicit calculation because of the evolving vorticity boundary condition on the walls, which is proportional to $1/h^2$. This is a limitation because an accurate solution obtained by a fine mesh would take more time steps to compute.

(b) In general, the viscous effects dominate at the walls resulting in high wall vorticity. Away from the walls the flow dominates and convects away the vorticity. This suggests mesh refinement near the walls.

(c) For Re = 200, a fine mesh with low time-step results in a region of recirculation downstream of the step which develops further in time. This is in agreement with the solution obtained by Hughes, et al.[32].

Driven Cavity Problem

This, like the step problem is a stringent test for the algorithm and is described in Figure 3.5.4 with the appropriate boundary conditions. A uniform mesh of 20×20 elements was chosen and the solutions were obtained for Re = 100, 400, and 800. In all the cases, the time step was fixed at 0.2 and the problem was run for 40 time steps. Transient results

3.5 NUMERICAL TEST CASES

Flow Past Step

This is a relatively stringent problem for testing the algorithm because of sharp boundaries which result in steep gradients of variables. Convergence in this problem is thus not expected to be as good as for problems involving smooth geometries like flow past a cylinder.(The latter case and associated phenomenon of vortex shedding is currently being studied by Glaisner[29], and, results obtained are in strong agreement with those obtained by Fornberg[30], Smith and Brebbia[31], and Brooks and Hughes[32]). Figure 3.5.1 gives a problem description and the appropriate boundary conditions used. This problem was solved using a crude(210 elements) mesh and a fine mesh (804 elements) for Re = 200 . The mesh was not refined near the walls in order to study the effects of a uniform mesh.

The solutions obtained for Re = 200 cases are shown in Figures 3.5.2 and 3.5.3 . Results obtained compare quite well with those obtained by Hughes et al.[32] using a penalty formulation. However, in our computations the Dirichlet boundary values are allowed to reach the full values after 10 time steps. Thus solutions obtained should be compared with caution.

The following observations can be made:

(a) As the mesh is refined, the time step has to be reduced even for the implicit calculation because of the evolving vorticity boundary condition on the walls, which is proportional to $1/h^2$. This is a limitation because an accurate solution obtained by a fine mesh would take more time steps to compute.

(b) In general, the viscous effects dominate at the walls resulting in high wall vorticity. Away from the walls the flow dominates and convects away the vorticity. This suggests mesh refinement near the walls.

(c) For Re = 200, a fine mesh with low time-step results in a region of recirculation downstream of the step which develops further in time. This is in agreement with the solution obtained by Hughes, et al.[32].

Driven Cavity Problem

This, like the step problem is a stringent test for the algorithm and is described in Figure 3.5.4 with the appropriate boundary conditions. A uniform mesh of 20×20 elements was chosen and the solutions were obtained for Re = 100, 400, and 800. In all the cases, the time step was fixed at 0.2 and the problem was run for 40 time steps. Transient results

are shown for Re = 100 in Figure 3.5.5, andthe last step results for Re = 400, and 800, in Figures 3.5.6 and 3.5.7. The solution can be compared with Hughes et al.[32] who used 20×21 elements . Figure 3.5.8 shows the results obtained by Hughes et al.[32].

The following observations can be made:

(a) Initially, the vorticity is generated by the top moving wall and is transported to the adjacent walls by the flow developed. However, as a consequence of this generation and transportation of vorticity, a circulating flow develops in the cavity. At steady state, the vorticity diffusion is balanced by the vorticity convected and recirculated.

(b) As a result of the circulating flow in the cavity, two small regions of recirculation develop on the lower corners.These grow with Reynolds number until Re = 800.

(c) In general, agreement is good for low Reynolds number with solution obtained by Hughes[32]. Note that both vorticity and stream function are practically constant after 40 steps for low Reynolds number.

CHAPTER 4

APPLICATION TO SIMULATION OF ELECTROPHORESIS SEPARATION PHENOMENA

Before actual simulation of any process it becomes necessary to identify the governing equations (PDE's, ODE's, algebraic equations, etc.) based on certain basic laws (mass, momentum, energy, charge balance, etc.) and also to understand the limitations/assumptions made in arriving at the equations. Electrophoresis simulation also requires the following:

- Development of special techniques to solve problems in **convection dominated flows.** Successful separation of particles is based on large differences in mobilities and low diffusion rates of individual species. Evidently, as explained in Chapter 1, convection dominated flows need **Petrov-Galerkin formulations** which have been developed in Chapter 2. Thus the schemes developed in Chapter 2 have been used in electrophoresis simulation.

- Prior knowledge of the **external flow field** (i.e., the velocity of the solvent in which the charged particles have been dissolved). In Chapter 3, a method has been developed to model the flow field based on the **vorticity-stream function formulation.**This formulation can be used to solve for the external flow field. However, it must be noted that in most electrophoretic separations the external velocity is kept at zero to avoid remixing of the separating species.

4.1 CLASSIFICATION OF SEPARATION TECHNIQUES

Although there are several classification of separation techniques the three distinct categories studied by us are listed below:

zone electrophoresis (ZE)
moving boundary electrophoresis (MBE)
isotachophoresis (ITP)

The above methods differ in the **applied initial condition** which leads to a different separation mode.

CHAPTER 4

APPLICATION TO SIMULATION OF ELECTROPHORESIS SEPARATION PHENOMENA

Before actual simulation of any process it becomes necessary to identify the governing equations (PDE's, ODE's, algebraic equations, etc.) based on certain basic laws (mass, momentum, energy, charge balance, etc.) and also to understand the limitations/assumptions made in arriving at the equations. Electrophoresis simulation also requires the following:

- Development of special techniques to solve problems in **convection dominated flows.** Successful separation of particles is based on large differences in mobilities and low diffusion rates of individual species. Evidently, as explained in Chapter 1, convection dominated flows need **Petrov-Galerkin formulations** which have been developed in Chapter 2. Thus the schemes developed in Chapter 2 have been used in electrophoresis simulation.

- Prior knowledge of the **external flow field** (i.e., the velocity of the solvent in which the charged particles have been dissolved). In Chapter 3, a method has been developed to model the flow field based on the **vorticity-stream function formulation.**This formulation can be used to solve for the external flow field. However, it must be noted that in most electrophoretic separations the external velocity is kept at zero to avoid remixing of the separating species.

4.1 CLASSIFICATION OF SEPARATION TECHNIQUES

Although there are several classification of separation techniques the three distinct categories studied by us are listed below:

zone electrophoresis (ZE)
moving boundary electrophoresis (MBE)
isotachophoresis (ITP)

The above methods differ in the **applied initial condition** which leads to a different separation mode.

In ZE, the whole separation column is filled with a single basic electrolyte system with a specific conductivity. The mixture of substances to be separated is injected at a certain location in the column and the passage of current mobilizes the substances at different rates and thus zones are created. Figure 4.1.1 illustrates this process schematically. The shape of the individual zones are influenced by the potential gradient. If the electrolyte is such that its conductivity is not affected by the substances to be separated, then the potential gradient remains constant and it is the most common type of ZE (this is the case simulated). In some cases the conductivity does change and the potential gradient is not a constant. Thus, when the species enters a region of high potential gradient (absolute) it speeds up, leading to a spreading of the front boundary . When it exits , the boundary sharpens. The opposite is true for the back boundary. A similiar deduction can be drawn for species entering or exiting low potential gradient(absolute) regions.

Some characteristic features of ZE are the following:

(i) particles with either sign can be separated.

(ii) concentrations decrease permanently.

(iii) zone boundaries can sharpen, or spread.

(iv) zone velocities are different for different species.

MBE resembles ZE closely and is characterized by separation of the column into three parts. Both sides are filled with the same basic electrolyte; the middle contains the mixture to be separated. Since the middle width is comparable to the column length, complete separation into individual zones cannot be accomplished. In yet another variation of this method, the compartment may be divided into only two regions - one containing the basic electrolyte and the other containing both the electrolyte and the mixture to be separated. Figure 4.1.2 shows the latter mode schematically. In the simulation, both species A and B are positively charged with A having a higher mobility. Therefore the leading zone contains only A followed by a zone containing both A and B. Only species A can be fully separated.

Some characteristic features of this method are the following:

(i) practically used to separate particles of one sign.

(ii) only one species is fully separated, others are mixed.

(iii) boundaries may sharpen or spread.

(iv) zone widths increase or decrease permanently.

(v) zone velocities are different for different substances but remain constant.

ITP is characterized by the fact that a cation/anion mixture cannot be separated by this method. The separation column is divided into three unequal parts. One part is filled with a *leader* electrolyte, followed by the mixture to be separated, and finally, the *terminating* electrolyte. If the mixture has anions to be separated, then the leader anions must have the highest mobility and the terminator the lowest in the column. On passing current, the mixture separates **completely** into individual substances with the anions arranged in the order of mobilities. The leader is in the front followed by the species to be separated, and finally the terminator. After steady state has been achieved, all the boundaries move with the same constant speed. Figure 4.1.3 depicts this method schematically.

Some characteristic traits of this method are the following:

(i) complete separation of species is achieved after steady state is reached.
(ii) concentrations can increase or decrease during transient phase.
(iii) concentrations are constant after steady state achievement.
(iv) zone widths increase or decrease during transient phase.
(v) zone widths are constant after steady state achievement.
(vi) zone velocities are same and constant after steady state achievement.

The above 3 separation techniques are used in one-dimensional separation. In **two dimensions**, there is a different classification,

zone electrophoresis - similiar to one-dimensional ZE
cross electrophoresis - oppositely charged species are made to cross each other so that a chemical interaction produces a new species.
diagonal electrophoresis - basically ZE along first direction followed by a chemical treatment of separated species, followed by ZE along second direction.
cross flow-through electrophoresis - an external bulk velocity is applied along one direction and the electric current perpendicular to it. Separation is achieved continuously along each electrode.

Remark Although there are several other criteria used to classify separation processes (amount separated, high/low voltage, continuous/batch etc.), the above classification methods are more amenable to mathematical modelling since they provide definite information regarding domain, initial concentration profiles, etc.

4.2 ASSUMPTIONS

The governing equations are derived with the following assumptions:

Fully ionized species - while charged or uncharged species can be easily handled by the model, the charged species are usually in equilibrium with their neutral counterpart. This represents a chemical reaction which complicates the model and is currently not being studied.

Individual species do not affect each other - the basic assumption made in deriving the flux equations is that flux of one species does not depend on the other. This is accurate only in dilute solutions.

Incompressible flow - since, in electrophoresis, one is dealing with common liquids at low velocities, this assumption is valid. However, if a chemical reaction changes the densities spatially and temporally, this assumption would have to be scrutinized.

Electrical heating effects negligible - the passage of an electric current induces heating of the liquid column which can in turn, induce thermal convection currents and remix the separating species. For this reason the separation column cross-section is kept low.

Electro-osmotic flow negligible - this flow is generated when an electric field is applied to the system and the charge in the diffuse part of double layer of the wall moves to the oppositely charged electrode. This drags particles close to the double layer along with it thus producing a net flow.

Electroneutrality - i.e., the sum total of all charge at a point (at the continuum level) is zero. Most fluids satisfy this property except in a region very close (100 Angstroms) to the electrodes.

4.3 GOVERNING EQUATIONS

The flux of each dissolved species is given by[33]

$$N_i = -z_i u_i F c_i \nabla\Phi - D_i \nabla c_i + c_i v \qquad (4.3.1)$$

electromigratory flux; diffusive flux; convective flux

where

c_i = unknown concentration of the i^{th} species

Φ = unknown electric potential

z_i = signed valence of the i^{th} species

u_i = mobility of the i^{th} species

F = Faraday's constant

v = bulk fluid velocity

D_i = diffusion coefficient for the i^{th} species

R_i = rate of generation of the i^{th} species

A material balance yields

$$\frac{\partial c_i}{\partial t} = -\nabla\bullet N_i + R_i \qquad (4.3.2)$$

Substituting eqs. (4.3.1) in (4.3.2) and using the incompressible flow assumption ($\nabla\bullet v = 0$), we get

$$\frac{\partial c_i}{\partial t} + v\bullet\nabla c_i = z_i u_i F \nabla\bullet(c_i \nabla \Phi) + \nabla\bullet(D_i \nabla c_i) + R_i \qquad (4.3.3)$$

or on simplification,

$$\frac{\partial c_i}{\partial t} + (v - z_i u_i F \nabla\Phi)\bullet\nabla c_i = z_i u_i F c_i \nabla^2\Phi + D_i \nabla^2 c_i + R_i \qquad (4.3.4)$$

Moreover the current density is given by

$$\mathbf{i} = F \sum_i z_i N_i \tag{4.3.5}$$

On multiplying eq.(4.3. 2) with $z_i F$ and summing over all species, we get

$$-\frac{\partial}{\partial t} F \sum_i z_i c_i = -\nabla \bullet F \sum_i z_i N_i + F \sum_i z_i R_i \tag{4.3.6}$$

Using the principle of electroneutrality and charge conservation ($\sum_i z_i R_i = 0$ and $\sum_i z_i c_i = 0$ respectively) gives

$$\mathbf{i} = -F^2 \nabla\Phi \sum_i z_i^2 u_i c_i - F \sum_i z_i D_i \nabla c_i \tag{4.3.7}$$

$$\nabla \bullet \mathbf{i} = 0 \tag{4.3.8}$$

Further assuming a constant current density, we see that

$$-\nabla \Phi = \mathbf{i}/\kappa + F/k \sum_i z_i D_i \nabla c_i \tag{4.3.9}$$

If electroneutrality is imposed explicitly, we get

$$-\nabla \Phi = \mathbf{i}/\kappa + F/\kappa \sum_{i \neq n} z_i (D_i - D_n) \nabla c_i \tag{4.3.10}$$

where

$$\kappa = F^2 \sum_i z_i^2 u_i c_i \tag{4.3.11}$$

If electroneutrality is imposed explicitly, we have

$$\kappa = F^2 \sum_{i \neq n} z_i c_i (z_i u_i - z_n u_n) \tag{4.3.12}$$

Thus the equations to be solved are the following :

$$\frac{\partial c_i}{\partial t} + (v - z_i u_i F \nabla\Phi)\bullet\nabla c_i = z_i u_i F c_i \nabla^2\Phi + D_i \nabla^2 c_i + R_i \qquad (4.3.13)$$

where the electric potential is evaluated from

$$-\nabla\Phi = i/\kappa + F/\kappa \sum_{i\neq n} z_i(D_i - D_n) \nabla c_i \qquad (4.3.14)$$

and the conductivity from

$$\kappa = F^2 \sum_{i\neq n} z_i c_i (z_i u_i - z_n u_n) \qquad (4.3.15)$$

Remarks

The above eqs. (4.3.13), (4.3.41), and (4.3.15) are thus used to evaluate the concentrations of n-1 species and the n^{th} species concentration can be evaluated from electroneutrality, i.e.,

$$z_n c_n = \sum_{i\neq n} z_i c_i \qquad (4.3.16)$$

4.4 STRONG FORM OF THE PROBLEM

The strong form of the problem based on the equations derived in previous section can now be written as follows (similar to the ones derived in the previous chapters except that there are n unknown species concentrations to be evaluated at a given node):

$$\frac{\partial c_i}{\partial t} + (v - z_i u_i F \nabla\Phi)\bullet\nabla c_i = z_i u_i F c_i \nabla^2\Phi + D_i \nabla^2 c_i + R_i$$

$$\text{on } \Omega \quad \text{and } i = 1,2,..,n-1 \qquad (4.4.1)$$

where

$$-\nabla\Phi = \mathbf{i}/\kappa + F/\kappa \sum_{i\neq n} z_i(D_i-D_n)\nabla c_i \qquad (4.4.2)$$

and

$$\kappa = F^2 \sum_{i\neq n} z_i c_i (z_i u_i - z_n u_n) \qquad (4.4.3)$$

The boundary Γ of the domain Ω, is assumed to have the following decomposition,

$$\Gamma = \overline{\Gamma_{g}i \cup \Gamma_{h}i} \qquad (4.4.4)$$

$$\varnothing = \Gamma_{g}i \cap \Gamma_{h}i \qquad (4.4.5)$$

where $\Gamma_{g}i$ and $\Gamma_{h}i$ represent the Dirichlet and Neumann type boundaries, respectively. Hence,

$$c_i(\mathbf{x},t) = g_i(\mathbf{x},t) \qquad \forall\, \mathbf{x} \in \Gamma_{g}i, t \in]0,T[\text{ and } i = 1,2,\ldots n-1 \qquad (4.4.6)$$

$$\mathbf{n}(\mathbf{x})\bullet\nabla c_i(\mathbf{x},t) = h_i(\mathbf{x},t) \quad \forall\, \mathbf{x} \in \Gamma_{h}i, t \in]0,T[\text{ and } i = 1,2,\ldots n-1 \qquad (4.4.7)$$

where $\mathbf{n}$ is the unit normal vector to the boundary, and g_i and h_i are prescribed functions.

The initial condition is

$$c_i(\mathbf{x},0) = c_{i0}(\mathbf{x}) \quad \mathbf{x} \in \Omega, i = 1,2,\ldots n-1 \qquad (4.4.8)$$

where c_{i0} is a given function.The initial/boundary-value problem is to find $c_i = c_i(\mathbf{x},t)$ which satisfies eqs. (4.4.1), and (4.4.6)-(4.4.8). It is assumed that the current density is known, i.e., $\mathbf{i} = \mathbf{i}(\mathbf{x},t)$ is specified.

4.5 FINITE-ELEMENT FORMULATION AND THE ALGORITHM

Adopting a procedure similiar to one in Section 2.2, a consistent finite-element spatial discretization of eq(4.4.1) leads to the following set of ordinary differential equations:

$$\mathbf{M}\,\dot{\mathbf{d}} + \mathbf{K}\,\mathbf{d} = \mathbf{F} \qquad (4.5.1)$$

where all the symbols have their usual meaning.

However solving this set of ODE's is different because the convection velocity induced due to the electric field has to be evaluated. In other words, these ODE's can be solved only if the potential gradient is known at each time step.

Thus the scheme used to solve this system is similiar to the Predictor/Multi-corrector algorithm used by Hughes and Brooks[20], except that several corrections are required to evaluate concentrations and the potential gradient.

The potential gradient is evaluated at nodes based on a 2^{nd} order finite-difference scheme, i.e., in evaluating $\nabla\Phi$ from the expression,

$$-\nabla\Phi = \mathbf{i}/\kappa + F/\kappa \sum_{i \neq n} z_i(D_i - D_n)\,\nabla c_i \qquad (4.5.2)$$

a 2^{nd} order finite-difference scheme based on nodal concentrations is used to approximate the ∇c_i term.

Remarks

(1) Since a finite-difference scheme is used to evaluate derivatives based on nodal concentrations, it restricts the usage to elements with boundaries parallel to the X and Y-axis.

(2) Depending on the spatial position and time, the flow for a particular species might be convection dominated and for another species diffusion dominated. This situation is possible because the convection term for each species is governed by the potential gradient (common to all species and a function of

space and time), and its particular valence and mobility.

(3) A Courant number based on "electro-migration" can be defined which will be useful in stability/accuracy analysis,

$$(EC_{\Delta t})_i = \frac{(F z_i u_i \nabla\Phi)\,\Delta t}{h} \qquad i = 1,2,....n-1 \qquad (4.5.3)$$

Here $(EC_{\Delta t})_i$ is the "Electro-migrative Courant Number" for the i^{th} species based on time step Δt, and element length h, along electromigation direction.

4.6 NUMERICAL TEST CASES

Although it is not possible to predict beforehand the course of separation process, in 1897 Kohlrausch established a general principle for understanding the general features which can be stated as follows:

" The passage of an electric current through an electrolyte system causes changes only where the system is nonhomogeneous."

Consequently,

(i) the passage of electric current through a homogeneous solution leaves the concentrations unchanged.

(ii) the passage of an electric current causes the boundary between two ionic species to advance and either degrade or self-stabilize in time.

(iii) concentration gradients are largely unaffected, but flatten out as a result of diffusion.

A review of numerical simulations indicates a paucity of work done in the field of electrophoresis. The models developed in [34] and [35] are specialized for either MBE or ITP in one-dimensional steady state cases. The general approach to electrophoresis presentedby Bier et al.[36] does explain all methods in one dimension. In two dimensions, surprisingly, no work seems to have been done - this despite the fact that two-dimensional electrophoresis is a dominant method in resolving proteins. The algorithm developed by us has the following advantages:

(i) has good stability and accuracy characteristics as demonstrated in Chapter 2.

(ii) can handle several species.

(iii) can handle external flow fields.
(iv) can handle irregular domains (however, see remark in Section 4.5).

One-dimensional simulations Based on the classification given in Section 4.1, one-dimensional simulations have been done for ZE, MBE, and ITP. The results have been compared with those of Bier et al.[36], and Fidler et al.[34]. However, Bier's simulations take into account chemical dissociation equilibrium which can affect the solution obtained depending on the dilution.

In all the simulations the two species to be separated are denoted by A and B, and the basic electrolyte in which they are introduced consists of P^+ (or L^+ and T^+) and Q^- ions.

Zone Electrophoresis in One Dimension

The initial condition consists of a uniform concentration distribution of P^+ (and Q^-) ions and a cosine-hill for both A^+ and B^- bearing opposite charges.

On the application of an electric field, each species migrates a distance proportional to its mobility and charge. In this way the species separate. The problem was run for 150 time steps ($\Delta t = 0.02$).The temporal evolution of A^+,B^-,P^+, and potential gradient ($\nabla\phi$) are shown in Figure 4.6.1. Broadening of the leading boundaries of A^+ and B^- indicates that the absolute value of $\nabla\phi$ is high off center .This is consistent with the $\nabla\phi$ plots.

Since the potential gradient is a function of the current density, concentrations and concentration gradients, adding the mixture S will disturb the existing uniform potential of the electrolyte. This is seen as a cosine-hill hump in the potential gradient initially. However as the species separate, it attains a much more complicated profile than is shown for this simple case.

On comparing this with the results obtained by Bier et al.[36] there is a similar trend observed except that the species to be separated has a sharpened leading boundary and smeared trailing boundary. This is because in [36] the species is an ampholyte (i.e., its mobility is a function of other species) and the electromigration velocity is thus dependent on the $\nabla\phi$, as well as the variable mobility. This was also simulated by making the mobility of A^+, a variable dependent on P^+ ion concentration in our computation (not shown) .

Moving Boundary Electrophoresis in One Dimension

The initial condition were chosen to compare the result with those of Bier et al.[36]. This initial condition is not the same as shown in Figure 4.1.2. The problem was run for 250

time steps and since B^+ has a higher mobility than A^+, the latter separates out fully as expected. This is to be contrasted with the example shown in Figure 4.1.2 where species A^+ with highest mobility separates out fully. This indicates that the initial condition and particle charge play a significant role in the fate of separation. Moreover, the boundaries can sharpen (self stabilize) or deteriorate (diffuse), as shown for the two boundaries.

The temporal evolution of A^+, B^+, P^+, and $\nabla\phi$ are shown in Figure 4.6.2 at regular intervals of 25 steps. Species A^+ is not affected too much by the current because it has a low mobility and hence, tends to diffuse. Species B^+ on the other hand, shows clearly the effects of electromigration with some initial profile adjustments. P^+ shows a tendency to reach spatial peaks which spread out in time. The potential gradient undergoes changes which are difficult to predict but shows plateaus in regions where concentrations are more or less constant.

These results are in general agreement with those of Bier et al.[36] for the descending arm case. However the comparison is qualitative, based on profiles.

Isotachophoresis in One Dimension

The initial condition for ITP is depicted in Figure 4.6.3. The mixture is introduced between the leader L^+ and terminator T^+ such that

$$U_L > U_A, U_B > U_T$$

Also note that the terminator T^+ is <u>not</u> strictly separated from the mixture which is not in general compliance with the requirements of ITP mentioned in Section 4.1 .

On passing current the species separate out in the order of their mobilities and finally, the separated species move as a single system . This problem was run for 1750 time steps and an intermediate and final condition are shown in Figure 4.6.3. Except for the leader, all other species undergo significant changes in zone width and peak concentrations. Moreover as a result of numerical smearing, the boundaries tend to overlap.

The temporal evolution of A^+, B^+, T^+, L^+, and $\nabla\phi$ are shown in Figure 4.6.4 at regular intervals of 150 steps. For T^+, in the initial stages the concentration levels off to zero. However later it levels off to a positive value signifying approach of a steady state.

Species B^+ follows a complicated evolution with increases, decreases, and plateaus in the concentration levels until it flattens out at steady state.

Species A^+ follows a complicated evolution with increases, decreases, and plateaus in the concentration levels until it flattens out at steady state. However the steady state concentration level is higher than B^+ while the width is less.

The leader L^+ shows relatively little change except for an initial boundary profile adjustment.

The potential gradient follows an initial period of adjustment until the species separate. After steady state is attained it develops local plateaus which correspond to the plateaus of each species.

On comparing this simulation with that of Zidler et al.[34] the following differences emerge:

(i) The initial concentration levels of A^+ and B^+ are not equal in [34].
(ii) Initially, the terminator T^+ is strictly separate from the mixture in [34].

The steady state results as obtained by us are in good agreement with those of Zidler et al.[34] except for the behavior of the terminator which is different because of the above two reasons. Moreover, the results by Bier et al.[36] also indicate that both increasing and decreasing profiles of the terminator are possible depending on the initial concentrations which is consistent with our results.

Two-dimensional simulations As pointed out earlier in this section, there is no result available to compare with in two dimensions. However, in order to test the algorithm and to demonstrate its capability, results for zone and cross (no reaction) electrophoresis have been shown. Although other methods have also been simulated, the results have not been shown here. For both cases the domain was taken as 0.66×1.0 units in the positive XY plane with a mesh of 20×30 square elements. For simplicity, the constant current density was applied in the Y-direction only.

Zone electrophoresis in Two Dimensions

Species A^+ and B^- , bearing opposite charges, are introduced as cosine hills centered at coordinates (0.33,0.5). The basic electrolyte, as usual, is made of P^+ and Q^- ion distributed uniformly (not shown).

The problem was run for 100 time steps and results plotted at steps 0, 50 and 100, in Figure 4.6.5. The profiles along Y-direction are similiar to those attained in the one-dimensional version of ZE. However, both diffusion and electro-migration act in the X-direction. Though diffusion is understandable, electro-migration might appear peculiar because, as stipulated earlier, the current was applied only in the Y-direction.

However, on careful examination of eq. (4.3.11) it becomes obvious that the potential gradient also depends on the concentration gradients which do exist along X-direction. This is confirmed by the nonzero $\partial\phi/\partial x$ which develops in time (not shown).

Cross Electrophoresis in Two Dimensions

Species A^+ is introduced as a cosine-hill centered at coordinates (0.33,0.25) and species B^- centered at (0.33,0.75) so that they cross over in the domain on applying current. This problem was run for 250 time steps and the results are shown at steps 0, 50, and 200 in Figure 4.6.6.

Species A^+ behaves quite normally, displaying the usual broadening and reduction in concentration level. However B^+ shows an increase in concentration which is accounted by the sharp potential gradient change at step 50(It does not affect A^+ because it has not reached there). However this sharpness diffuses later which is consistent with Kauhlraucsh's principle. Moreover, it is apparent that the potential gradient is predominantly controlled by B^+ because it is seen to drift along with the profile of B^+ rather than that of A^+.

CHAPTER 5

CONCLUSIONS

The results from Chapter 2 show that by choosing a proper weighting function and an appropriate form for the algorithmic Courant number, a variety of problems can be solved giving improved results. Choosing the form $C_{2\tau} = 2/\sqrt{15} + (1 - 2/\sqrt{15})\, C_{\Delta t}$ with SUPG and $C_{2t} = 1/4 + (1 - 1/4)\, C_{\Delta t}^4$ form with TW (or SW) gives optimal results for a range of Courant numbers, for one-dimensional problems. For two-dimensional problems, in addition to the above forms of $C_{2\tau}$, the form $C_{2\tau} = C_{\Delta t}$ also performs well. In general, the extension of one-dimensional schemes to multi-dimensions should be done with care. However, the proposed weighting functions perform satisfactorily in multi-dimensions as is clear from the results.

Based on the results obtained, and from the stability and accuracy analysis performed, one can deduce that the proposed transient schemes are versatile, produce wiggle-free solutions, and show minimal damping and a good frequency ratio response.

Numerical test cases run for flow field simulations in Chapter 3, indicate that the vorticity-stream function algorithm behaves quite well at low Reynolds number. However, there is limitation on the time step, which depends on the mesh size and is thus crucial for the stability/accuracy of the solution.

As Reynolds number increases, sharp changes occur in the solution which lead to resolution problems. Though these can be resolved by mesh refinement (which is an extra computational burden), in complex domains it is not possible initially to predict regions of steep gradients.

For high Reynolds number this model is not appropriate because turbulent flows are three-dimensional in nature[37]. Also, resolving the small scale structures would require refinement beyond feasible limits[37].

Moreover, if the pressure is to be determined, the primitive approach, in terms of the velocity and the pressure, is often advantageous. For flow in finite-sized enclosures and flow over arbitrary three-dimensional bodies, this assumption of two-dimensional flow may not be applied and the general three-dimensional circumstance is to be considered. The problem is extremely complicated in that case, and though the vorticity-stream function approach may be extended to this flow, the primitive variable method is often more appropriate.Thus other approaches like penalty formulation, primitive variable approach, etc., should also be tested with the newly developed Petrov-Galerkin

schemes.

The numerical scheme proposed for electrophoresis simulation is capable of simulating ZE, MBE, and ITP in one dimension. The results obtained are in good agreement with those obtained by others. In general, electric current application mobilizes the particles, which in turn, alter the potential gradient distribution. Thus the electromigration velocity will change as a result of the changing potential gradient. In many cases, complicated concentration and potential gradient profiles are achieved which are difficult to predict otherwise.

However, a combination of Petrov-Galerkin finite-element and 2^{nd} order finite-difference discretization was used in the algorithm which does place a restriction on the domain shape. In order to avoid such a restriction, the algorithm should be modified for quadratic elements and thus a pure finite-element scheme can be used on any domain. This would require testing of the Petrov-Galerkin weighting functions which have been developed and tested only for linear elements. However, it is expected that the performance would be more or less the same.

The effects of thermal heating/osmotic flow have been neglected in our model. By including such effects and learning to control them, it is possible to keep them to a minimum and thus develop better commercial techniques.

Reaction terms have not been included as yet in the test cases; clearly, to take into account equilibria between neutral and charged species, this is essential. This would require a better understanding of individual physical problems.

The assumption of a constant current density, while valid for one-dimensional problems, is not a good approximation for two-dimensional cases; it is expected that better models will be developed. Two-dimensional simulations are quite expensive but provide invaluable help in understanding the physical process. In short, more work needs to be done to simulate electrophoresis separation fully, but in the meantime the existing model does provide useful insight into the physics of the problem.

To sum up, the motivation for developing accurate time-dependent Petrov-Galerkin schemes was to simulate flow field and electrophoresis separation phenomena; nevertheless, the equations considered might be those governing thermal convection/ diffusion, chemical convection/diffusion/ reaction, etc. Our results indicate a strong potential for future work in this area and it is expected that such formulations will be used to obtain better transient solutions for Navier-Stokes and Euler equations which have become "classical" challenges over the years.

REFERENCES

[1] G. DeVahl Davis and G. Mallinson,"An Evaluation of Upwind and Central Difference Approximations by a Study of Recirculating Flow", Computers and Fluids, vol. 4, pp. 29-43, 1976 .

[2] P.M. Gresho and R.L. Lee,"Don't Suppress the Wiggles-They Are Telling You Something !", in: T.J.R. Hughes, ed., Finite Element Methods for Convection Dominated Flows, T.J.R. Hughes (ed.), AMD vol. 34, pp. 37-62, ASME, New York, 1979 .

[3] B.P. Leonard,"A Survey of Finite Difference Opinion on Numerical Muddling of the Incomprehensible Defective Confusion Equation", Finite Element Methods for Convection Dominated Flows, T.J.R. Hughes (ed.), AMD vol. 34, pp. 1-18, ASME, New York, 1979.

[4] I. Christie, D.F. Griffiths, A.R. Mitchell and O.C. Zienkiewicz, "Finite Element Methods for Second Order Differential Equations with Significant First Derivatives", International Journal for Numerical Methods in Engineering, vol. 10, pp. 1389-1396, 1976.

[5] J.C. Heinrich, P.S.. Huyakorn, O.C. Zienkiewicz and A.R. Mitchell,"An Upwind Finite Element Scheme for Two-dimensional Convective Transport Equation", International Journal of Numerical Methods in Engineering, vol. 11, pp. 134-143, 1977.

[6] T.J.R. Hughes ,"A Simple Scheme for Developing "Upwind" Finite Elements", International Journal for Numerical Methods in Engineering, vol. 12, pp. 1359-1365, 1978.

[7] T.J.R. Hughes and J. Atkinson,"A Variational Basis for "Upwind" Finite Elements", IUTAM Symposium on Variational Methods in the Mechanics of Solids, Northwestern University, Evanston, IL, 1978.

[8] T.J.R. Hughes and A. Brooks,"A Multi-dimensional Upwind Scheme with No Crosswind Diffusion", Finite Element Methods for Convection Dominated Flows,

T.J.R. Hughes (ed.), AMD vol. 34, pp. 19-36, ASME, New York, 1979.

[9] T.J.R. Hughes and A. N. Brooks,"A Theoratical Framework for Petrov-Galerkin Methods with Discontinuous Weighting Functions: Application to the Streamline Upwind Procedure", Finite Elements in Fluids, R.H. Gallagher et al. (eds.), vol.4, pp. 46-65, Wiley, London, 1984.

[10] A.N. Brooks and T.J.R. Hughes,"Streamline Upwind/Petrov- Galerkin Formulations for Convection Dominated Flows with Particular Emphasis on the Incompressible Navier-Stokes Equations", Computer Methods in Applied Mechanics and Engineering, vol. 32, pp. 199-259, 1982.

[11] T.J.R. Hughes and T.E. Tezduyar,"Finite Element Methods for First-order Hyperbolic Systems with Particular Emphasis on the Compressible Euler Equations", Computer Methods in Applied Mechanics and Engineering, vol. 45, pp. 217-284, 1984.

[12] T.J.R. Hughes, M. Mallet, Y. Taki, T.E. Tezduyar, and R. Zanutta,"A One-dimensional Shock Capturing Finite Element Method and Multi-dimensional Generalizations", Numerical Methods for the Euler Equations of Fluid Dynamics, F. Argrand et. al. (eds.), SIAM, pp. 371-408, 1985.

[13] T.J.R. Hughes, M. Mallet and L.P. Franca,"Entropy-stable Finite Element Methods for Compressible Fluids: Applications to High Mach Number Flows with Shocks", to appear in Finite Element Methods for Nonlinear Problems, Springer-Verlag.

[14] C. Johnson, U. Navert and J. Pitkaranta,"Finite Element Methods for Linear Hyperbolic Problems", Computer Methods in Applied Mechanics and Engineering , vol.46, pp. 285-312, 1984.

[15] H. Schlichting,"Boundary Layer Theory", McGraw-Hill Book Company, seventh edition, 1979.

[16] P.J. Roache, " Computational Fluid Dynamics",Hermosa Publishers,1972.

[17] R. Peyret & T.D. Taylor,"Computational Methods for Fluid Flow", Springer-Verlag, New York Inc., 1983.

[18] D.J. Shaw " Electrophoresis", Academic Press London and New York, 1969.

[19] C.J.O.R. Morris and P. Morris " Separation Methods in Biochemistry ", John Wiley & Sons, New York, 1976.

[20] T.J.R. Hughes, K.S. Pister and R.L. Taylor,"Implicit-explicit Finite Elements in Nonlinear Transient Analysis", Computer Methods in Applied Mechanics and Engineering, vol. 17/18, pp. 159-182, 1979.

[21] T.E. Tezduyar and T.J.R. Hughes,"Development of Time-accurate Finite Element Techniques for First Order Hyperbolic Systems with Particular Emphasis on the Compressible Euler Equations", Final Report, NASA-Ames University Consortium Interchange No. NCA2-OR745-104, May 1982 .

[22] R.F. Warming and R.M. Beam,"On the Construction and Application of Implicit Factored Schemes for Conservation Laws", SIAM-AMS Proceedings, vol. II, 1978.

[23] W.H. Raymond and A. Garder,"Selective Damping in a Galerkin Method for Solving Wave Problems with Variable Grids", Monthly Weather Review, vol. 104, pp. 1583-1590, 1976.

[24] K.W. Morton and A.K. Parrot,"Generalized Galerkin Methods for First Order Hyperbolic Equations", Journal of Computational Physics, vol. 36, no. 2, 1980.

[25] G.D. Mallinson and G. De Vahl Davis, " The Method of the False Transient for the Solutions of Coupled Elliptic Equations", Journal of Computational Physics, vol. 12 , pp. 435-461, 1973.

[26] A.K. Runchal, D.B. Spalding and M. Wolfshtein," Numerical Solution of the Elliptic Equations for Transport of Vorticity, Heat and Matter in Two-dimensional Flow", High speed Computing in Fluid Dynamics, Physics of Fluids Supplement II , 1969.

[27] R. Glowinski, private communications, 1986.

[28] R. Glowinski and E. Dean,"Finite Element Implementation of an Absorbing Boundary Condition for the Bi-harmonic Equation", preprint.

[29] F. Glaisner, University of Houston - University Park, M.S. Thesis in progress, 1986.

[30] B. Fornberg," A Numerical Study of Steady Viscous Flow Past a Circular Cylinder", Journal of Fluid Mechanics , vol. 98, pp. 819-855, 1980.

[31] S.L. Smith and C.A. Brebbia," Improved Stability Techniques for the Solution of the Navier-Stokes Equations", Applied Mathematical Modelling, vol.1, pp. 226- 234, June 1977.

[32] T.J.R.Hughes, W.K. Liu, and A. Brooks," Finite Element Analysis of Incompressible Viscous Flows by the Penalty Function", to appear in the Journal of Computational Physics.

[33] John Newman, " Electro-Chemical Systems ", Prentice-Hall International Series, 1973.

[34] J. Vacik, W. Ostrowski, F.M. Everaerts, J.L. Beckers, N. Catsimpoolas et al., " Electrophoresis, a Survey of Techniques and Applications, part A: Techniques ", Journal of Chromatography Library, Z. Deyl et al. (eds.), Elsevier Scientific Publishing Company, vol. 18, 1979.

[35] F.M. Everaerts, J.L. Beckers, T.P.E.M. Vergheggen, " Isotachophoresis Theory, Instrumentation and Application ", Journal of Chromatography Library, vol. 6, Elsevier Scientific Publishing Company, 1976.

[36] M. Bier, O.A. Palusinski, R.A. Mosher, D.A. Saville, " Electrophoresis: Mathematical Modelling and Computer Simulation ", Science, vol. 219, No. 4590, pp. 1281-1287, 1983.

[37] A.K.M.F. Hussain,"Coherent Structures - Reality and Myth ", The Physics of Fluids, vol.26, pp. 2816-2850, Oct. 1983.

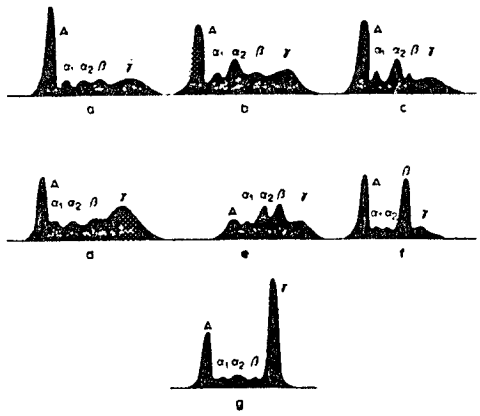

Figure 1.1.1 Electrophoresis. Characteristic examples of separation of pathological blood serum proteins : (a) normal ; (b) acute inflammation ; (c) subcute chronic inflammation ; (d) cirrhosis of the liver ; (e) nephrotic syndrome; (f) β-myeloma; (g) γ-plasmocytoma[19].

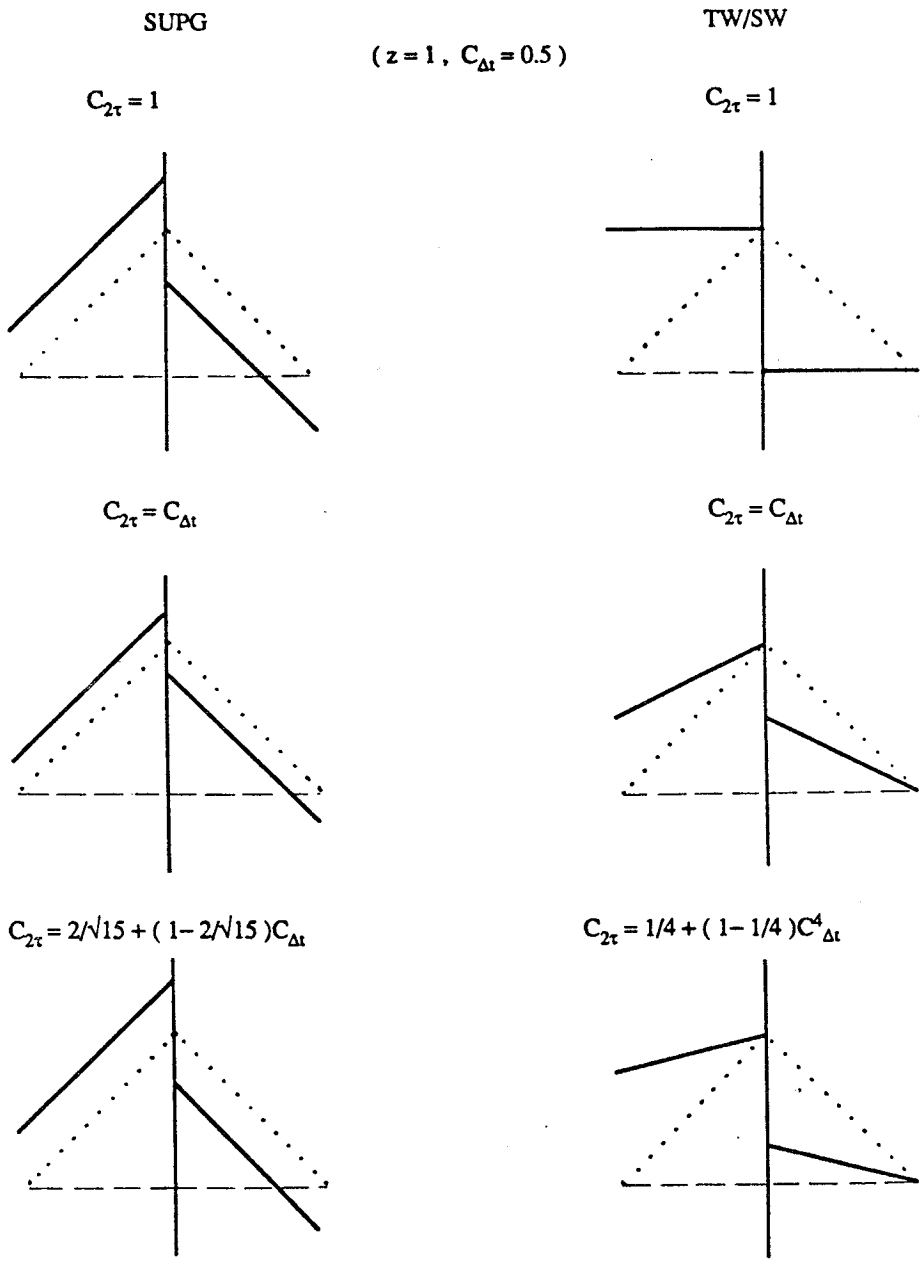

Figure 2.3.1 Weighting functions for Petrov-Galerkin schemes for 1-D linear elements.
(Dotted lines represent weighting function leading to Galerkin formulation.)

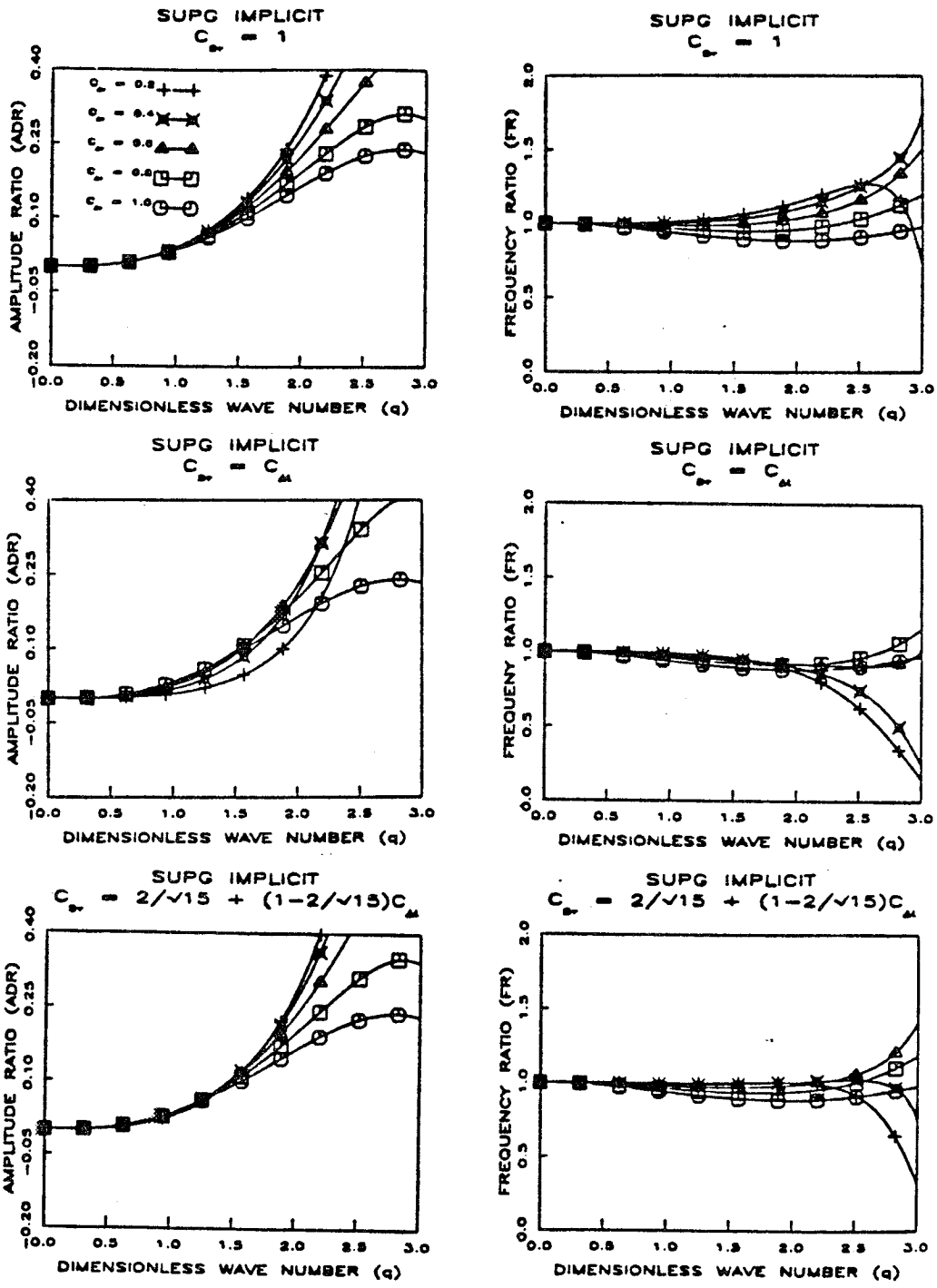

Figure 2.3.2 Stability and accuracy characteristics for implicit SUPG formulation.

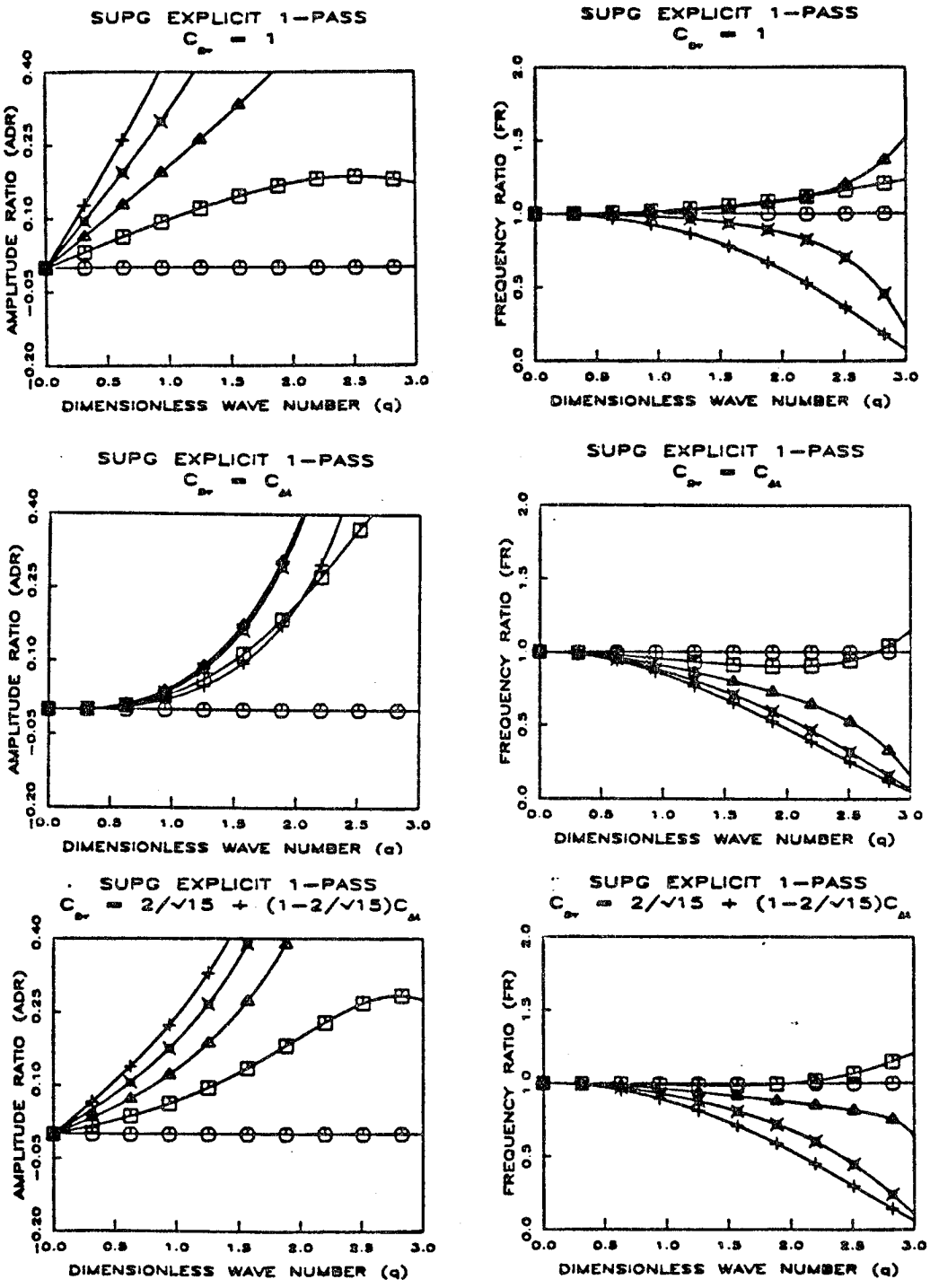

Figure 2.3.3 Stability and accuracy characteristics for explicit 1-pass SUPG formulation.

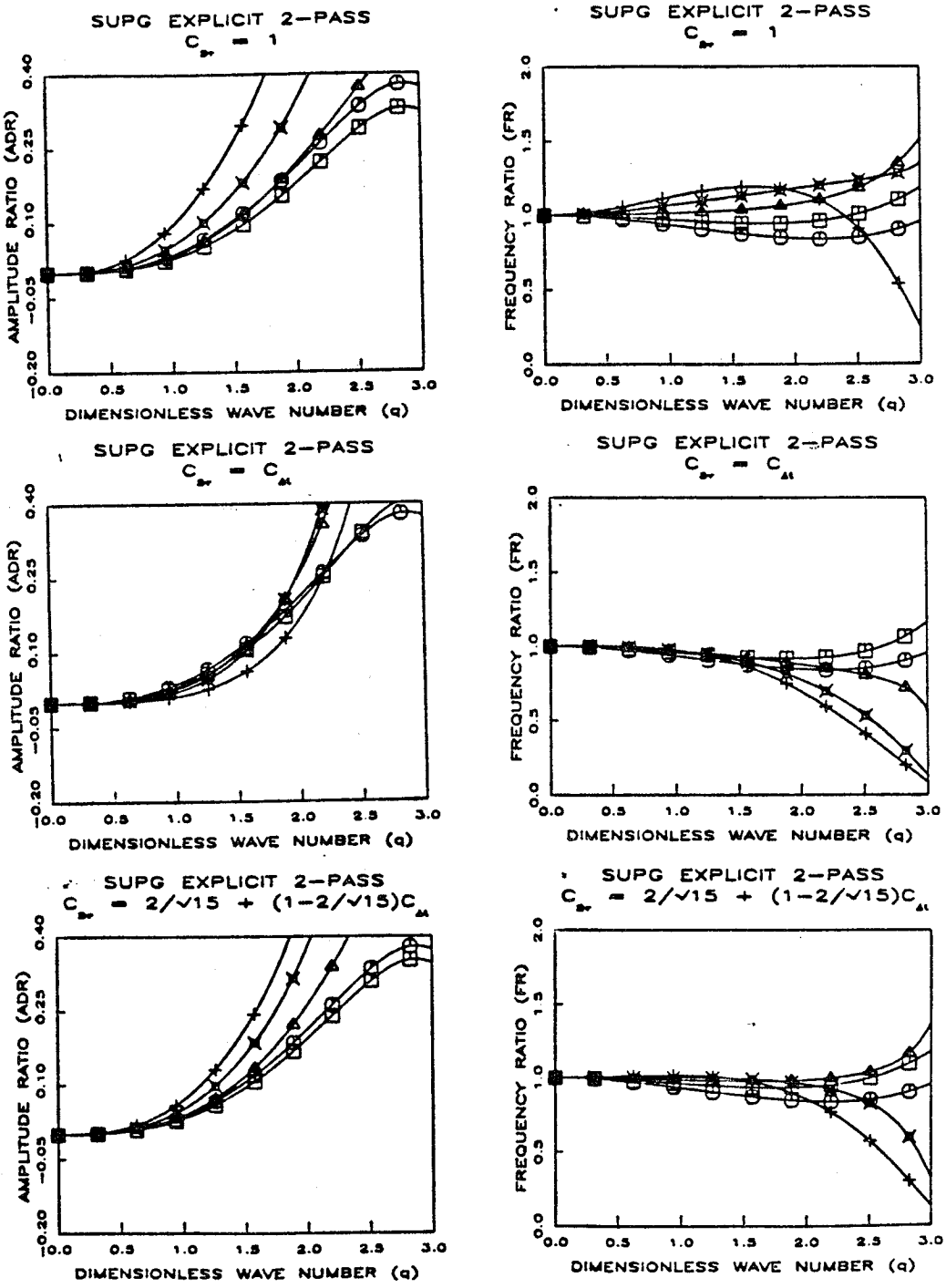

Figure 2.3.4 Stability and accuracy characteristics for explicit 2-pass SUPG formulation.

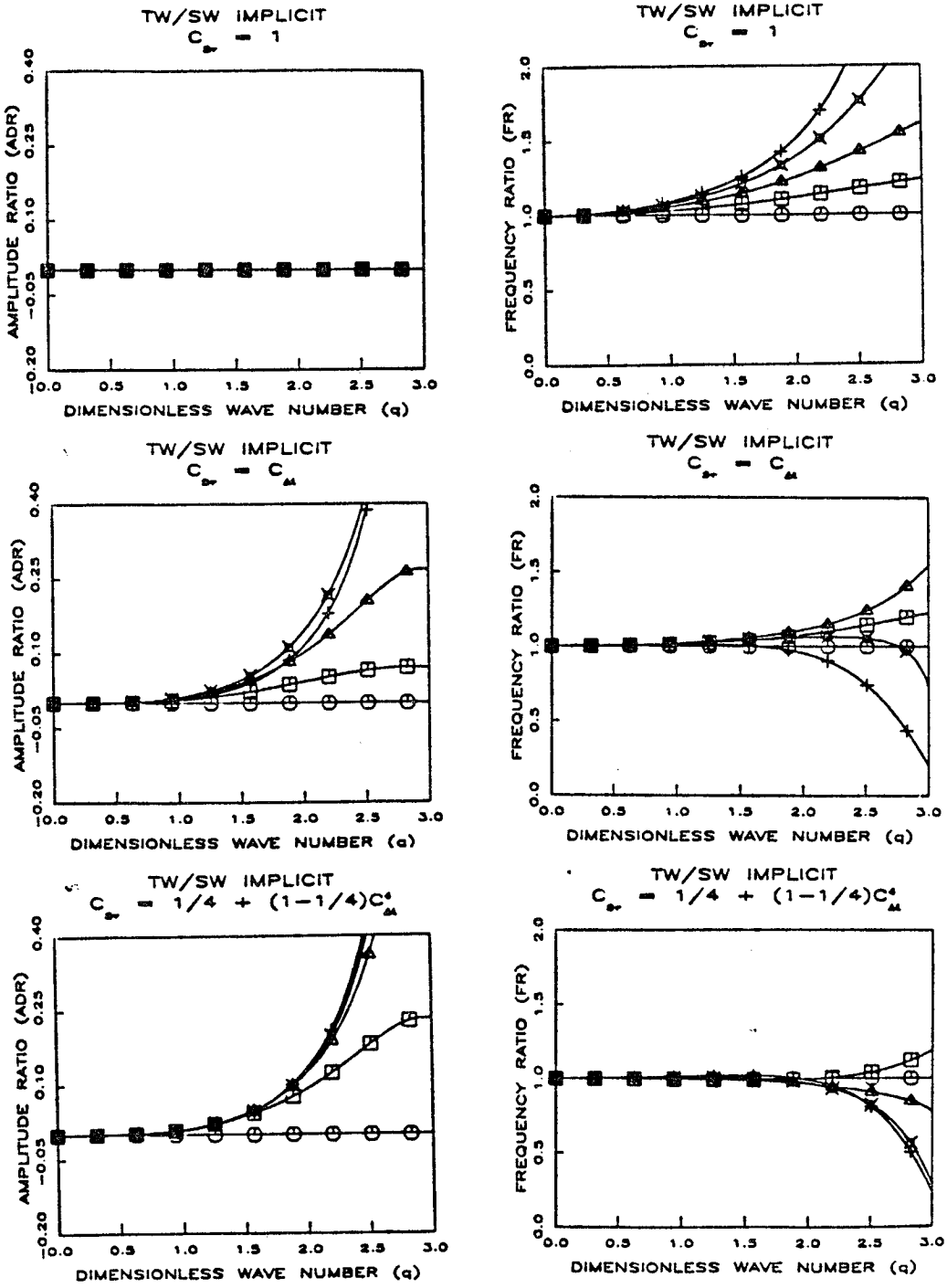

Figure 2.3.5 Stability and accuracy characteristics for implicit TW/SW formulation.

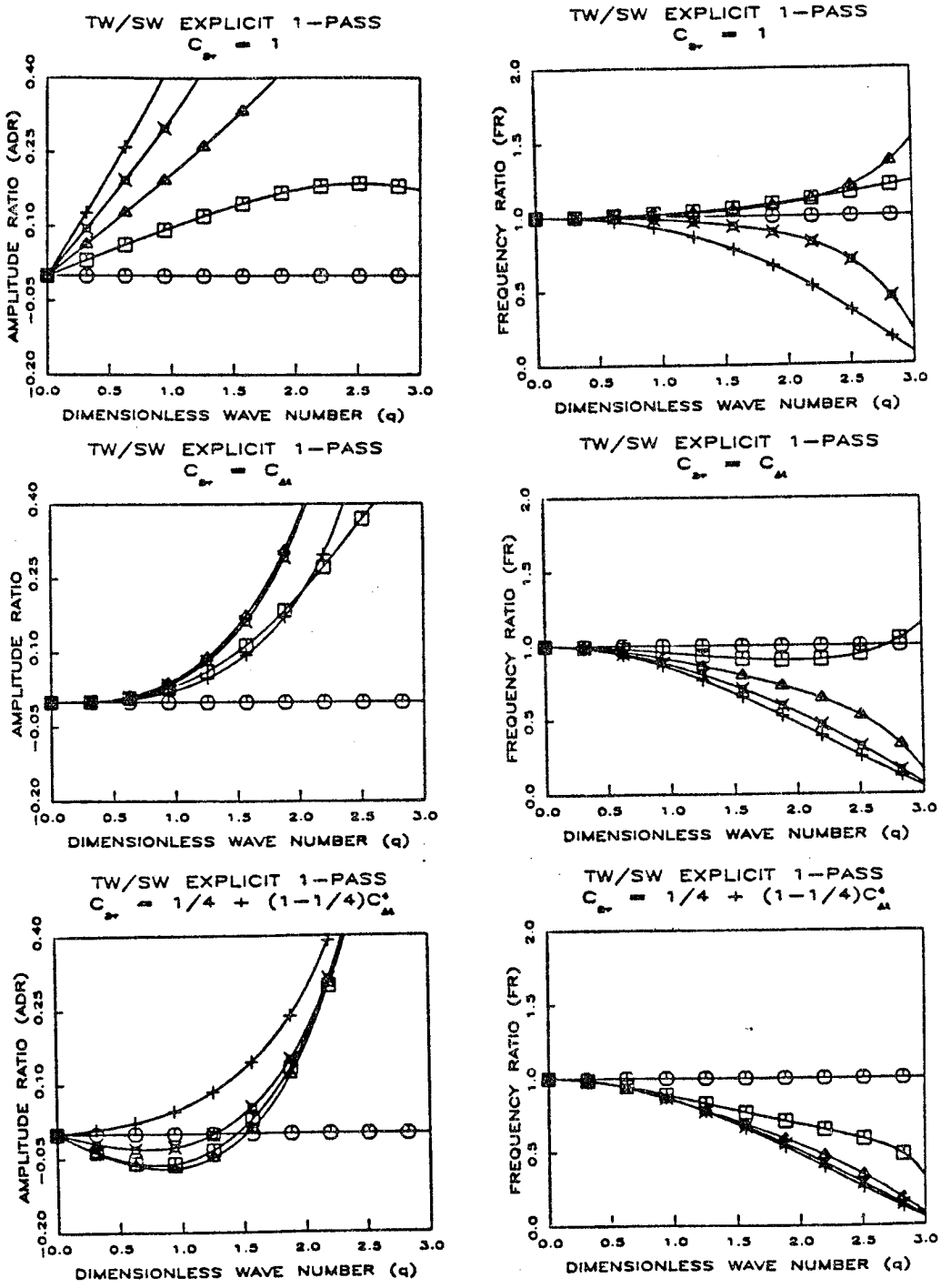

Figure 2.3.6 Stability and accuracy characteristics for explicit 1-pass TW/SW formulation.

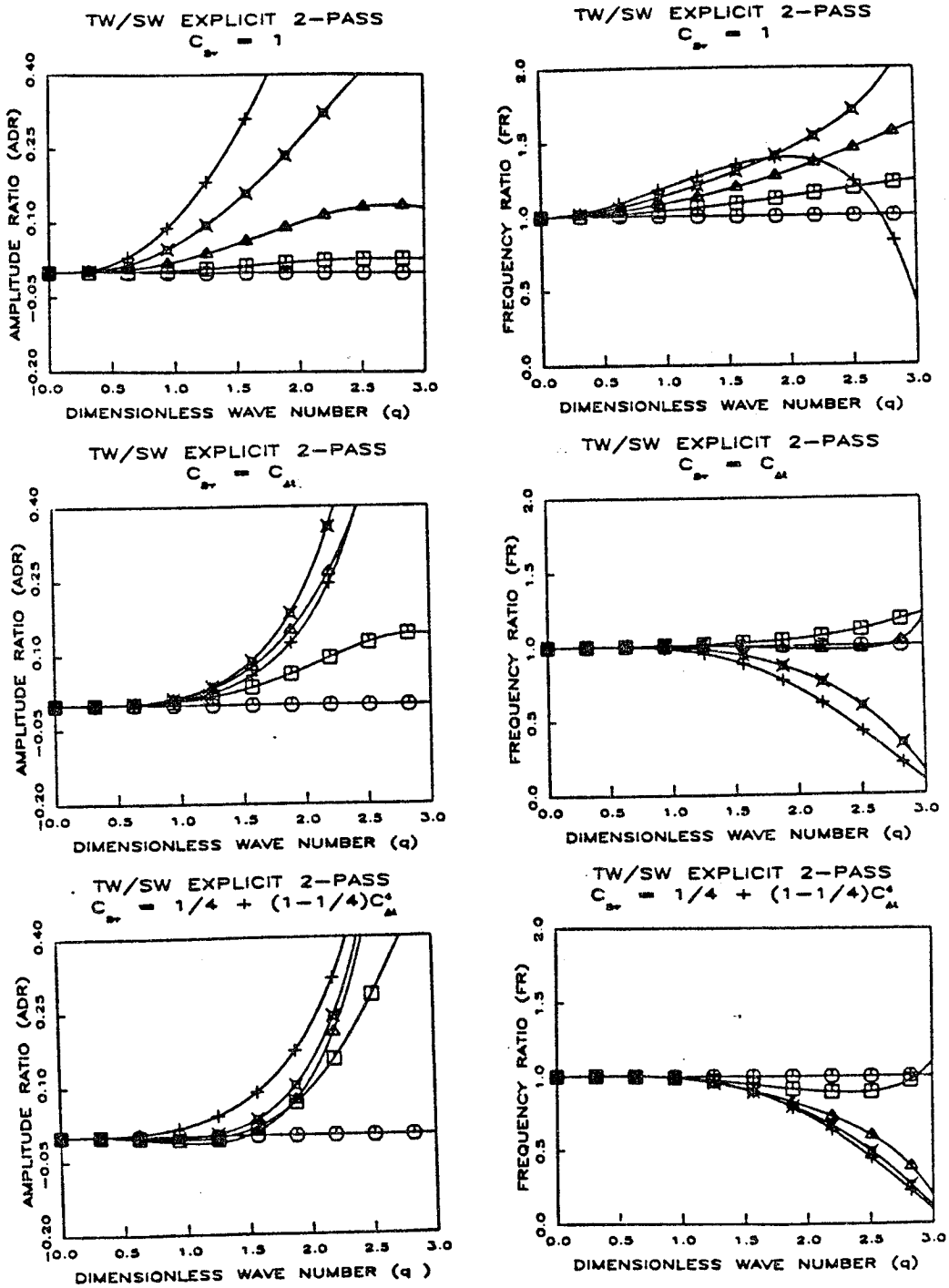

Figure 2.3.7 Stability and accuracy characteristics for explicit 2-pass TW/SW formulation.

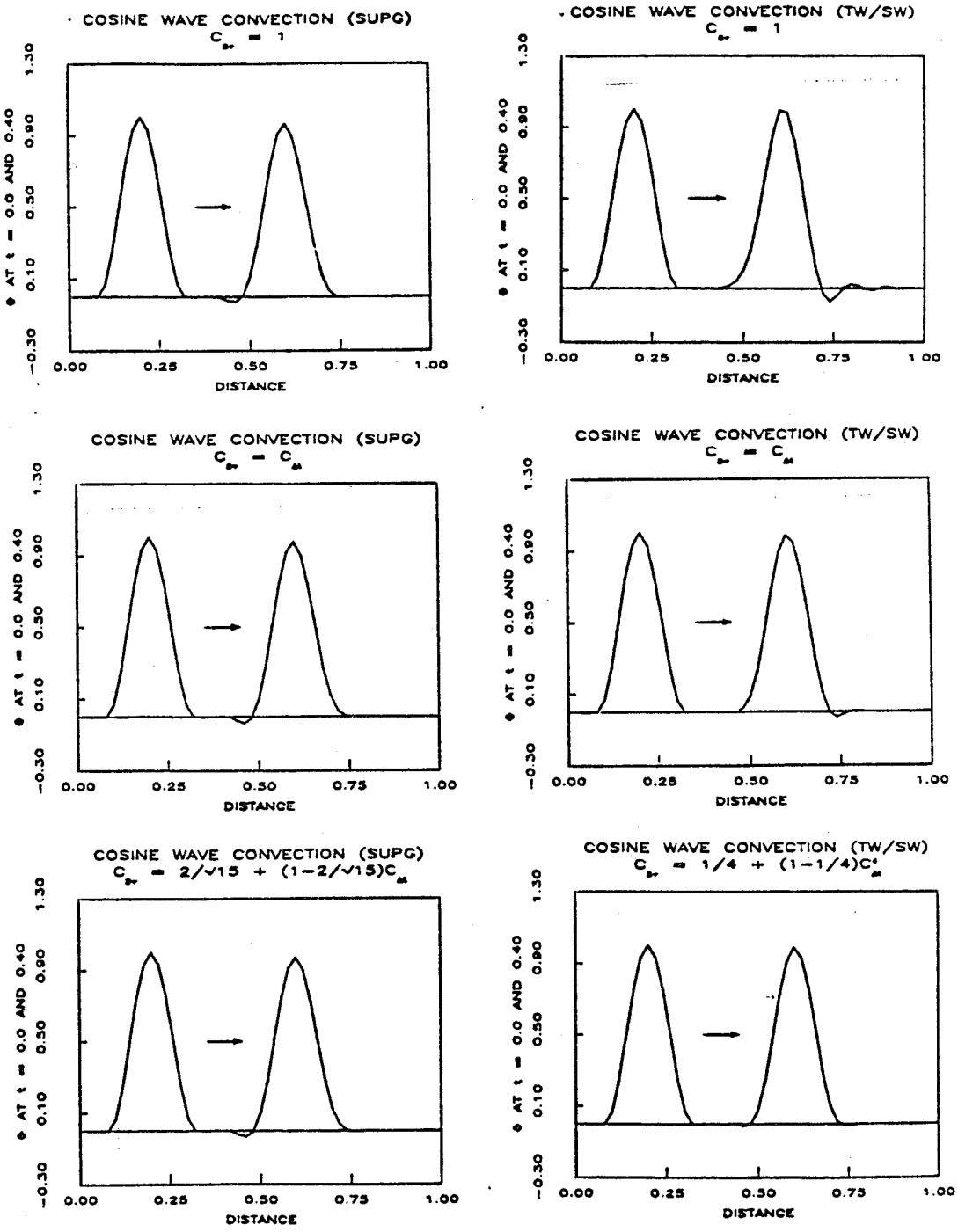

Figure 2.4.1 Convection of a cosine wave.

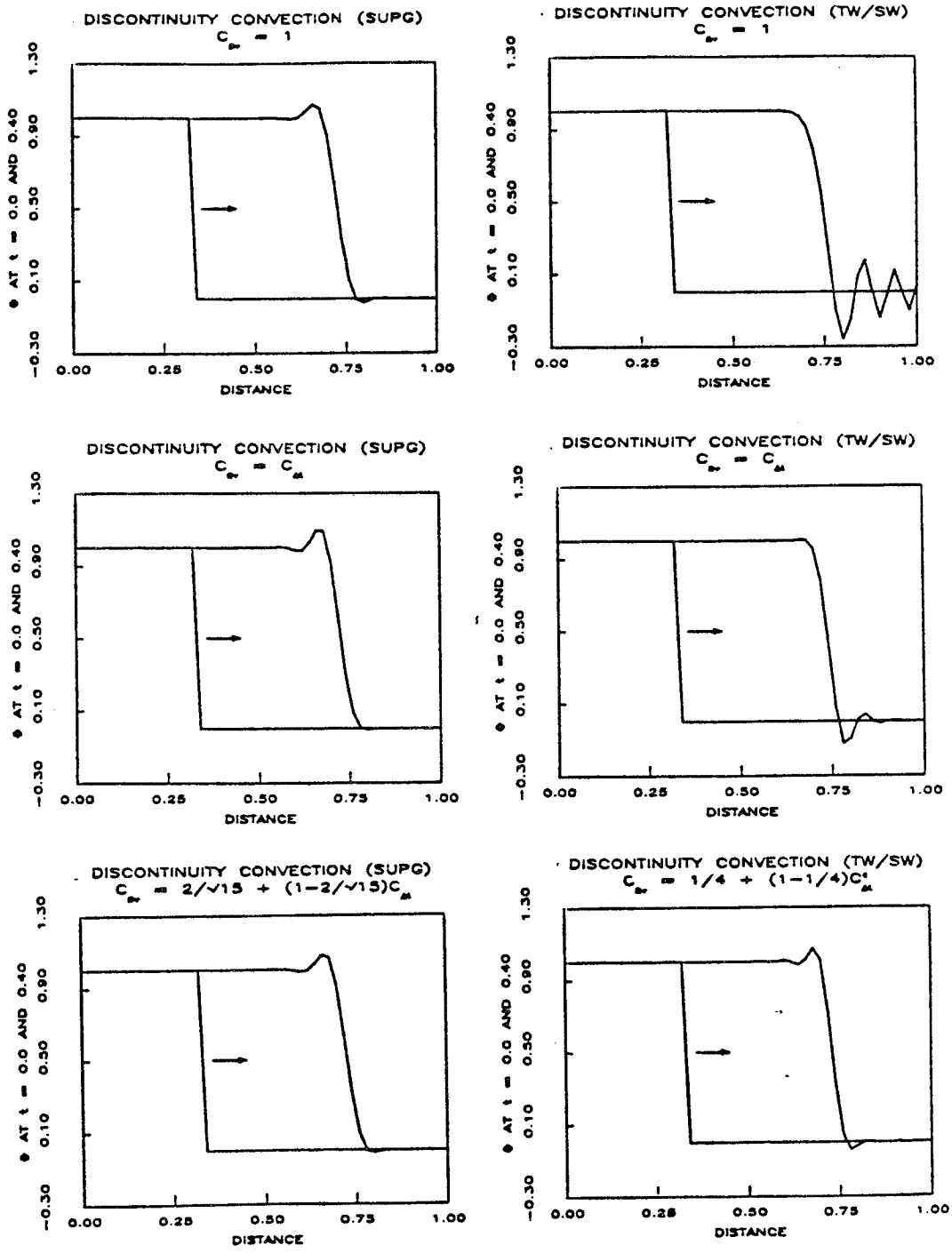

Figure 2.4.2 Convection of a discontinuity .

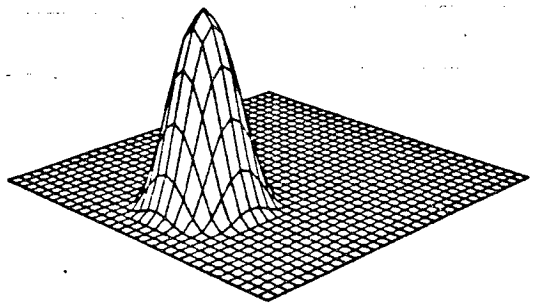

Figure 2.4.3 Initial condition for translating puff and rotating puff problems.

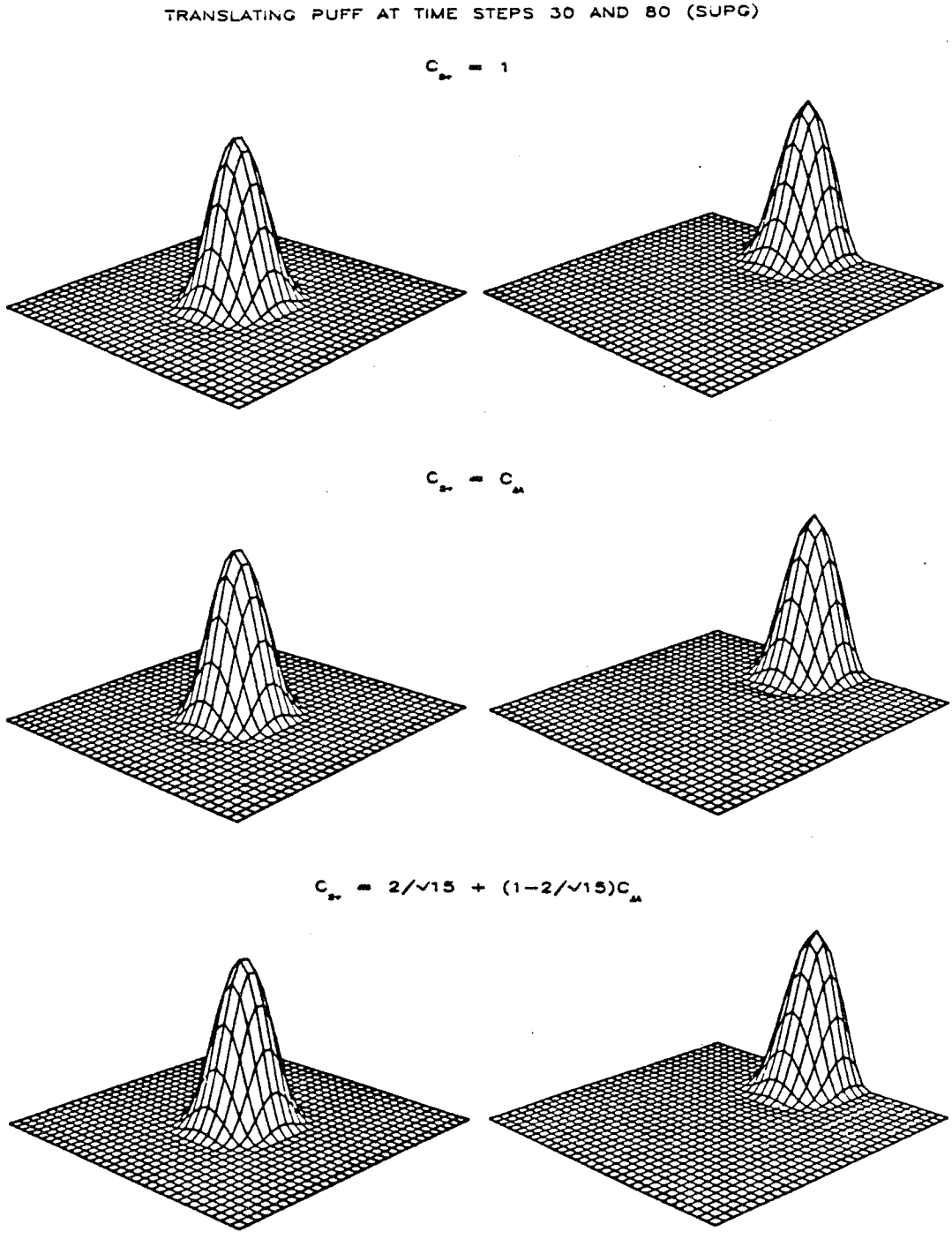

Figure 2.4.4 Translating puff elevation plots (SUPG).

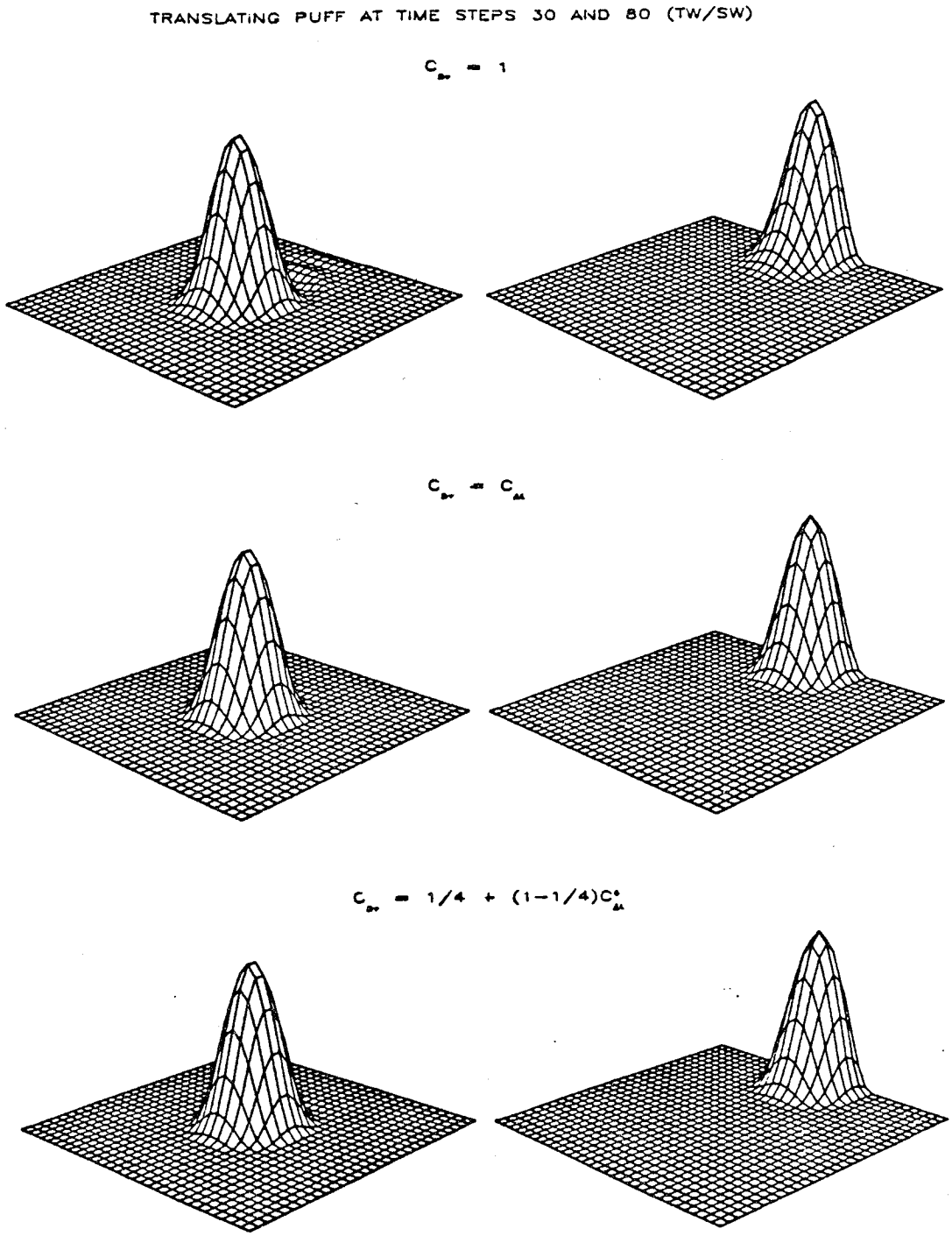

Figure 2.4.5 Translating puff elevation plots (TW/SW).

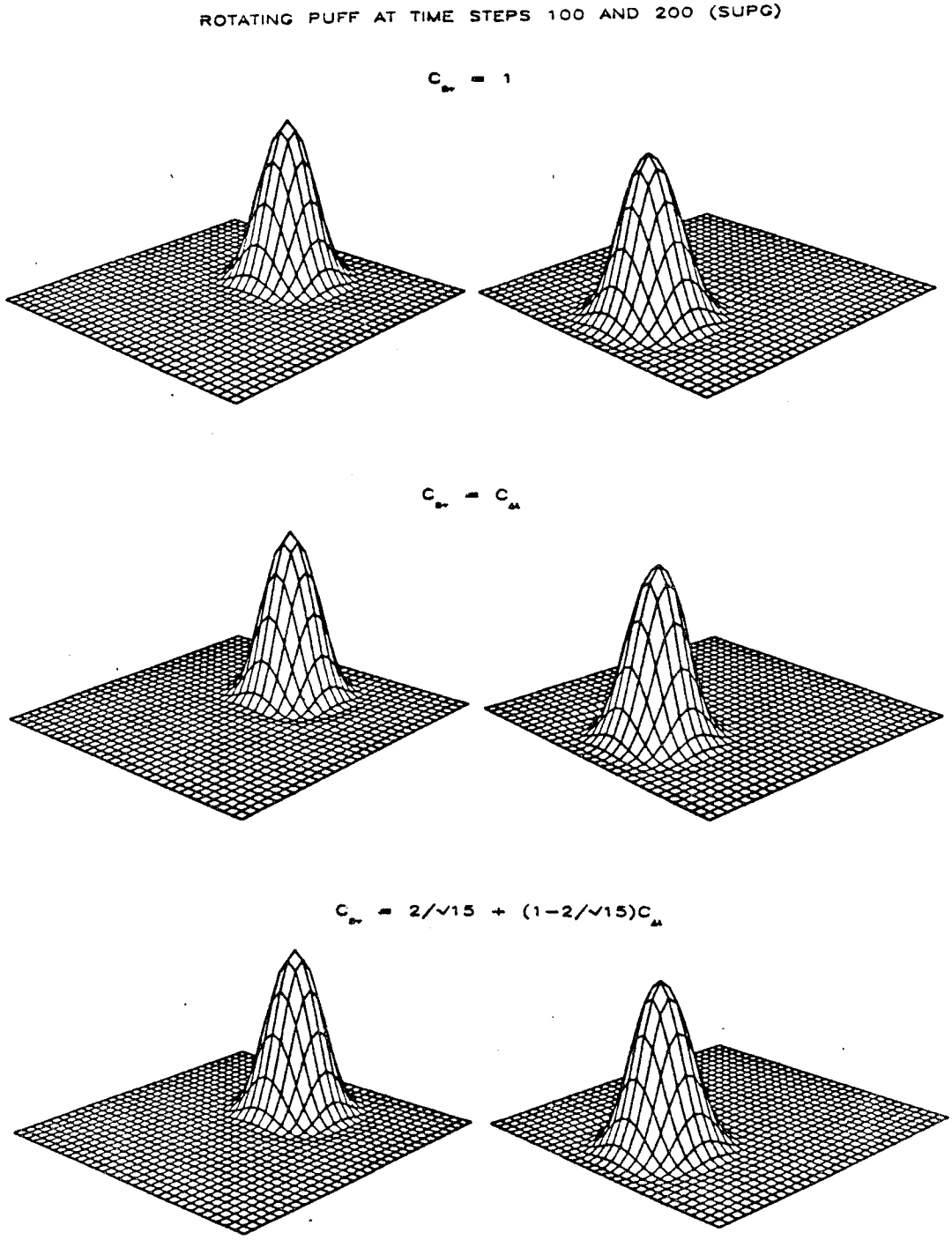

Figure 2.4.6 Rotating puff elevation plots (SUPG).

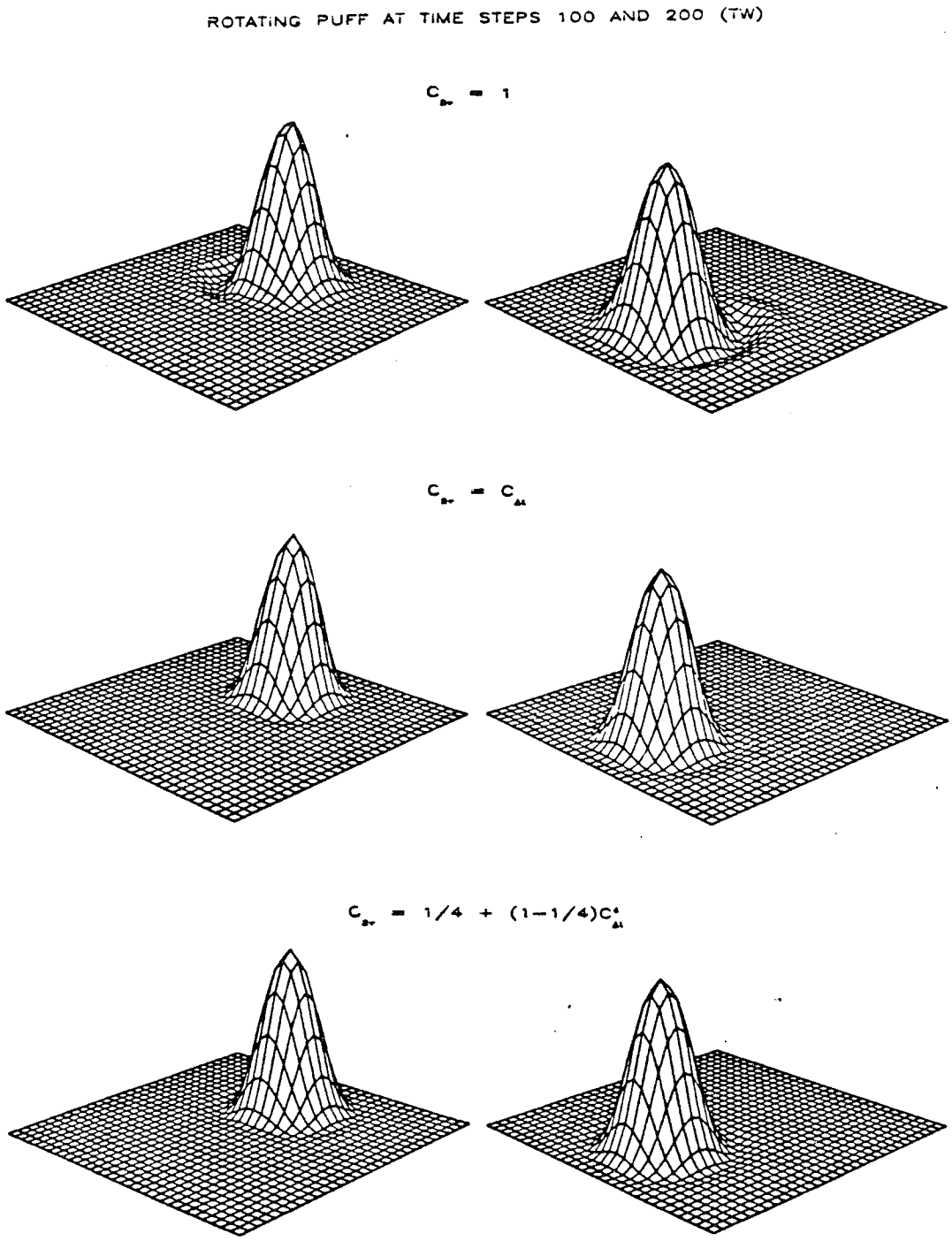

Figure 2.4.7 Rotating puff elevation plots (TW).

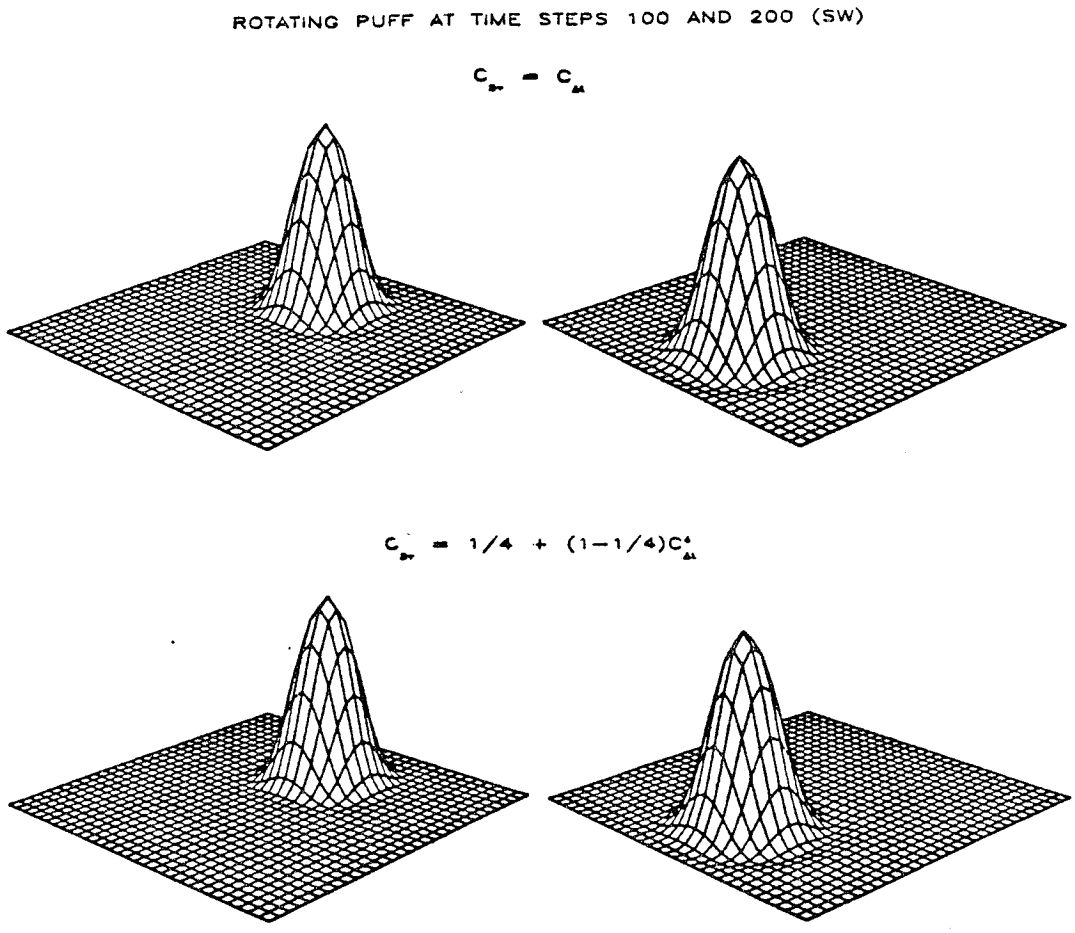

Figure 2.4.8 Rotating puff elevation plots (SW).

WALL DETAILS

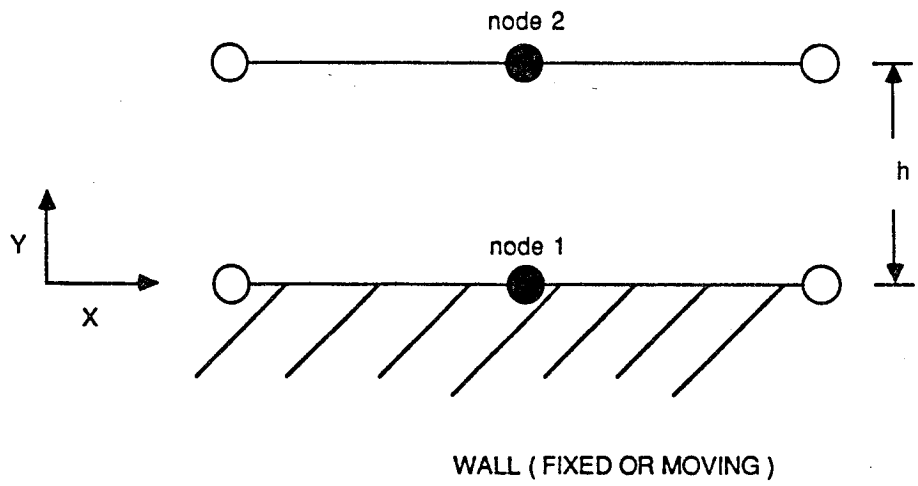

Figure 3.2.1 Vorticity -stream function formulation. Wall boundary details.

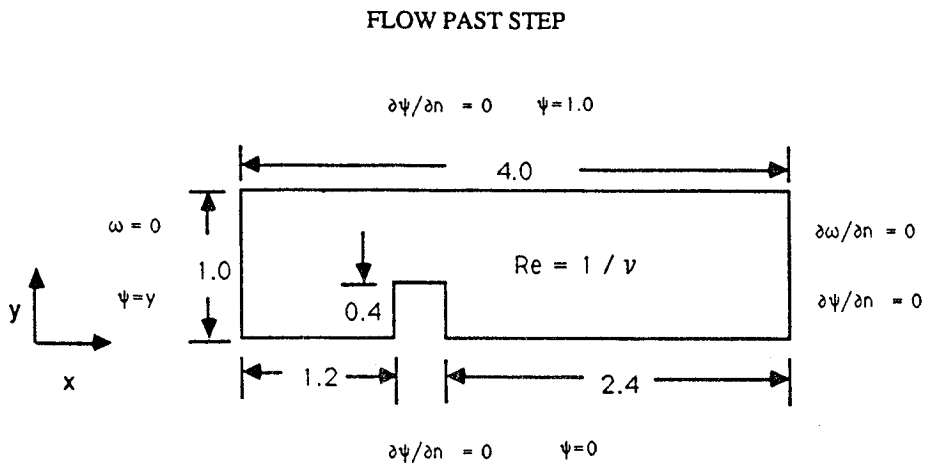

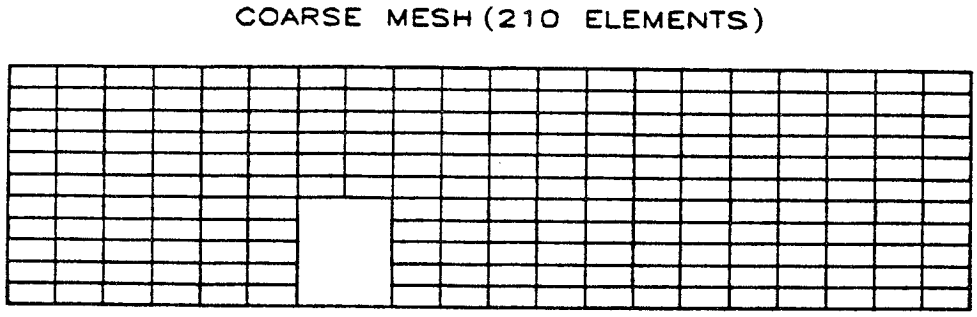

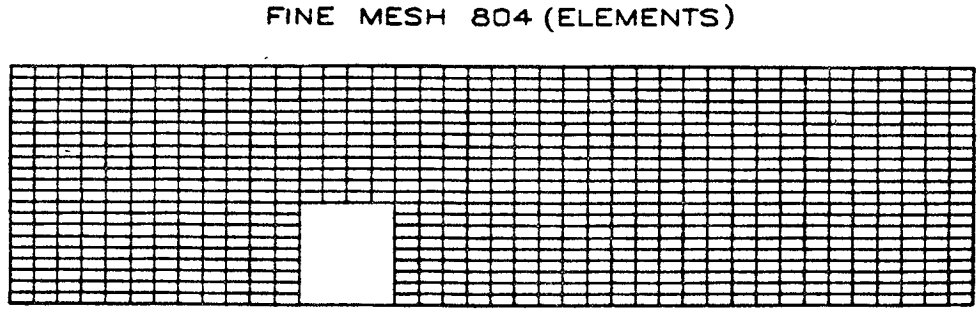

Figure 3.5.1 Flow past a step. Problem description, boundary conditions, and mesh employed.

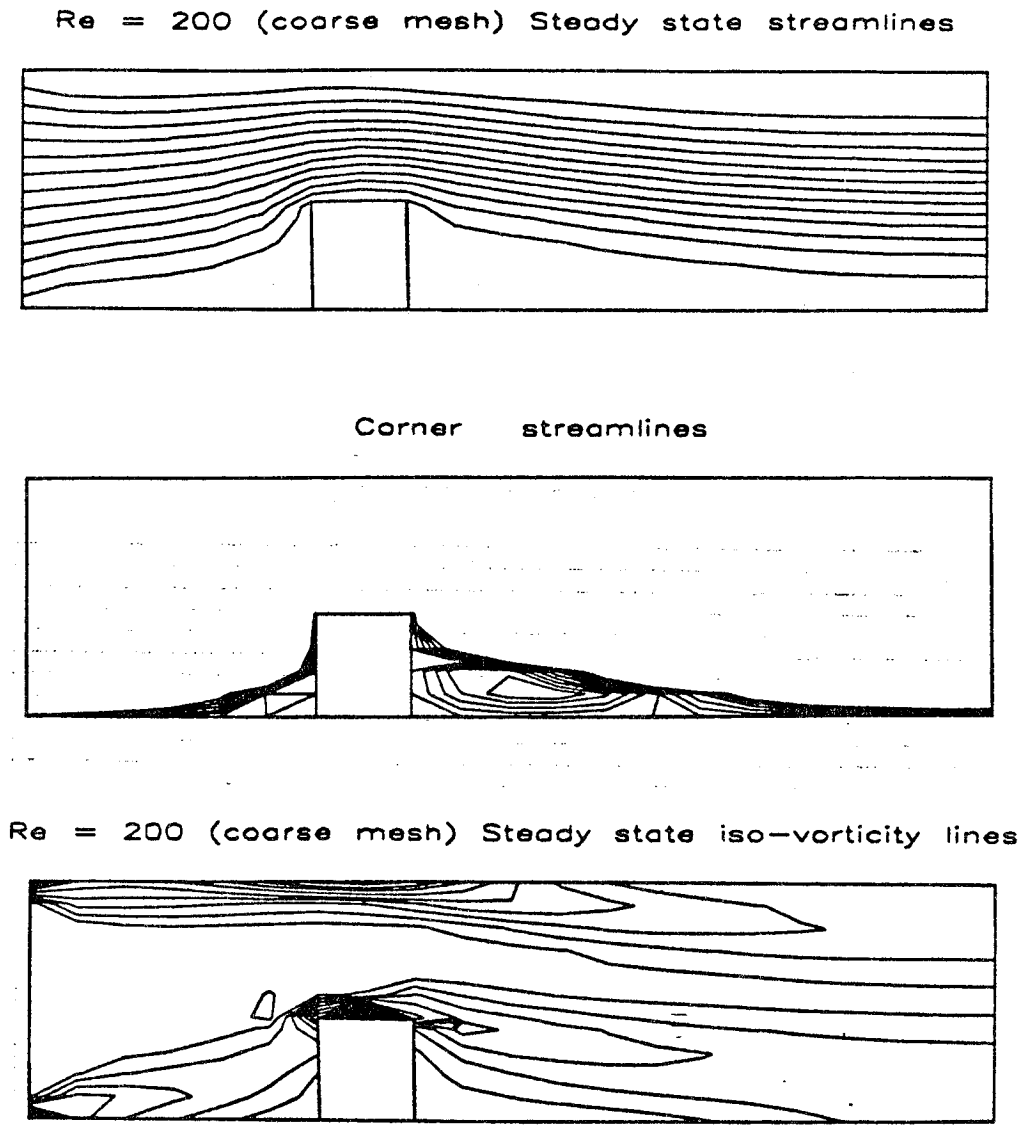

Figure 3.5.2 Flow past a step at Re = 200. Steady state streamlines and iso-vorticity lines (coarse mesh).

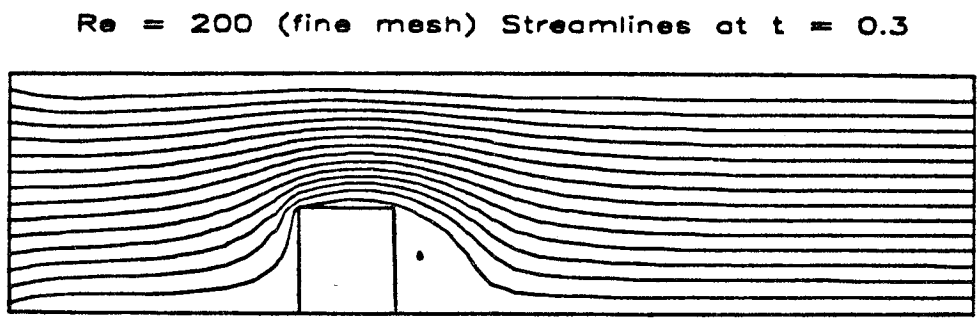

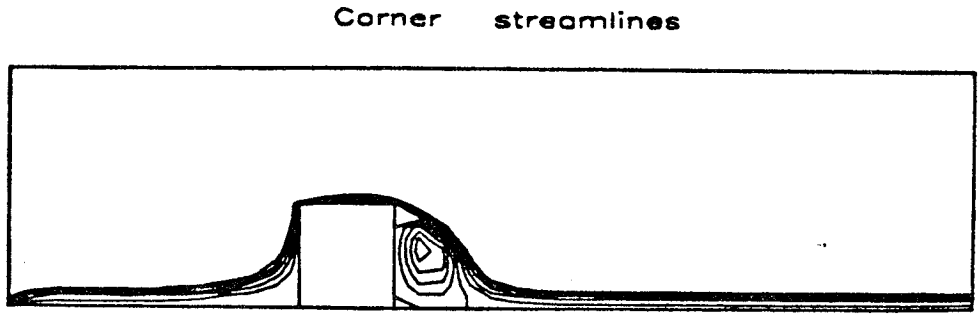

Figure 3.5.3 Flow past a step at Re = 200. Streamlines at various time steps(fine mesh).

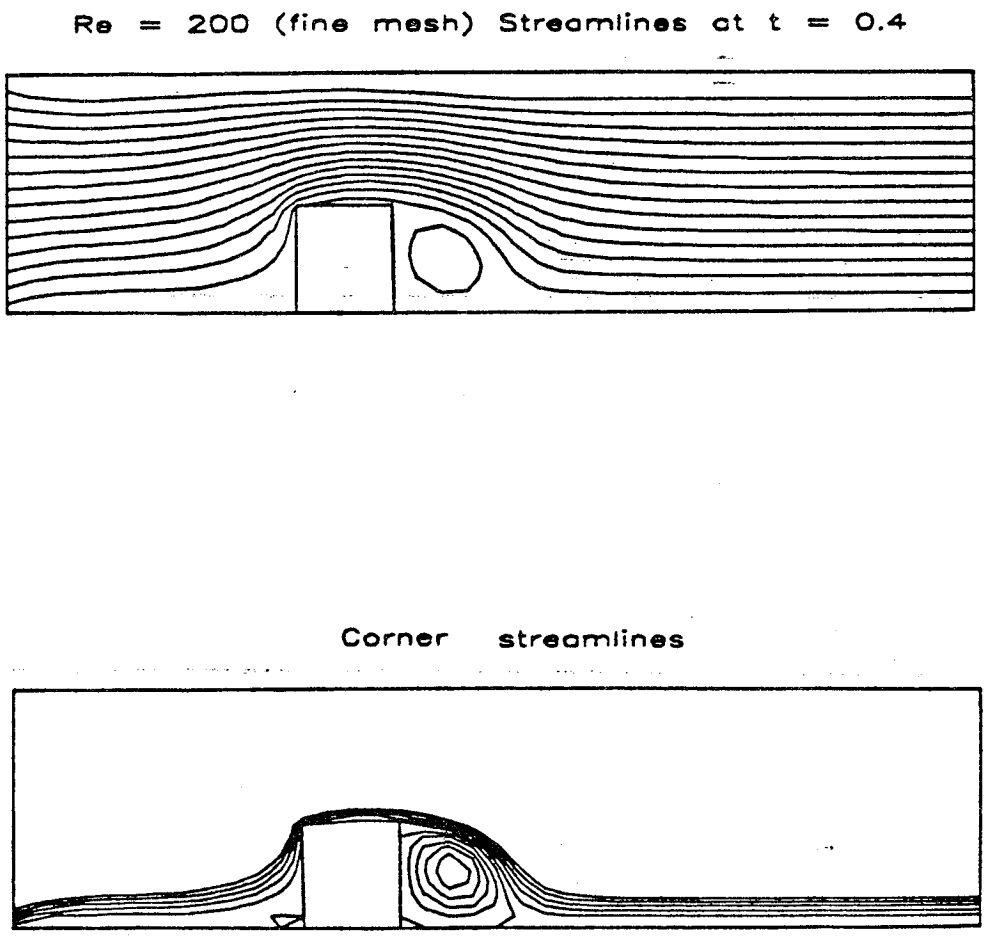

Figure 3.5.3 Flow past a step at Re = 200. Streamlines at various time steps(fine mesh).

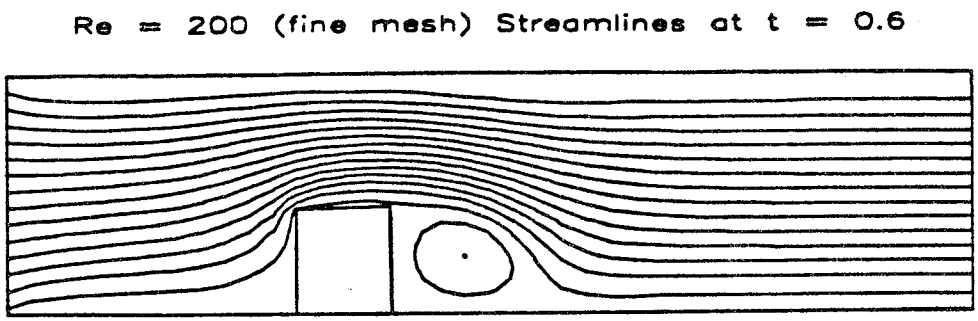

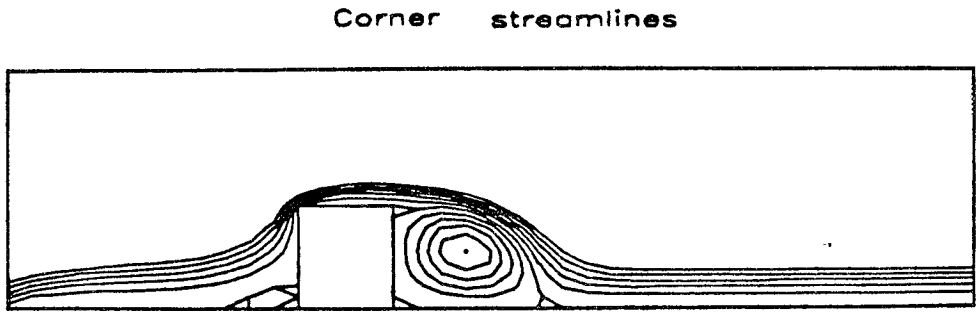

Figure 3.5.3 Flow past a step at Re = 200. Streamlines at various time steps(fine mesh).

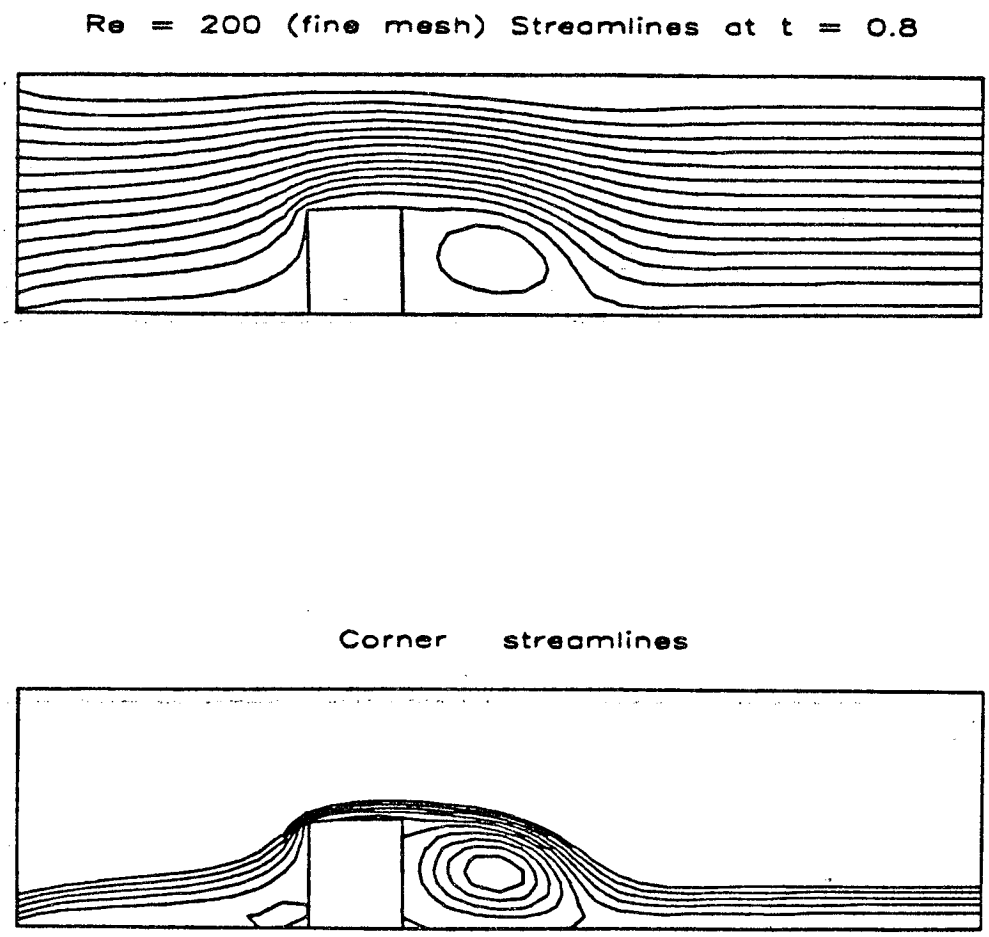

Figure 3.5.3 Flow past a step at Re = 200. Streamlines at various time steps(fine mesh).

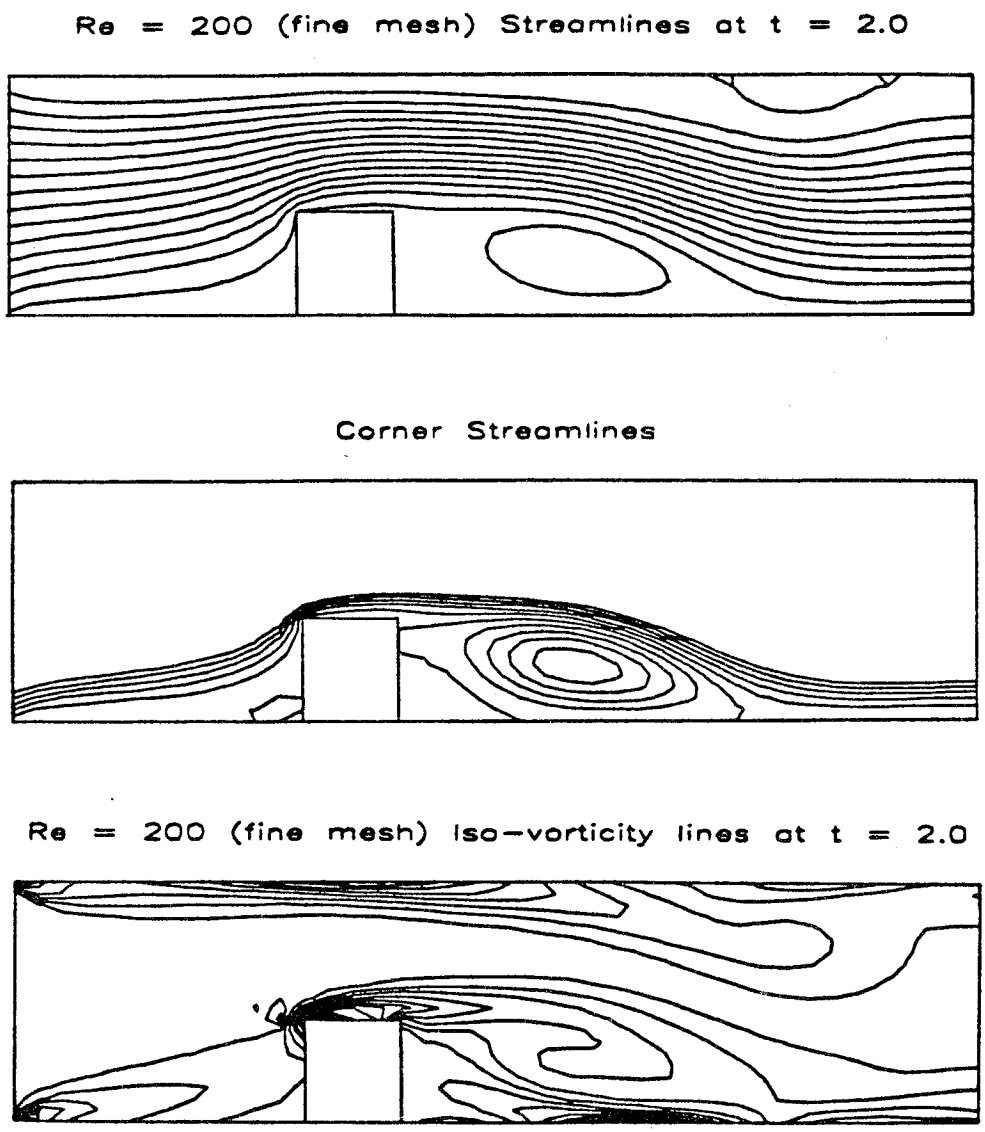

Figure 3.5.3 Flow past a step at Re = 200. Steady state streamlines and iso-vorticity lines. (fine mesh).

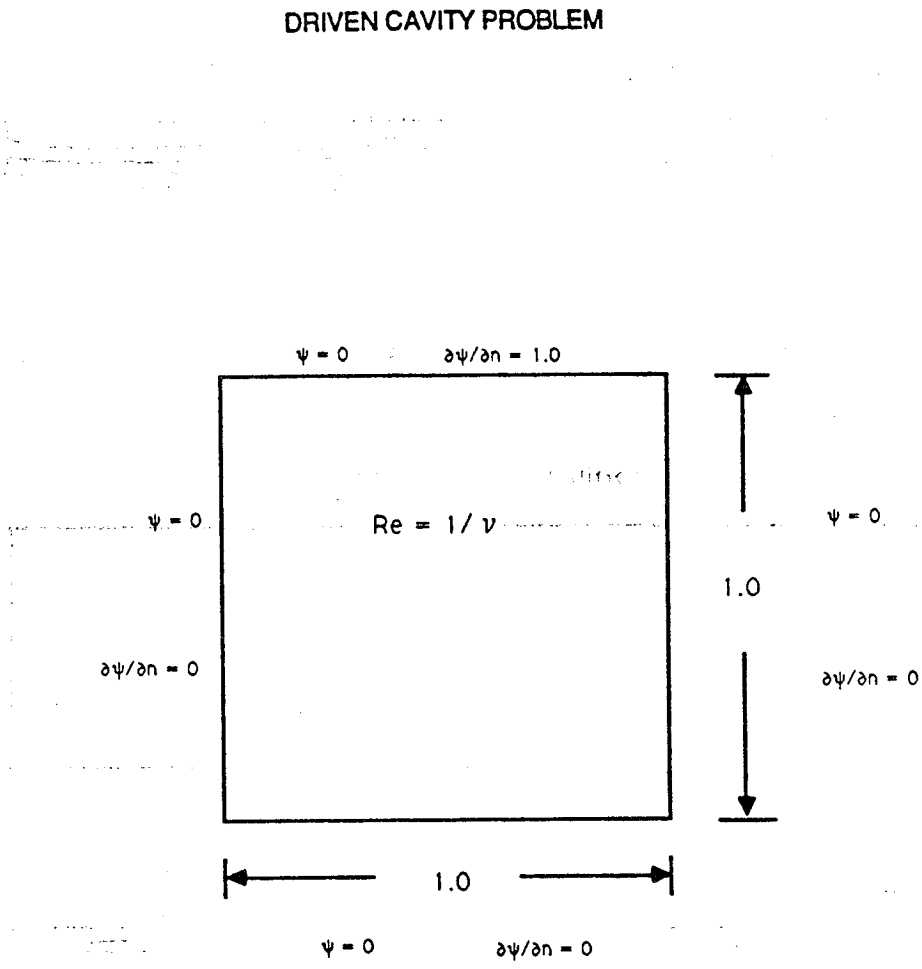

Figure 3.5.4 Driven cavity. Problem description and boundary conditions.

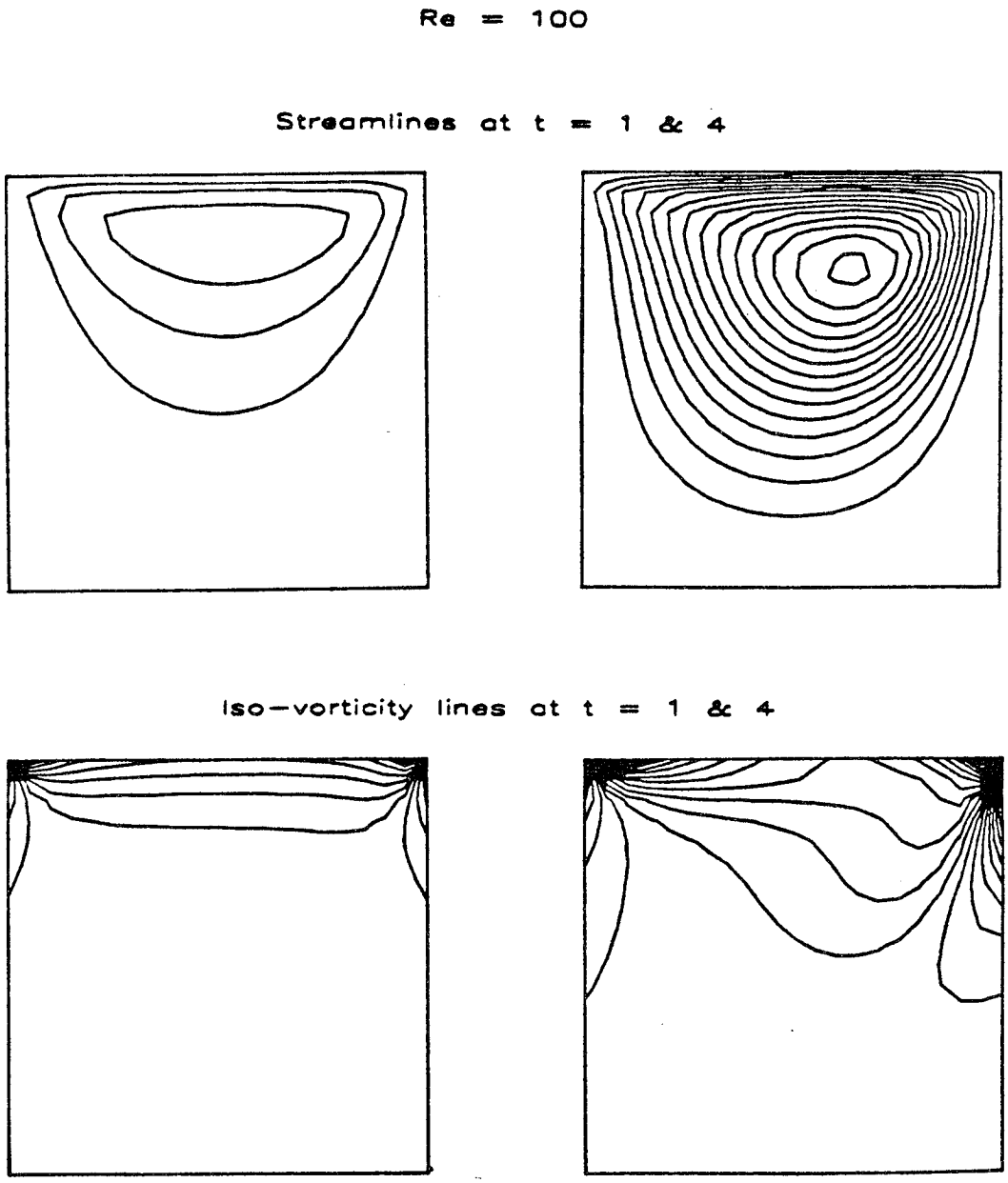

Figure 3.5.5 Driven cavity at Re = 100. Streamlines and iso-vorticity lines at various time steps.

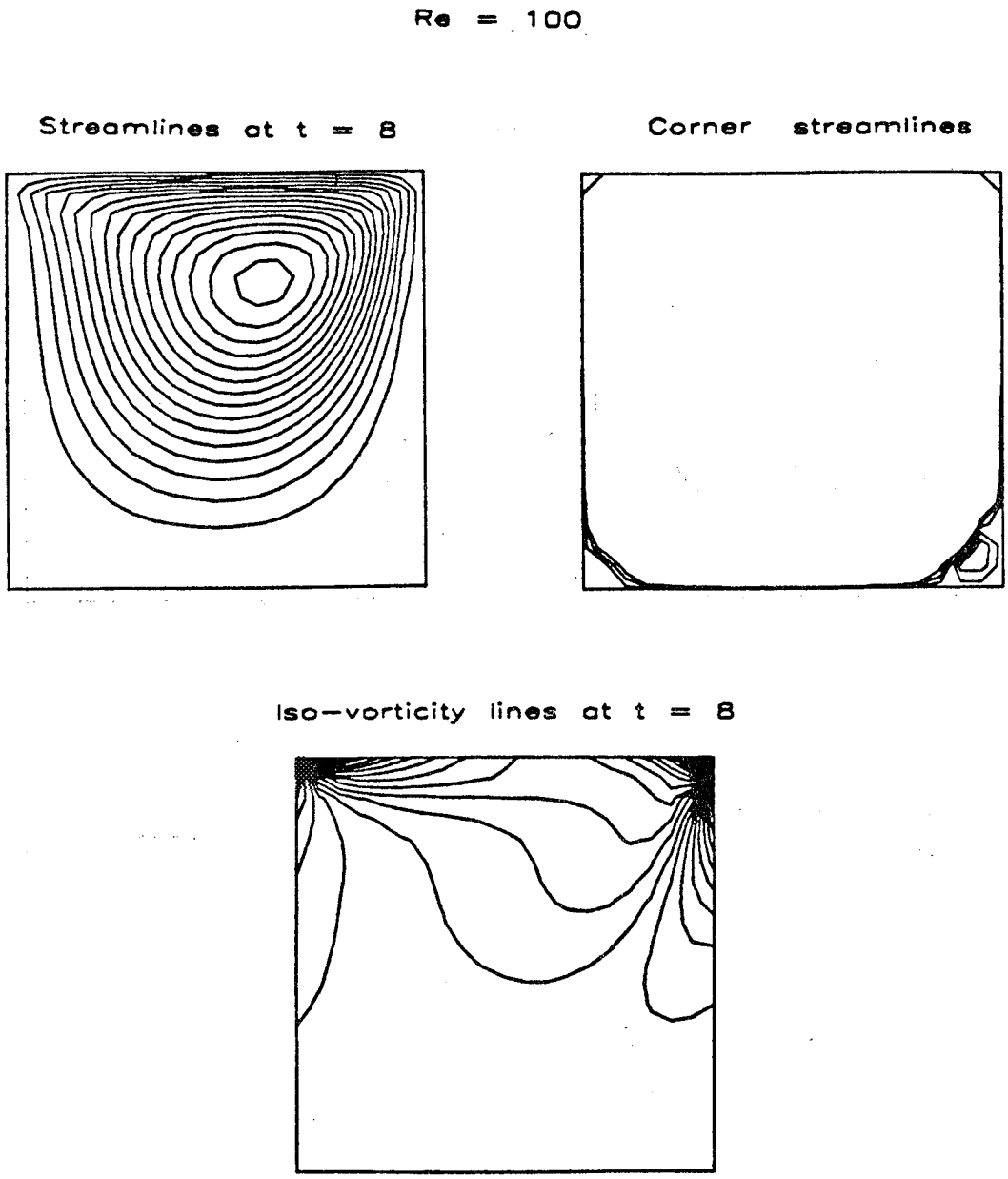

Figure 3.5.5 Driven cavity at Re = 100. Steady state streamlines and iso-vorticity lines.

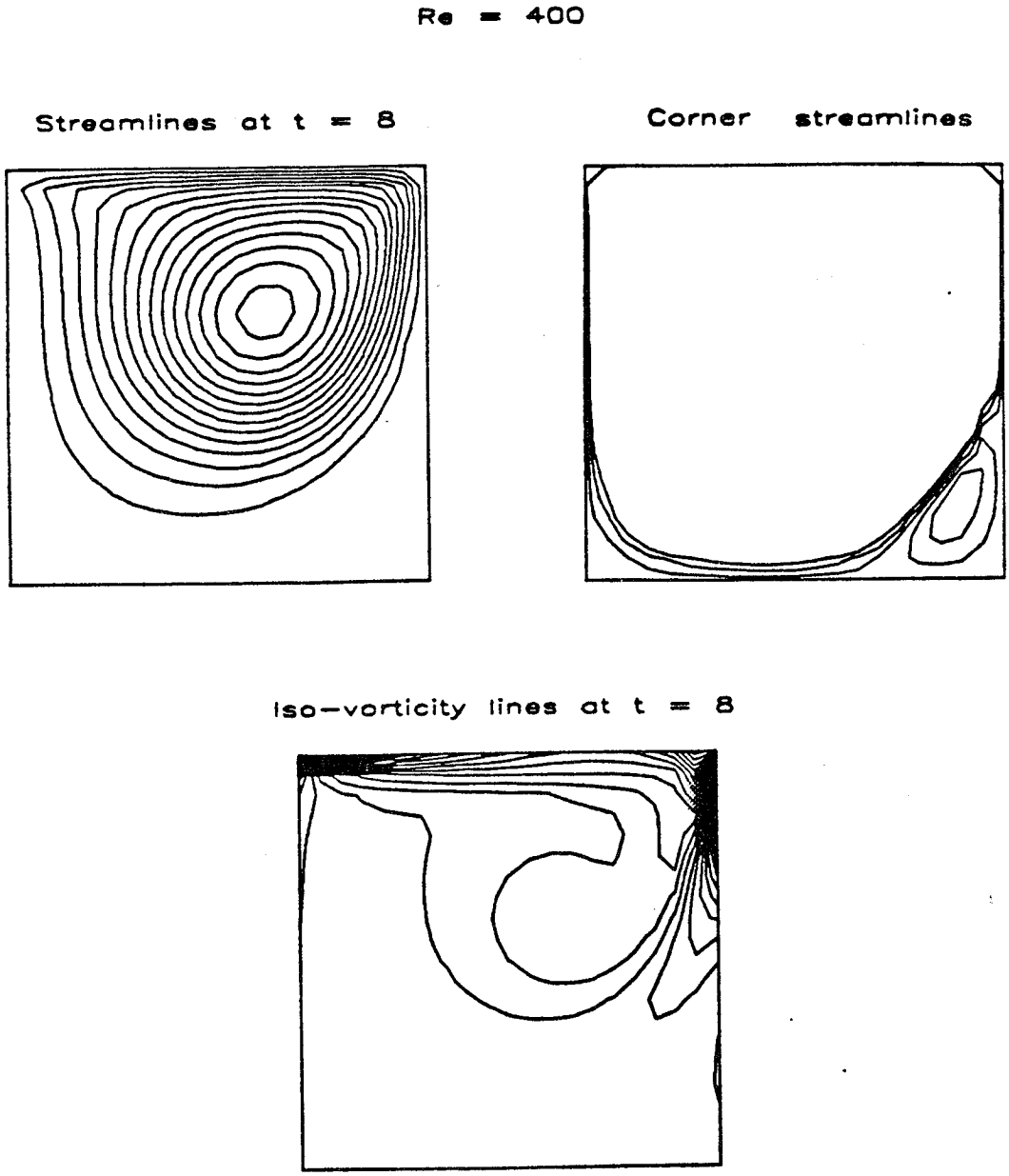

Figure 3.5.6 Driven cavity at Re = 400. Steady state streamlines and iso-vorticity lines.

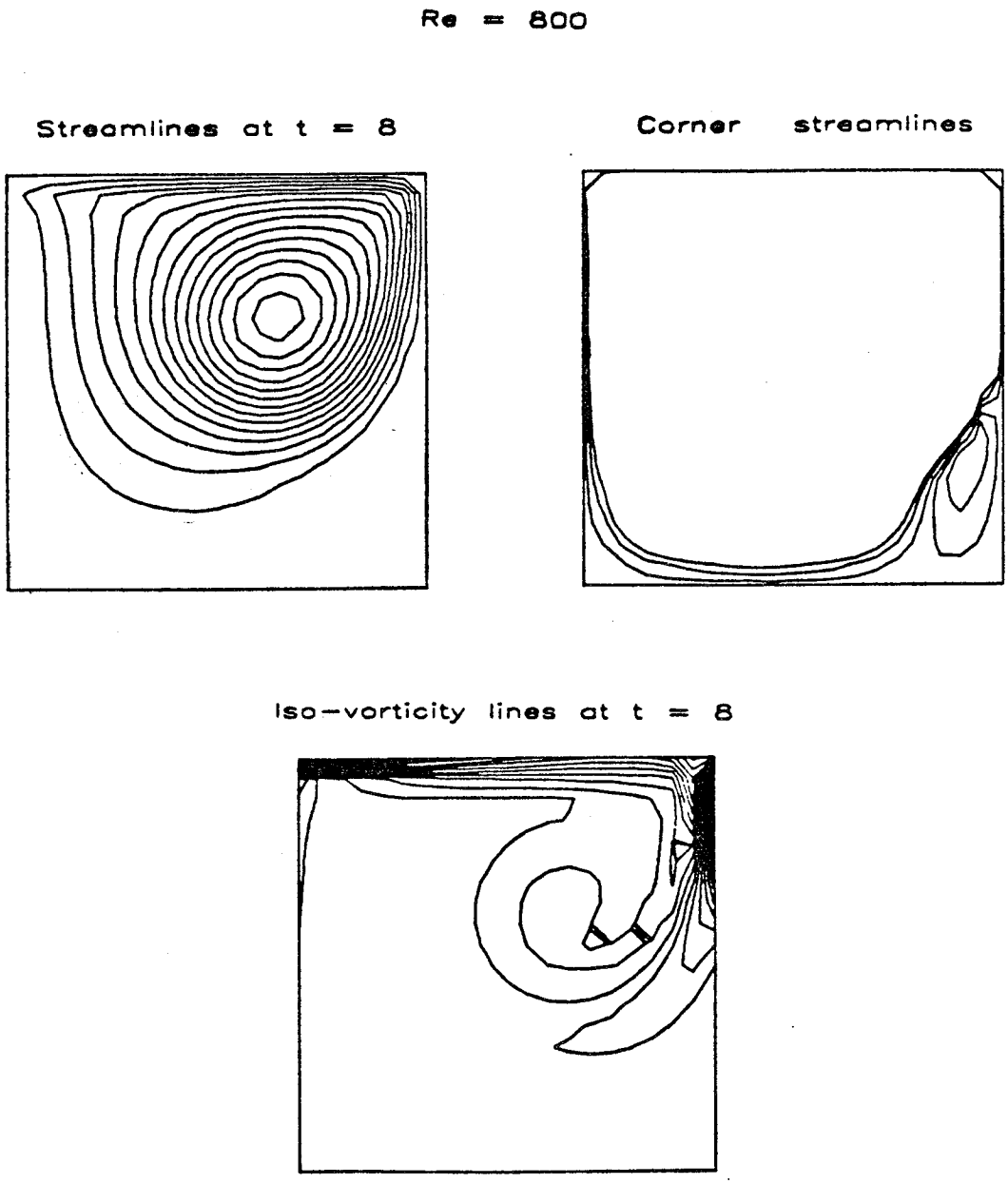

Figure 3.5.7 Driven cavity at Re = 800. Steady state streamlines and iso-vorticity lines.

Re = 100 Re = 400

Streamlines

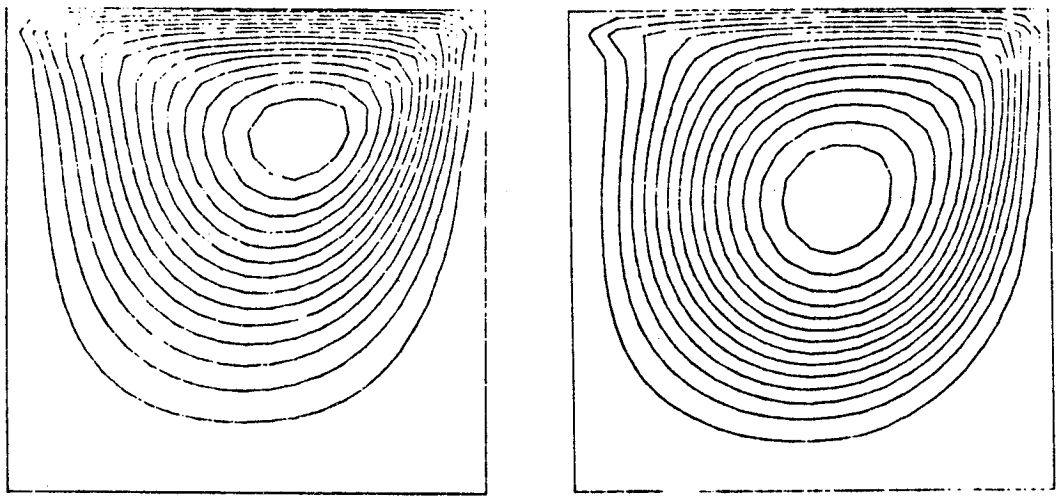

Iso-vorticity lines

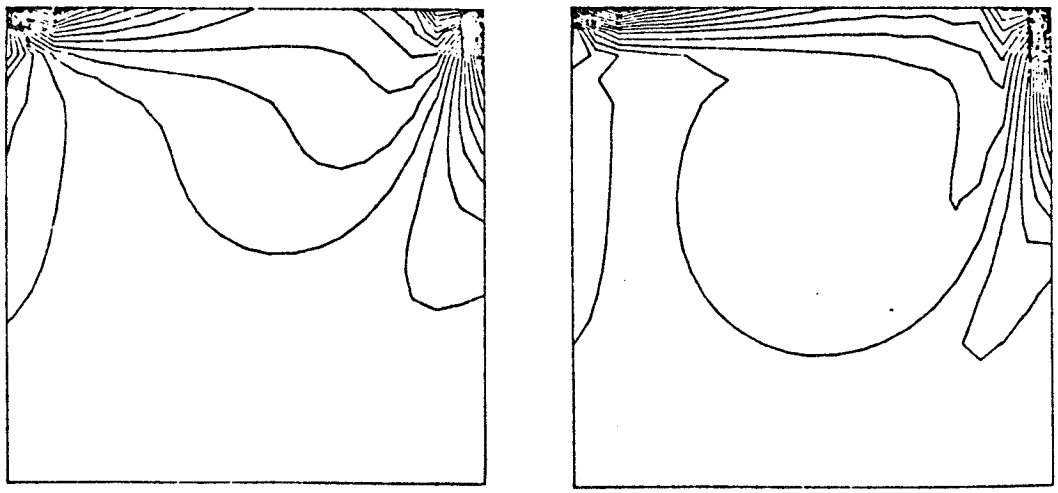

Figure 3.5.8 Driven cavity at Re = 100 and 400. Steady state streamlines and iso-vorticity lines obtained by Hughes et al. [32].

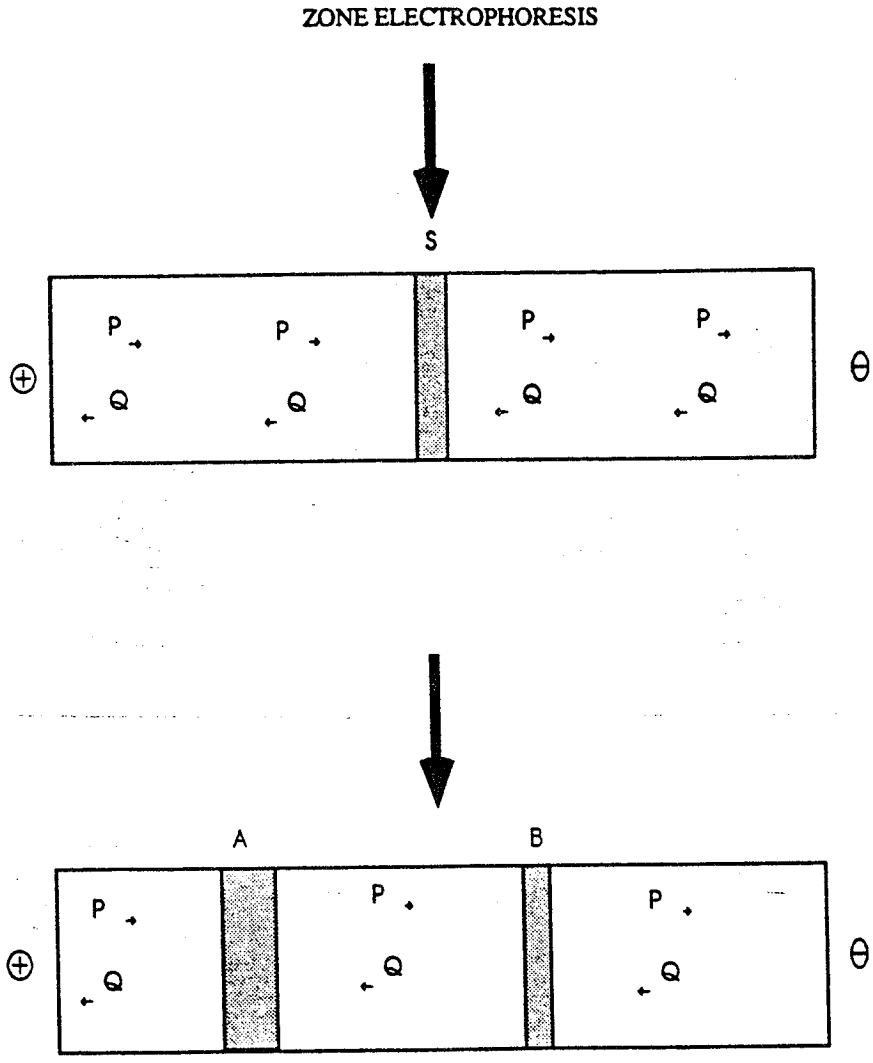

Figure 4.1.1 Zone electrophoresis. A mixture S consisting of anions and cations to be separated is injected in the electrolyte consisting of P^+ and Q^- ions. On the passage of an electric current the species separate out into zones depending on the charge and mobility.

MOVING BOUNDARY ELECTROPHORESIS

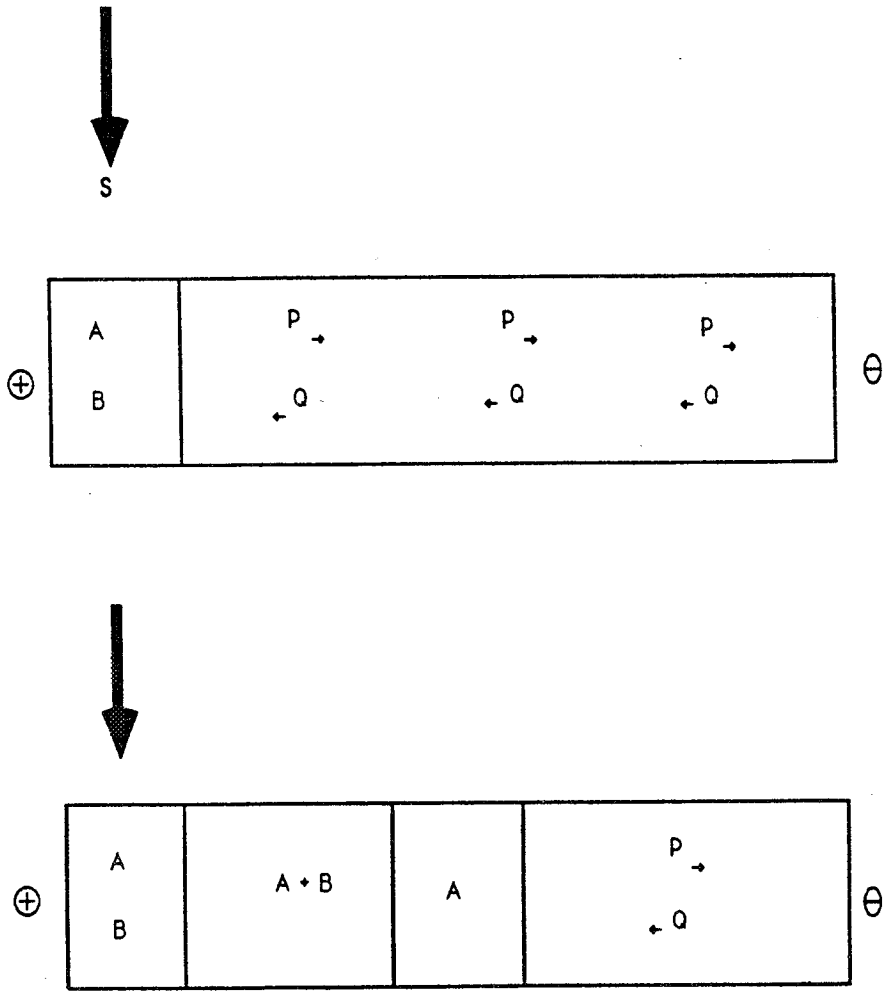

Figure 4.1.2 Moving boundary electrophoresis. The sample S consisting of species A and B is introduced into the cathode compartment. On the passage of current species A separates out fully because it has a higher mobility. This is followed by a mixture of A+B.

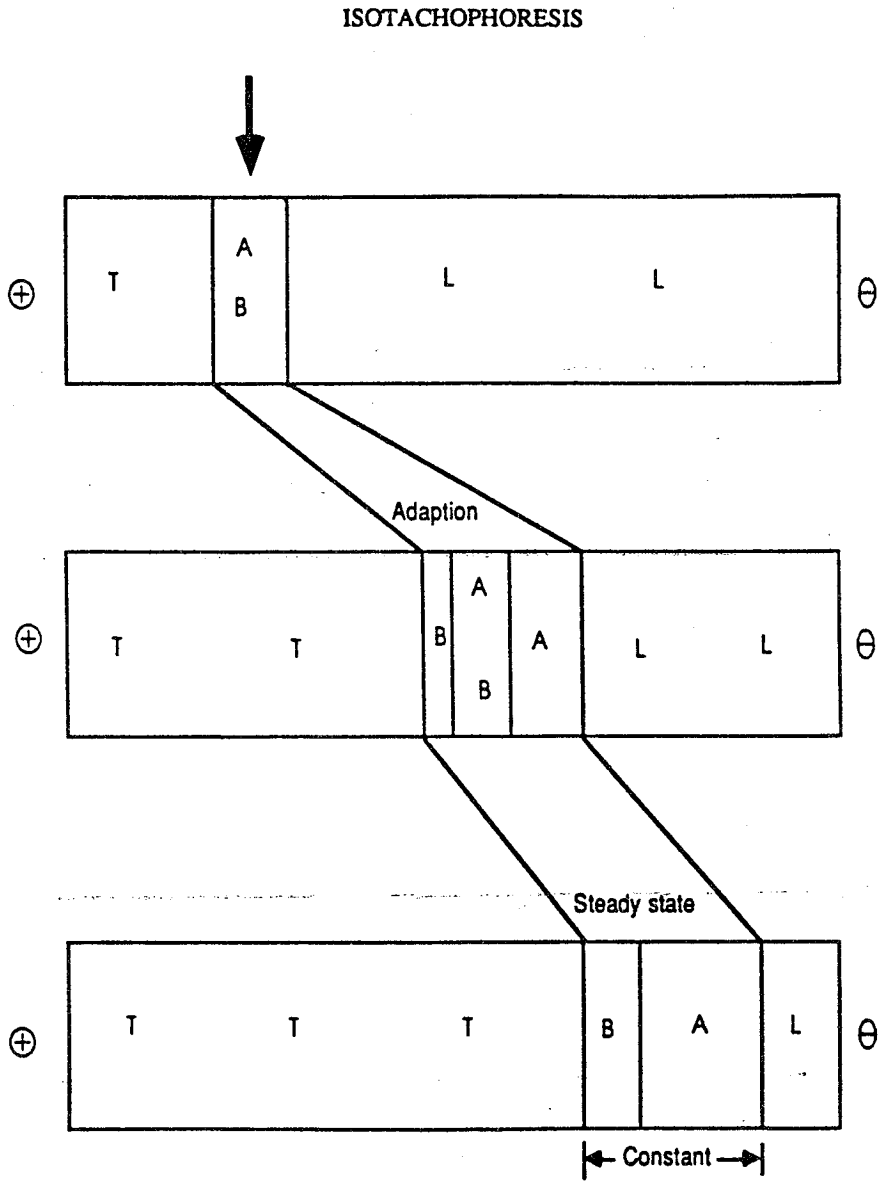

Figure 4.1.3 Isotachophoresis. The sample S consisting of A+B species is introduced between leading(L) and terminating(T) anionic species. On the passage of current mixed zones are obtained(like in MBE). On achieving steady state species A and B separate out and move at the same constant speed.

ZONE ELECTROPHORESIS IN ONE DIMENSION

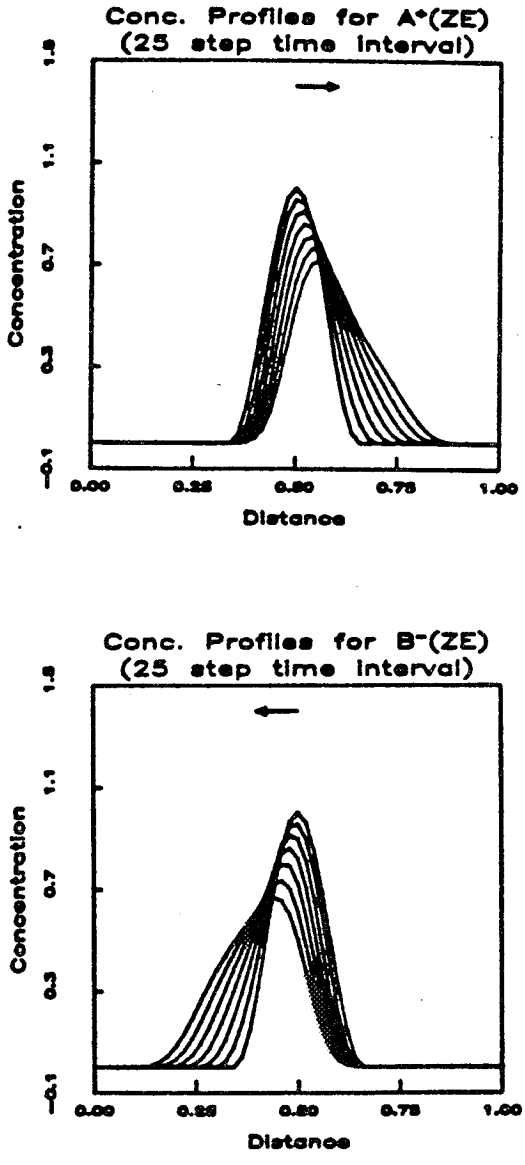

Figure 4.6.1 Zone electrophoresis in 1-D. Temporal evolution of species A^+ and B^-.

ZONE ELECTROPHORESIS IN ONE DIMENSION

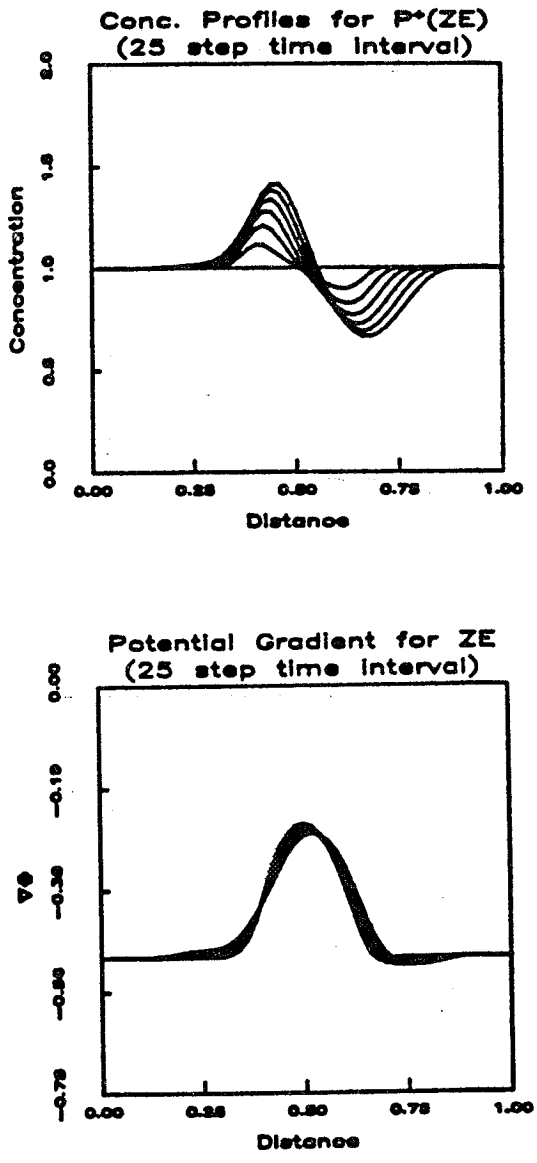

Figure 4.6.1 Zone electrophoresis in 1-D. Temporal evolution of P^+ and potential gradient.

MOVING BOUNDARY ELECTROPHORESIS IN ONE DIMENSION

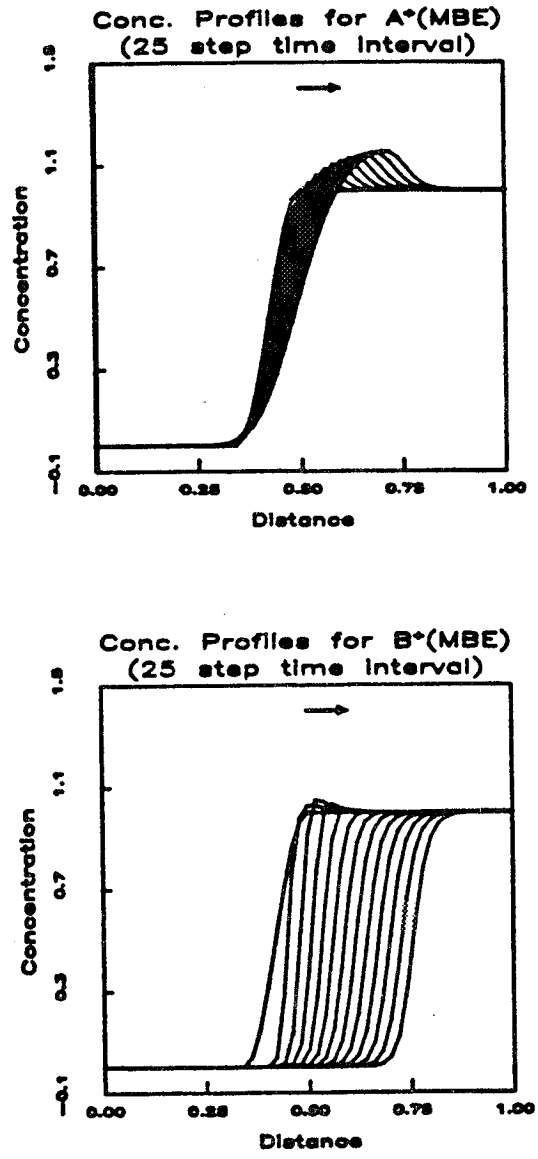

Figure 4.6.2 Moving boundary electrophoresis in 1-D. Temporal evolution of species A^+ and B^+.

MOVING BOUNDARY ELECTROPHORESIS IN ONE DIMENSION

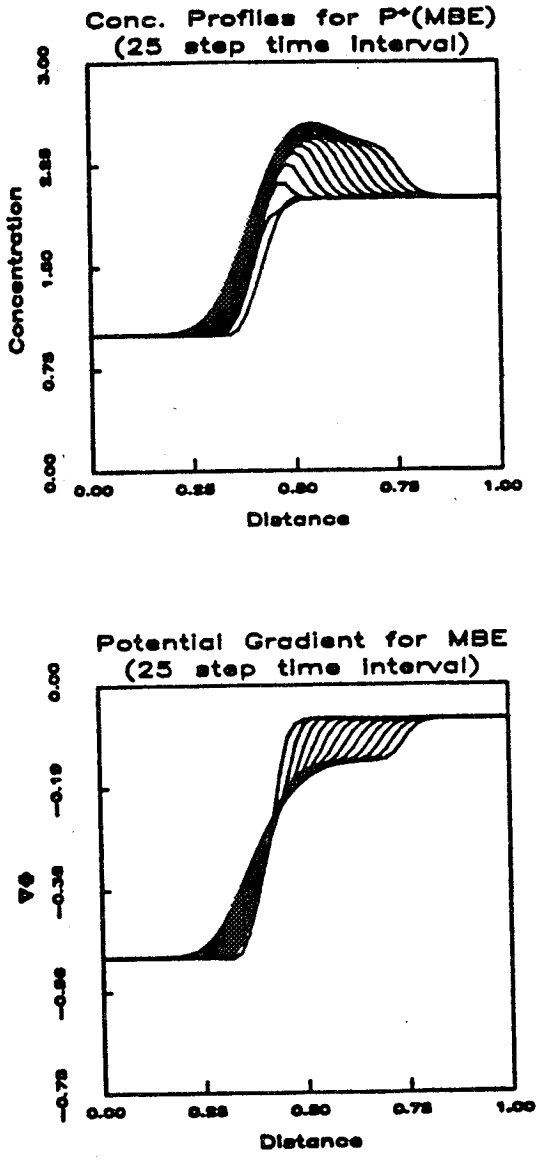

Figure 4.6.2 Moving boundary electrophoresis in 1-D. Temporal evolution of P^+ and potential gradient.

ISOTACHOPHORESIS IN ONE DIMENSION

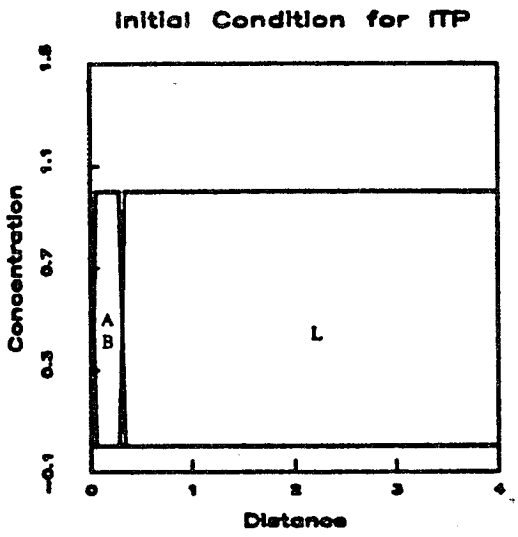

Figure 4.6.3 Isotachophoresis in 1-D. Initial condition showing concentration profiles of terminator T^+, species B^+ and A^+, and leader L^+ (in order of increasing mobility).

ISOTACHOPHORESIS IN ONE DIMENSION

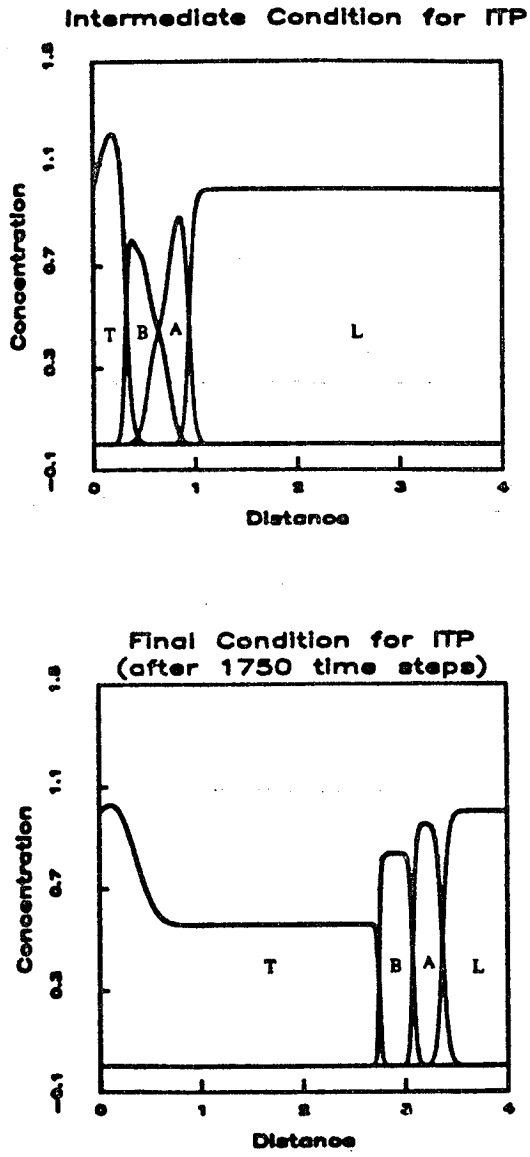

Figure 4.6.3 Isotachophoresis in 1-D. Intermediate and final condition showing concentration profiles of terminator T^+, species B^+ and A^+, and leader L^+ (in order of increasing mobility).

ISOTACHOPHORESIS IN ONE DIMENSION

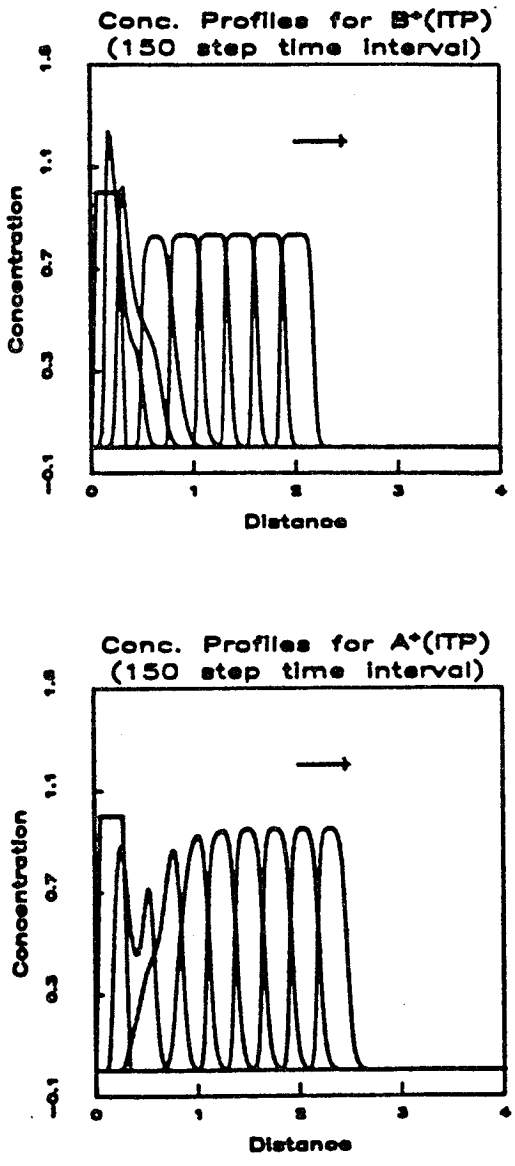

Figure 4.6.4 Isotachophoresis in 1-D. Temporal evolution of potential gradient.

ISOTACHOPHORESIS IN ONE-DIMENSION

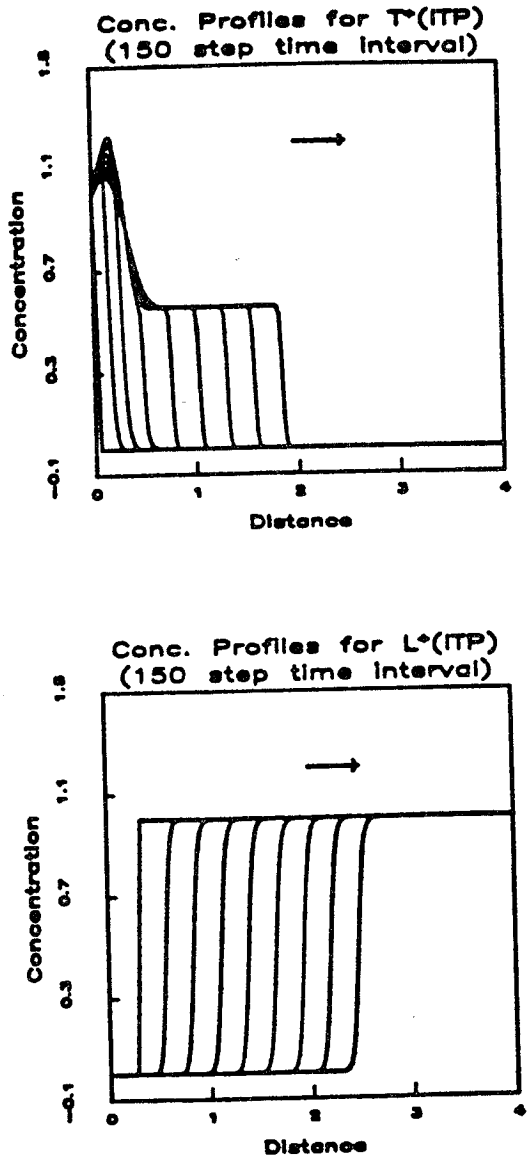

Figure 4.6.4 Isotachophoresis in 1-D. Temporal evolution of terminator T^+ and leader L^+.

ISOTACHOPHORESIS IN ONE DIMENSION

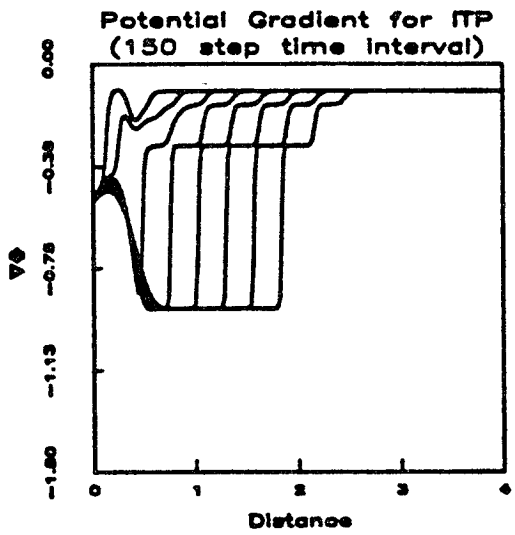

Figure 4.6.4 Isotachophoresis in 1-D. Temporal evolution of potential gradient.

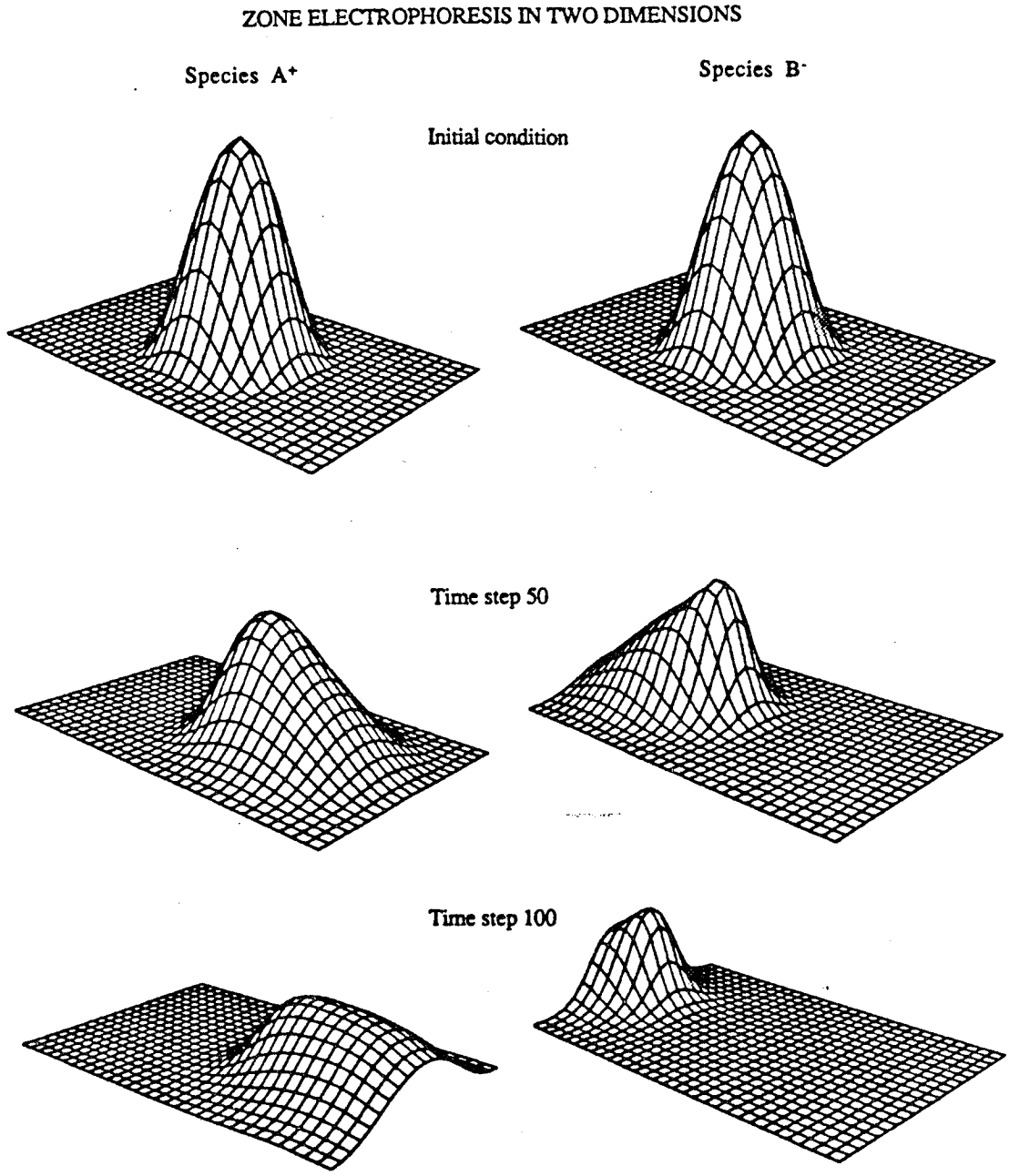

Figure 4.6.5 Zone electrophoresis in 2-D. Temporal evolution of species A^+ and B^-.

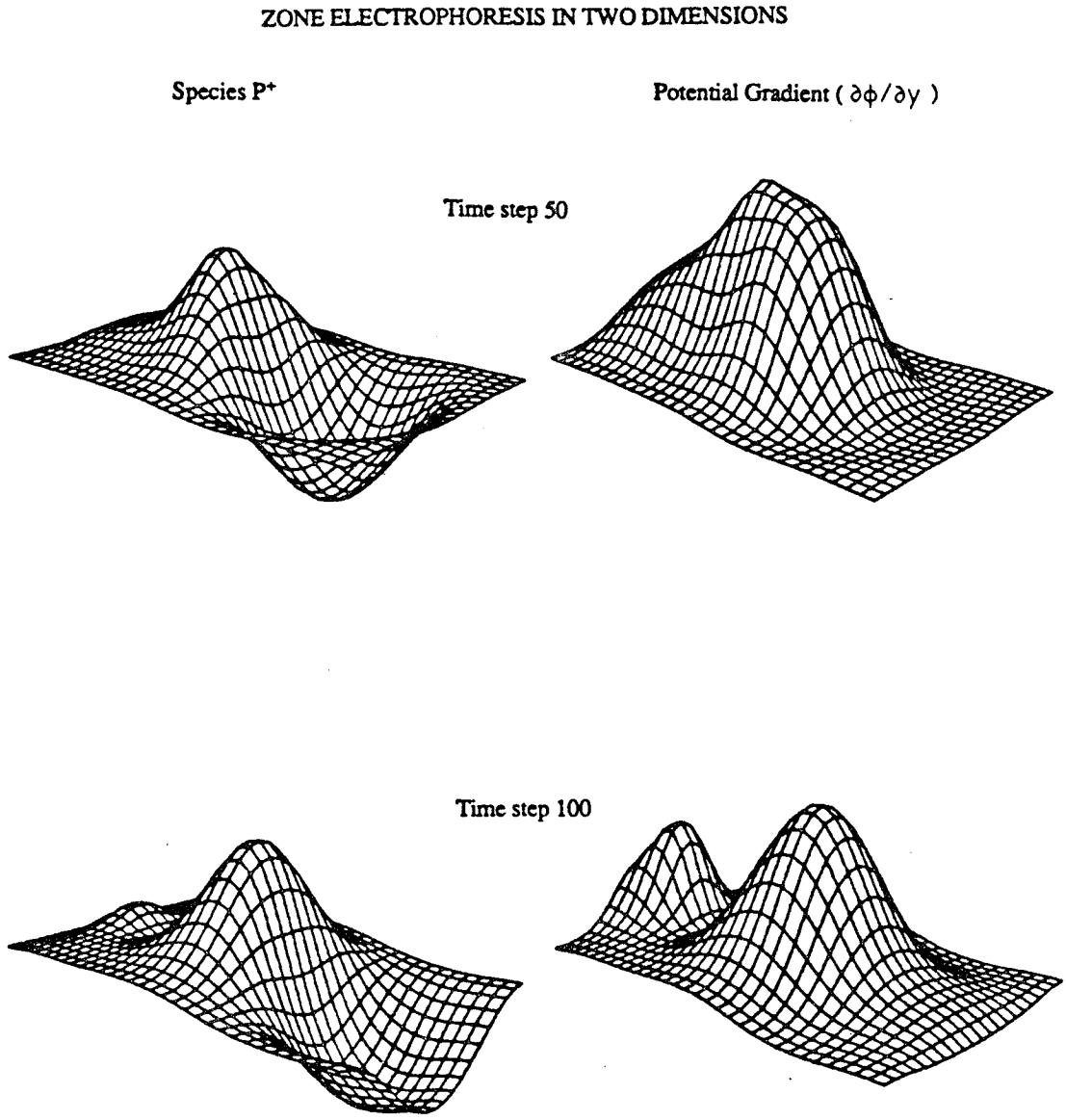

Figure 4.6.5 Zone electrophoresis in 2-D. Temporal evolution of P^+ and potential gradient.

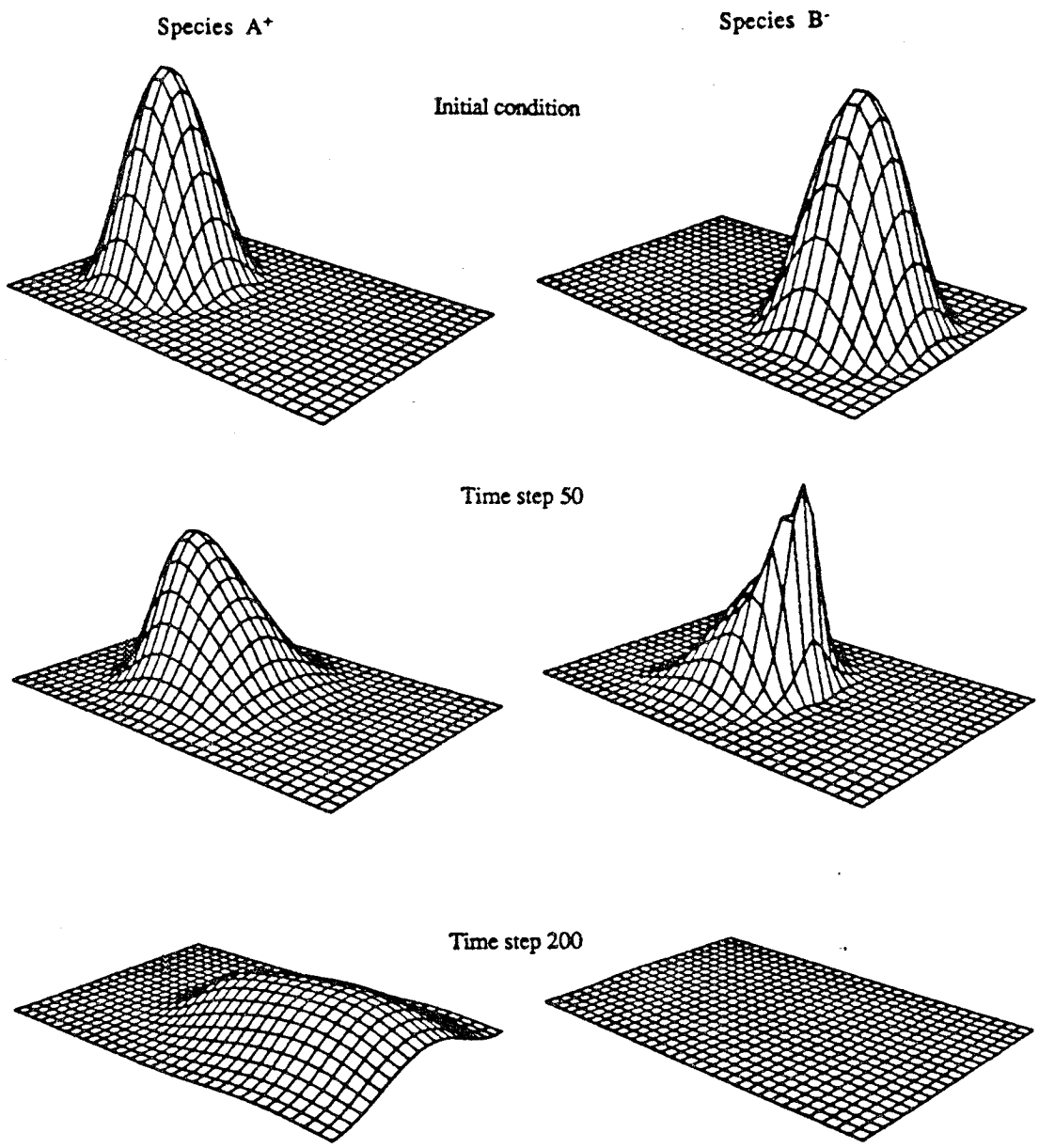

Figure 4.6.6 Cross electrophoresis in 1-D. Temporal evolution of species A^+ and B^-.

C-2

CROSS ELECTROPHORESIS IN TWO DIMENSIONS

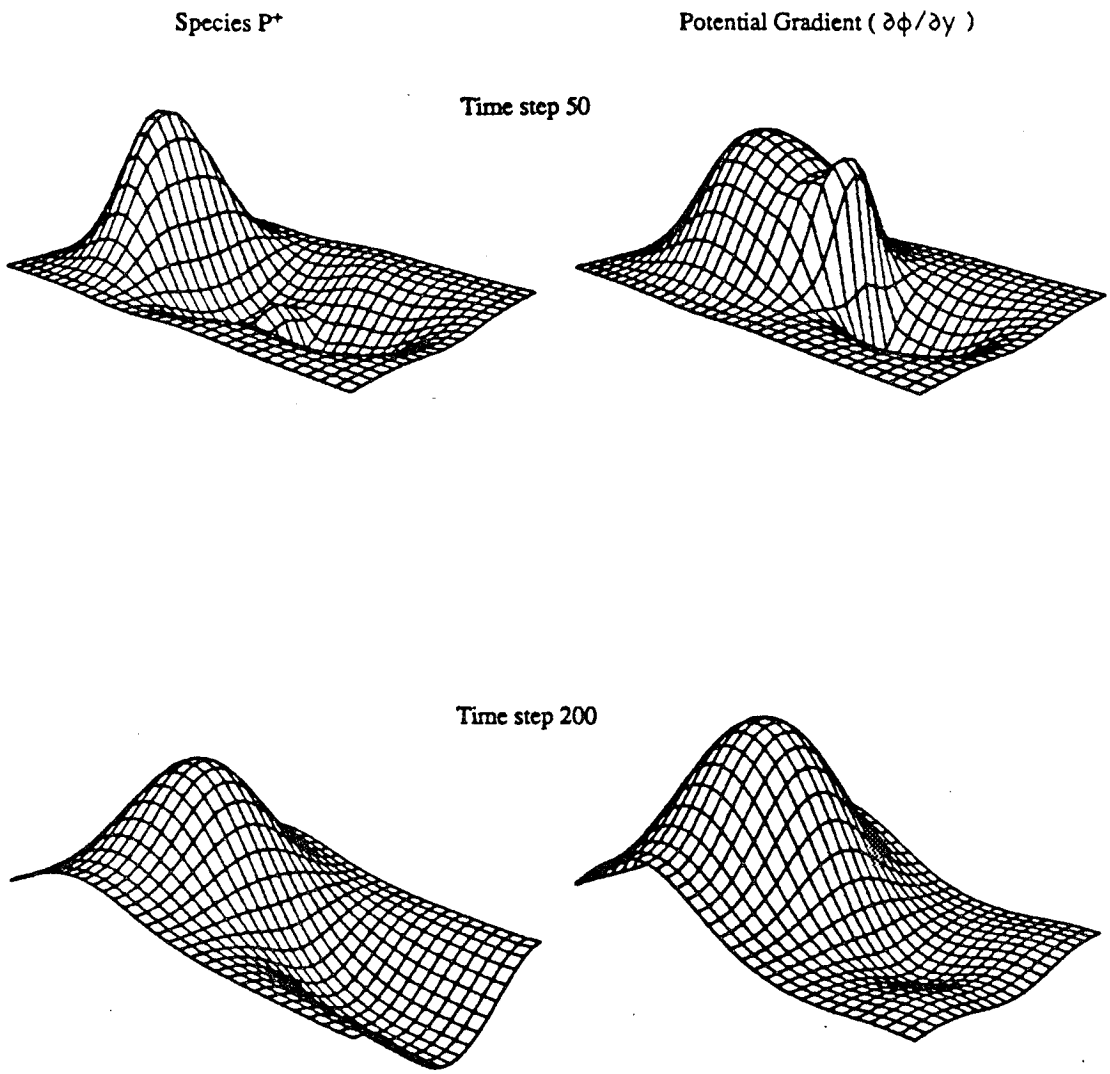

Figure 4.6.6 Cross electrophoresis in 1-D. Temporal evolution of P^+ and potential gradient.